Billiards in Nearly Isosceles Triangles

W. Patrick Hooper * and Richard Evan Schwartz †

April, 23 2013‡

Abstract

We prove that any sufficiently small perturbation of an isosceles triangle has a periodic billiard path. Our proof involves the analysis of certain infinite families of Fourier series that arise in connection with triangular billiards, and reveals some self-similarity phenomena in irrational triangular billiards. Our analysis illustrates the surprising fact that billiards on a triangle *near* a Veech triangle is extremely complicated even though billiards *on* a Veech triangle is very well understood.

1 Introduction

This paper concerns periodic billiard paths in triangles. In some cases, quite a bit is known about periodic billiard paths in triangles, and in some cases surprisingly little is known. For example, it is still unknown if every triangle has a periodic billiard path.

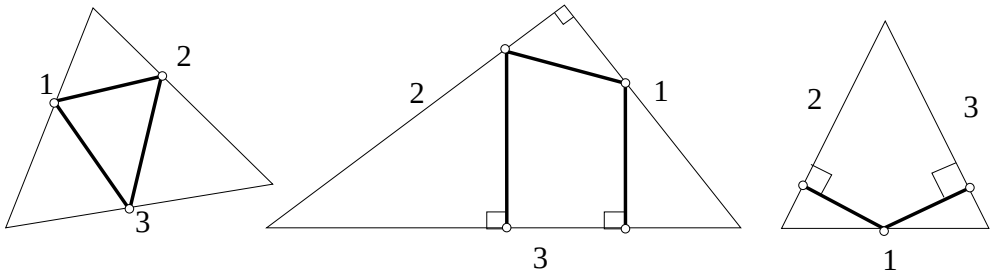

Figure 1.1: Periodic paths having combinatorial type 123 and 312321 and 2131.

One can show in elementary geometric ways that acute, right, and isosceles triangles always have periodic billiard paths. The famous Fagnano path, which goes back to 1775, exists on a triangle if and only if the triangle is acute. The Fagnano path has combinatorial type 123, meaning that it hits side 1 of the triangle, then side 2, then side 3, and then closes up. Assuming the sides are appropriately labelled, a periodic billiard path of combinatorial type 312321 exists on a triangle if and only if the triangle is right and a periodic billiard

*Supported by N.S.F. Postdoctoral Fellowship DMS-0803013

†Supported by N.S.F. Research Grant DMS-0305047

‡This improves the published paper [HS09]; it corrects some errors in §9. See remark 9.1.

path of combinatorial type 2131 exists on a triangle if and only if the triangle is isosceles. Examples of these paths are shown in Figure 1.1.

Periodic billiard paths in right triangles have been fairly extensively studied. The path 312321, mentioned above, is part of a broader class of periodic billiard paths in right triangles, introduced in [VGS92], which start out perpendicular to a side of the triangle. One sometimes calls these "perpendicular billiard paths". In [CHK95] it is shown that almost every perpendicular billiard path is periodic. In [Tro05] this result is refined, for right triangles with small angle lying in $(\pi/6, \pi/4)$: For such triangles, all but one perpendicular billiard path is periodic, and the union of these periodic perpendicular paths is dense in the phase space. In [GZ03] and [Vor05], some classes of periodic billiard paths in triangles are introduced and shown to be *unstable* – meaning that paths of the same combinatorial type do not exist on nearby acute or obtuse triangles. Finally, in [Hoo07] it is shown that all periodic billiard paths in right triangles are unstable.

Every rational triangle – i.e., a triangle whose angles are rational multiples of π – has a periodic billiard path. Indeed, any given rational polygon has a dense set of periodic billiard paths [BGKT98]. See also [Mas86] and [Vor05]. The subject of billiards on rational polygons is a deep and extensive one. For instance, see [Vee89] for connections between rational billiards and Teichmüller Theory. See [MT02] and [Tab95] for surveys on rational billiards.

Much less is known about periodic billiard paths in obtuse, irrational triangles. The paper [VGS92], the first to make serious inroads into this question, produces some infinite families of stable periodic billiard paths in obtuse triangles. A periodic billiard path on a triangle is called *stable* if all sufficiently nearby triangles have a combinatorially identical periodic billiard path. The paper [HH00] continues the program started in [VGS92], producing additional families of stable periodic billiard paths on obtuse triangles. The papers [Hoo06], [Sch06a], [Sch06b] exhibit additional infinite families of periodic billiard paths for some obtuse triangles. In particular, in [Sch06a], [Sch06b] it is shown that a triangle has a periodic billiard path provided that all its angles are at most 100 degrees.

We already mentioned above that the periodic billiard path 2131 exists on any isosceles triangle. Unfortunately, this path is unstable: It disappears as soon as we perturb the triangle so that it is no longer isosceles. One might wonder if there is more to the story for such perturbations. Here is the main result of this paper.

Theorem 1.1 *Any sufficiently small perturbation of an isosceles triangle has a periodic billiard path.*

1.1 Overview of the Proof

The parameter space of (obtuse) triangles is an open triangle $\Delta \subset \boldsymbol{R}^2$, where the point (x, y) corresponds to the obtuse triangle whose small angles are x and y radians. To each infinite periodic word W, with digits in the set $\{1, 2, 3\}$, we assign the region $O(W) \subset \Delta$ as follows: A point belongs to $O(W)$ if W describes the combinatorics of a periodic billiard path in the corresponding triangle. By this we mean that we label the sides of the triangle 1, 2, and 3, and then read off W as the sequence of successive edges encountered by the billiard path. We call $O(W)$ an *orbit tile* and W a *combinatorial type*.

The open line segment $\{x = y\} \subset \Delta$ parametrizes the obtuse isosceles triangles. We prove Theorem 1.1 by covering a neighborhood of this segment by orbit tiles. This innocent-sounding approach gives rise to an extremely intricate covering involving infinitely many combinatorial types. As we go along, we will try to explain why the complexity seems necessary.

We define the *Veech points*

$$V_n = (\pi/2n, \pi/2n); \qquad n = 3, 4, 5... \tag{1.1}$$

These points are special because they correspond to triangles which have Veech's famous lattice property [Vee89]. First of all, we will prove the following result.

Theorem 1.2 *A point on the obtuse isosceles line lies in the interior of an orbit tile provided it is not of the form V_n.*

Theorem 1.2 involves a doubly-infinite family of tiles – with infinitely many tiles existing between consecutive Veech points. See Figure 1.3 below. Experimentally, the family in Theorem 1.2 seems to be the most efficient one by far. Theorem 1.2 focuses our attention on the Veech points.

We find it useful to treat the points V_n in a uniform way. We decompose neighborhoods of the Veech points into quadrants. Let $B(\epsilon)$ denote the ball of radius ϵ, centered at the origin. Let $B_{\pm,\pm}(\epsilon)$ denote the intersection of B_ϵ with the open $(\pm, \pm)$ quadrant. Now define

$$N_{\pm,\pm}(n, \epsilon) = V_n + B_{\pm,\pm}(\epsilon). \tag{1.2}$$

Finally, let $N(n, \epsilon)$ denote the ϵ neighborhood of V_n.

Theorem 1.3 *For each $n \geq 4$ there are words A_n, B_n, and C_n, and some $\epsilon_n > 0$ such that*

- $N_{--}(n, \epsilon_n) \subset O(A_n)$.
- $N_{-+}(n, \epsilon_n) \subset O(B_n)$
- $N_{+-}(n, \epsilon_n) \subset O(C_n)$.
- $B(\epsilon_n) - \overline{N}_{++} \subset O(A_n) \cup O(B_n) \cup O(C_n)$

The last statement is present to take care of the boundaries of the quadrants. See Figures 1.2 and 1.4 below. It is worth remarking that the words A_n are part of a larger family discovered in [VGS92]. See also [HH00].

Theorem 1.3 focuses our attention on the regions $N_{++}(n, \epsilon)$. Theorem 1.3 and Conjecture 1.6 together imply that these regions do not have finite covers by orbit tiles, at least when n is a power of 2. We deal with all values of n at once, by introducing a doubly infinite family $\{W_{nk}\}$ of words. Here $n = 4, 5, 6...$ and $k = 0, 1, 2....$ Figure 1.4 below shows some of the corresponding orbit tiles for $n = 4$.

Theorem 1.4 *For each $n \geq 3$, there is some $\epsilon = \epsilon_n$ such that*

$$\overline{N}_{++}(n, \epsilon) - \{V_n\} \subset \bigcup_{k=0}^{\infty} O(W_{nk}).$$

Theorems 1.2, 1.3, and 1.4 take care of neighborhoods of all points except V_2 and V_3. The example we work out in the next chapter shows that $V_3 \in O(W)$ for a certain word W of length 22. See Corollary 2.4. Alternatively, Theorem 1.5 handles a neighborhood of V_3. Finally, in [Sch06b] we proved that a neighborhood of V_2, the point corresponding to the right-angled isosceles triangle, is contained in the union of 9 orbit tiles. This completes the proof of Theorem 1.1.

It is worth remarking that some of the complexity in our proof seems necessary. We will prove the following result.

Theorem 1.5

1. *For $k = 3, 4, 5...$ the triangle V_{2^k} does not lie in the interior of an orbit tile.*
2. *For $n \geq 3$ and not a power of two, V_n does lie in the interior of an orbit tile.*

In a separate and independent way, Statement 2 of Theorem 1.5 handles all the Veech points except V_{2^k} for $k = 3, 4, 5...$ However, this result does not really save us any time in our analysis, because we still need to use the analysis above to cover the remaining Veech points. Statement 1 suggests that perhaps the remaining points will be trouble. Indeed, computer evidence strongly supports the following conjecture.

Conjecture 1.6 *For $k = 3, 4, 5...$ no neighborhood of V_{2^k} has a finite covering by orbit tiles.*

Remark: In [Sch06a] it is proved that no neighborhood of $(\pi/3, \pi/6)$ has a finite covering by orbit tiles. Thus, the covering constructed in [Sch06a] and [Sch06b] for the "100 degree result"mentioned above is necessarily infinite, partly because of the "trouble spot" at the point corresponding to the $(30, 60, 90)$-triangle. In the same way, Conjecture 1.6 states that there are an infinite number of "trouble spots" at various Veech points.

1.2 Some Pictures of the Tiles

We discovered all the results in this paper using our computer program, McBilliards, a well-documented Java-based program which is publicly available. [1] The reader can see great pictures of our tiles using McBilliards. Here we reproduce a few of these pictures.

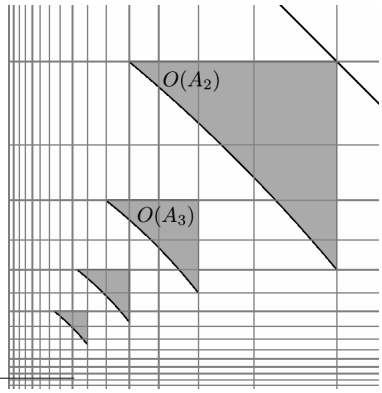

[1] `http://mcbilliards.sourceforge.net`

Figure 1.2: The orbit tiles $O(A_n)$ for $n = 2, 3, 4, 5$.

Figure 1.2 shows a picture the first few orbit tiles in the A series. The horizontal grid lines have the form $x_2 = \pi/n$ for $n = 4, 5, 6...$ and the vertical grid lines have the form $x_1 = \pi/n$ for $n = 4, 5, 6$. The right-angled tips of these tiles are the Veech points.

The tiles in the A series are also part of the tiles of we use to prove Theorem 1.2. Theorem 1.2 uses a double-infinite family $\{Y_{n,m}\}$ of words with $m \in \boldsymbol{N}$ and $n \in \{2, 3, 4...\}$. We have $A_n = Y_{n,1}$. For n fixed, the tiles $\{Y_{n,m}\}$ live between the two consecutive Veech points V_n and V_{n+1}. Figure 1.3 shows some of these tiles.

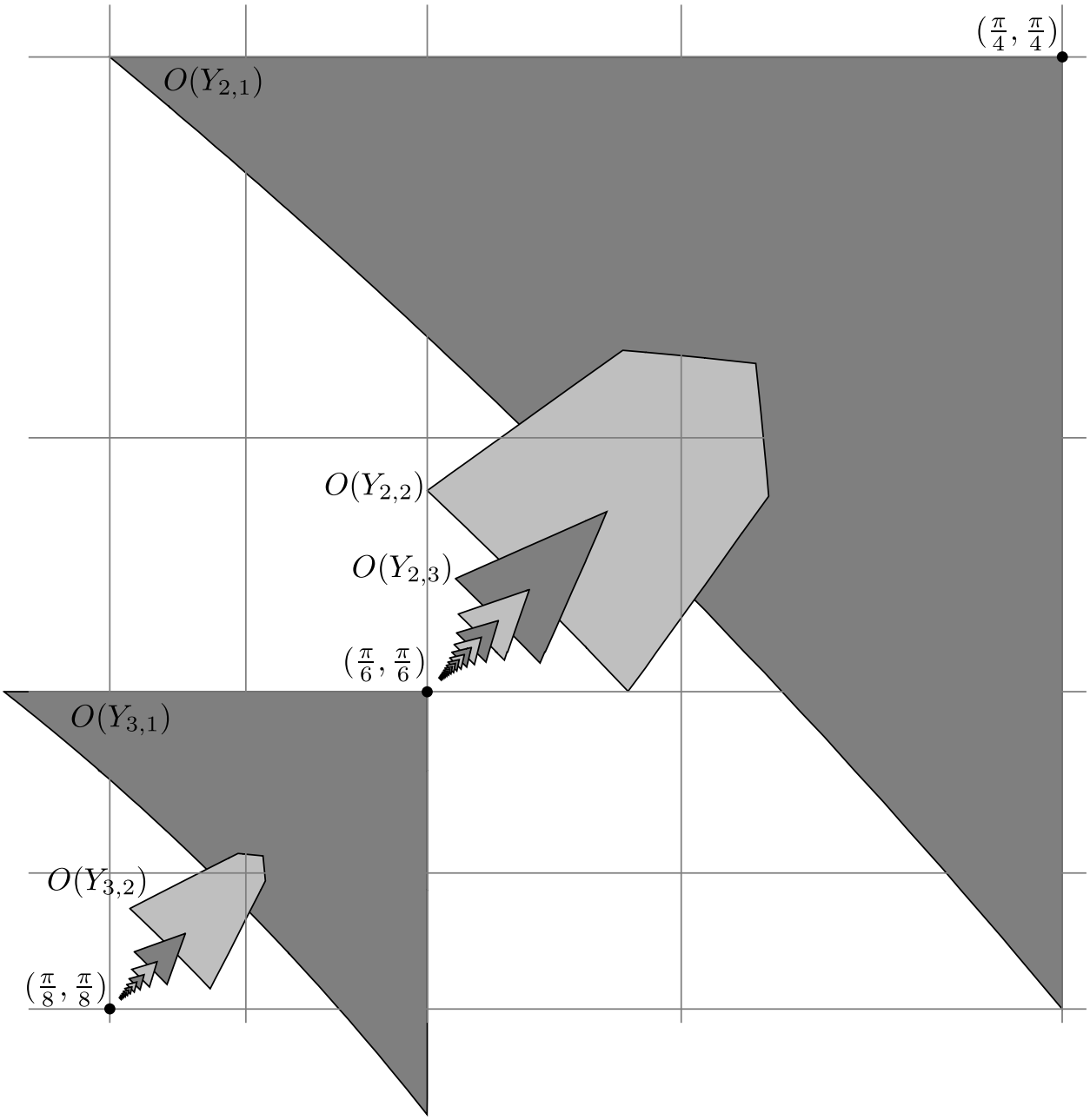

Figure 1.3: Some of the tiles $O(Y_{n,m})$ with $n \in \{2, 3\}$ and $m \in \{1, 2, 3, \ldots\}$.

Figure 1.4 shows a neighborhood of the point $V_4 = (\pi/8, \pi/8)$, a point in the bottom left corner of Figure 1.3. The tiles $O(B_4)$ and $O(C_4)$ are tiny in comparison to the size of $O(A_4)$, so much of $O(A_4)$ is off the screen. The union covers a neighborhood of V_4.

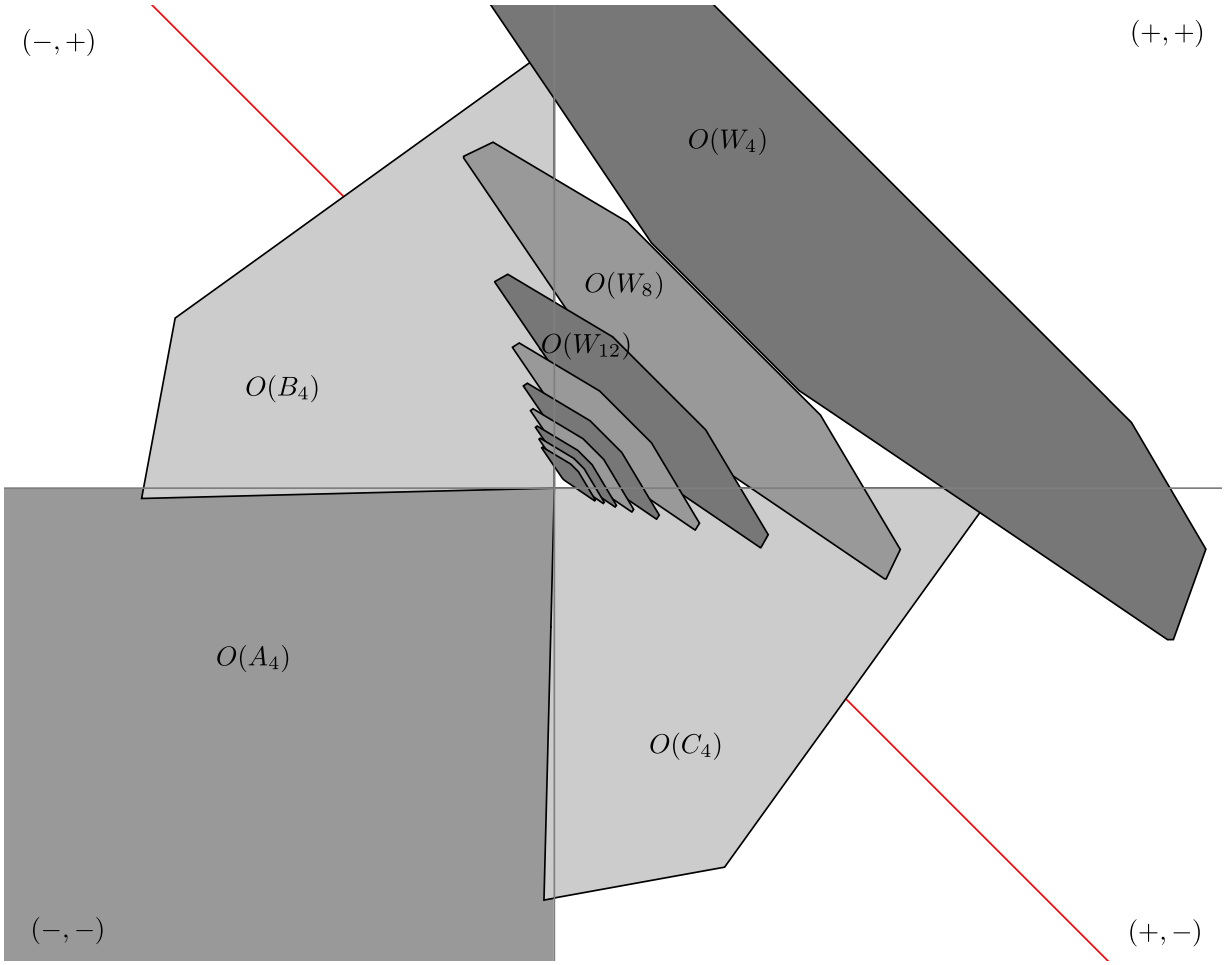

Figure 1.4: The orbit tiles $O(A_4)$ and $O(B_4)$ and $O(C_4)$ and $O(W_{4k})$ for $k = 1, ..., 9$.

1.3 Asymptotic Self-Similarity and Fourier Series

Let $O_{nk} = O(W_{nk})$. The following self-similarity result, which is the central technical result in the paper, implies Theorem 1.4.

Theorem 1.7 (Central Lemma) *Let S_{nk} be the dilation which maps V_n to 0 and expands distances by*

$$\zeta_n k^2; \qquad \zeta_n := 2(n-1)\cot(\pi/2n) \approx 4n^2/\pi$$

If n is held fixed and $k \to \infty$ then the closure of $S_{nk}(O_{nk})$ Hausdorff-converges to the convex quadrilateral Q_n with vertices

$$v_1 = (-\frac{1}{n}, 1 - \frac{1}{n}); \quad v_2 = (1 - \frac{1}{n}, -\frac{1}{n}); \quad v_3 = (a_n, a_n); \quad v_4 = (\mu_n a_n, \mu_n a_n);$$

where

$$a_n = \frac{1}{2} - \frac{1}{2n}; \quad \mu_n = \frac{1}{2} - \frac{\tan^2(\pi/2n)}{2}.$$

The convergence is such that any compact subset $Q_n' \subset Q_n$ is contained in $S_n(O_{nk})$ for k sufficiently large in comparison to n.

An example of the limiting quadrilateral Q_n is shown in figure 1.5, below.

Proof of Theorem 1.4: Fixing n, Theorem 1.7 implies that there are constants $0 < \epsilon_1 < \epsilon_2$ such that, for k sufficiently large, $O(W_{nk})$ contains the set $V_n + \Lambda_k$, where Λ_k is the convex hull of

$$(\epsilon_1/k^2, 0); \quad (\epsilon_2/k^2, 0); \quad (0, \epsilon_1/k^2); \quad (0, \epsilon_2/k^2)$$

for k large. But the union of the sets $V_n + \Lambda_k$ covers $N(n, \epsilon)$ for some $\epsilon > 0$. These sets "bunch up" as $k \to \infty$. Compare Figure 1.4. So, Theorem 1.7 proves Theorem 1.4. ♠

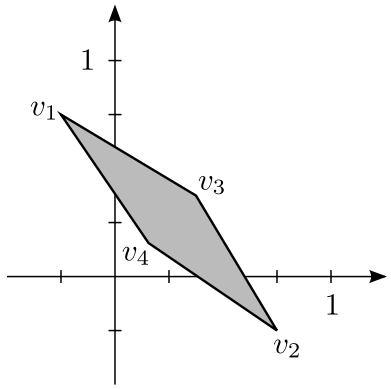

Figure 1.5: The limiting quadrilateral Q_4.

Our technique for proving Theorem 1.7 involves looking at the Fourier transforms of the analytic functions which define the edges of the orbit tiles of interest to us. The Fourier transforms of these functions are functions defined on $\boldsymbol{Z}^2$. It turns out that the supports of these Fourier transforms grow "linearly" with the parameter k in a way we make precise in §6. To deal with with the situation as $k \to \infty$ we prove the Quadratic Rescaling Theorem, a result which describes the asymptotic limits of a family of functions which vary with the prescribed growth. One of the main technical innovations in the paper is a combinatorial method for understanding such growing families of Fourier series. Our technique seems to be more general than the application we give here, but so far this is the main application.

1.4 Paper Outline

In §2 we will give background information about triangular billiards, and in particular discuss how one computes the orbit tile $O(W)$ based on the combinatorics of the word W. All of the constructions in §2 are programmed into McBilliards. The interested reader can see these constructions in action when using the program.

In section 3, we prove theorem 1.2.

In §4 we will prove Theorem 1.3.

§5-8 are devoted to the proof of the Central Lemma, namely Theorem 1.7. In §5 we will introduce our words W_{nk}, and prove some preliminary results about the orbit tiles $O_{nk} := O(W_{nk})$. In particular, we will isolate a region $R_{nk} \subset \Delta$ with the property that (independent of n and k) a certain 16 functions define $O_{nk} \cap R_{nk}$.

In §6 we will prove the Quadratic Rescaling Theorem, a result that is designed to analyze infinite families of defining functions, such as the 16 families we isolate in §5. In §7 and §8 we will use the Quadratic Rescaling Theorem to finish the proof of Theorem 1.7.

In §9, which is logically independent from the rest of the paper, we prove theorem 1.5. This classifies the Veech triangles V_n which lie in the interior of an orbit tile.

2 Billiard Paths and Defining Functions

2.1 Unfoldings

The *unfolding* of a word W with respect to a triangle T, which we denote by $U(W,T)$, is the union of triangles obtained by reflecting T out according to the digits of W. This construction is discussed in detail in [Sch06a] and in e.g. [Tab95]. We will persistently abuse our notation in the following sense: A point X in parameter space represents a triangle $T = T_X$. We will often write $U(W,X)$ in place of $U(W,T)$.

There is a sequence of vertices which runs across the top of $U(W,T)$. We call these the *top vertices* and label them $a_1, a_2, ...$ from left to right. There is a sequence of vertices which runs across the bottom of $U(W,T)$ and we label these $b_1, b_2, ...$ from left to right. Figure 2.1 shows an example of an unfolding, with respect to the Veech point V_3.

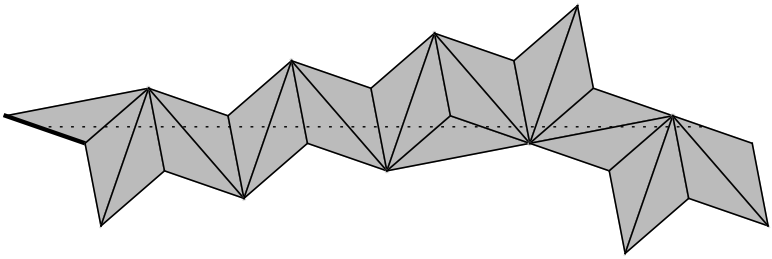

Figure 2.1: $U(2323132313123232313131, V_3)$ with a centerline

It is worth pointing out that one of the apparent edges of the unfolding in Figure 2.1 is not actually an edge of reflection. Figure 2.2 shows the unfolding of the same word with respect to a different point.

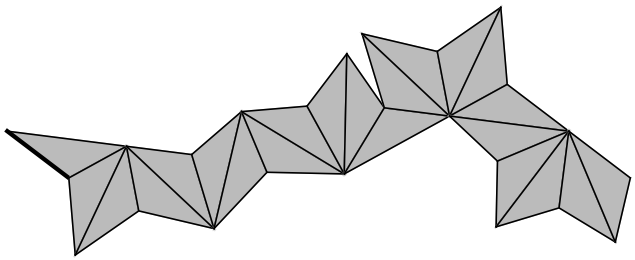

Figure 2.2 $U(2323132313123232313131, (\pi/5, \pi/6))$

Remark: We mainly care about unfoldings of isosceles triangles or triangles that are very nearly isosceles. From here on in, most of our pictures show unfoldings of isosceles triangles. However, as with Figure 2.2, we sometimes show an unfolding of a non-isosceles triangle so as to illustrate a point.

The first side of U has been highlighted in both examples. W represents a periodic billiard path in T iff the first and last sides of $U(W,T)$ are parallel and the interior of $U(W,T)$ contains a line segment L, called a *centerline*, such that L intersects the first and last sides at corresponding points. In both examples above, the first and last sides are parallel. However, the centerline only exists for Figure 2.1. In particular, Figure 2.1 shows

that the given word describes a periodic billiard path for the triangle corresponding to V_3. As in Figures 2.1 and 2.2 we always rotate the picture so that the first and last sides are related by a horizontal translation. We call this horizontal translation the *holonomy*.

2.2 Stability and Hexpaths

A word W is called *stable* if the first and last sides of $U(W,T)$ are parallel for any triangle T. This implies that $O(W)$ is an open set. In this section we will explain a combinatorial criterion for stability. The proof is well known, and we omit it. See [Sch06a] for details.

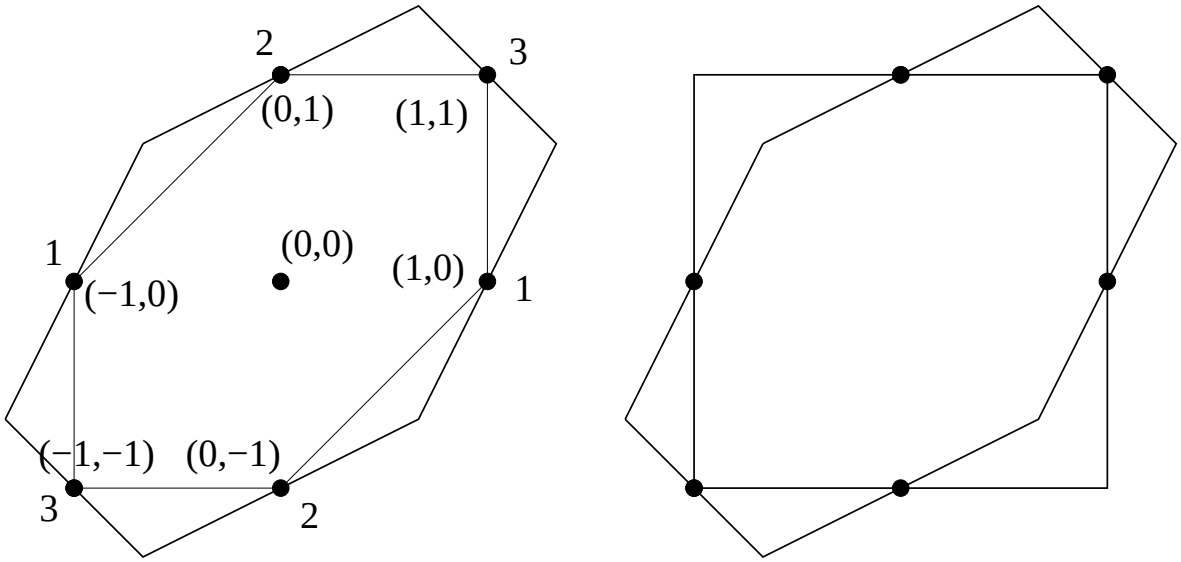

Figure 2.3: The fundamental hexagon

Let H_0 be the outer hexagon shown in Figure 2.3. The shape if H_0 is a bit strange, but the inscribed hexagon has vertices on the integer lattice $\boldsymbol{Z}^2$ as shown. Also, H is well related to a square of side-length 2, as shown on the right hand side of Figure 2.3. The sides of H_0 are divided into 3 types, according to their label. Let $\mathcal{H}$ denote the tiling of $\boldsymbol{R}^2$ by translates of H_0. By $\mathcal{H}$ we really mean the union of edges of the tiling. By construction, the midpoints of edges in $\mathcal{H}$ lie in $\boldsymbol{Z}^2$.

Given the word W, we can draw a path in $\mathcal{H}$ by following the edges as determined by the word: we move along the dth family when we encounter the digit d. Figure 2.4 shows the path corresponding to the examples given in Figures 2.1 and 2.2. The dot in the picture indicates the start of the path. We call this path the *hexpath* and denote it by $H(W)$.

Lemma 2.1 (Hexpath) *The word W is stable iff $H(W)$ is a closed path.*

This condition in the Hexpath Lemma is equivalent to the better known condition, which appears as lemma 3.3.1 in [Tab95]. We have restricted this lemma to our context.

Lemma 2.2 *A word W is stable iff the number of times each letter $\ell = 1,2,3$ appears in an odd position in W equals the number of times ℓ appears in an even position.*

This condition can easily be verified for the example we have been considering. In addition it happens for squares of words of odd length.

Corollary 2.3 (Odd squares are stable) *If W is a word of odd length, then W^2 is stable.*

Now we can take care of the loose end from the introduction.

Corollary 2.4 *V_3 is contained in the interior of an orbit tile.*

Proof: Figure 2.1 shows that the given word describes a periodic billiard path for the triangle corresponding to V_3. Figure 2.4 below shows that the hexpath corresponding to this word is closed. Hence, the corresponding billiard path is stable. ♠

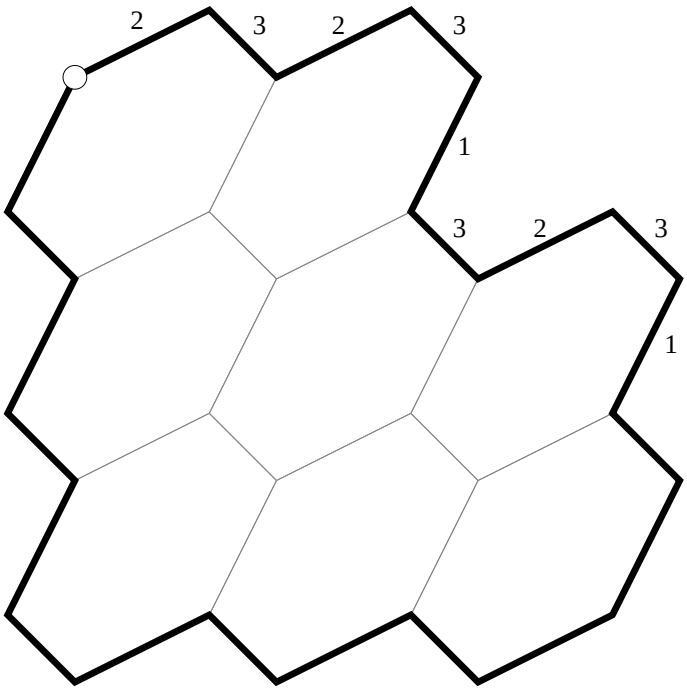

Figure 2.4: The hexpath for $W = 2323132313123232313131$.

2.3 The Squarepath

It turns out that the hexpath $H(W)$ contains precisely the same information as a certain rectilinear path, which we call the *squarepath*. Each vertex of the hexpath has a unique type 3 edge emanating from it. The squarepath is obtained by connecting the midpoints of these type-3 edges together, in order. We denote the squarepath by $\widehat{Q}(W)$. We can also define similar paths based on the edges of type 1 or 2. These paths are somewhat more complicated, though they will be of theoretical importance for us. In practice, however, we will always try to work with the type 3 edges.

If we mark off points on the squarepath at integer steps (starting with a vertex) the resulting points are naturally in bijection with the type 3 edges of the unfolding. In the next section we will elaborate on this bijection. Figure 2.5 shows the squarepath for the examples we have been considering The hexpath is drawn underneath in grey.

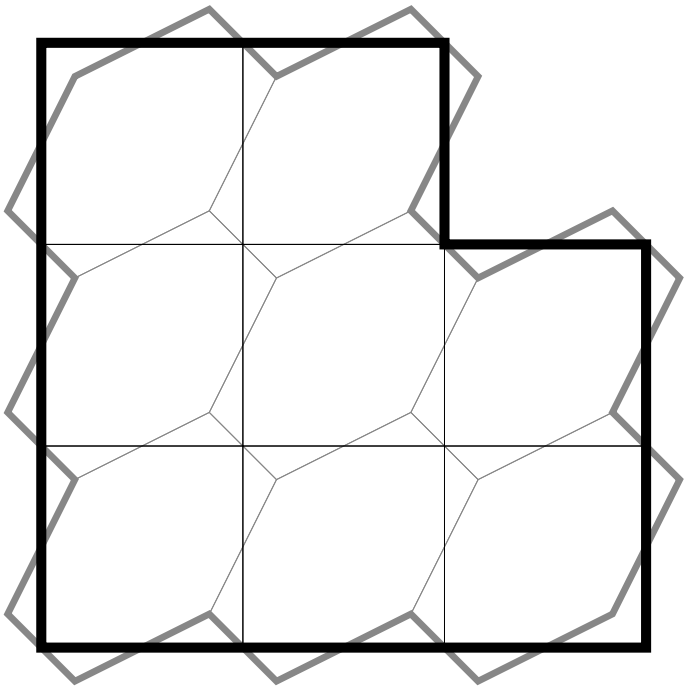

Figure 2.5: $\widehat{Q}_3(W)$ in black and $H(W)$ in grey.

It is possible to reconstruct $H(W)$ from $\widehat{Q}(Q)$, when $\widehat{Q}(W)$ is a closed loop. When $\widehat{Q}(W)$ is embedded, this loop bounds a finite union of squares. We simply replace each square by the associated hexagon. Then $H(W)$ is the boundary of the union of hexagons. In general, $H(W)$ is the union of all the edges of $\mathcal{H}$ which intersect $\widehat{Q}(W)$. There is a natural ordering to these edges, and so the union of all these edges naturally has the structure of a closed loop.

It turns out that there is a simple algorithm for deducing the combinatorics of the unfolding from the squarepath. Say that a *k-dart* is a union of k triangles, arranged around a common vertex, in the pattern shown in Figure 2.6 for $k = 2, 3, 4..$ A k-dart is just an unfolding with respect to either the word $(13)^{k-1}1$ or the word $(23)^{k-1}2$.

Remark: We shall almost always consider darts made from isosceles triangles. Indeed, the idea of grouping the unfolding into darts is mainly a combinatorial trick, and in our applications we might as well perform the trick with respect to unfoldings of isosceles triangles. However, some of our pictures show darts made from triangles that are not quite isosceles.

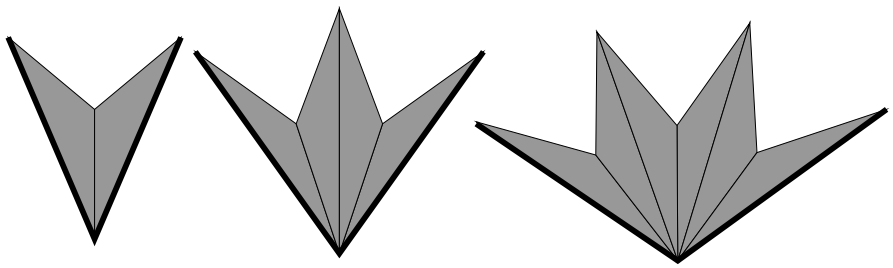

Figure 2.6: k-darts for $k = 1, 2, 3$

We say that the 3-*spine* of the dart is the union of the two outermost long edges. We have highlighted the spines of our darts in Figure 2.6.

The relation of $U(W, *)$ to $\widehat{Q}(W)$ is as follows:

- The maximal darts of the unfolding are in bijection with the edges of the square path. (The maximal k-darts correspond to edges of length $2k$.) The maximal darts are glued together along their 3-spines.
- Two consecutive maximal darts lie on opposite sides of their common 3-edge iff $\widehat{Q}(W)$ makes a northwest or southeast turn at the vertex corresponding to this 3-edge.

To make this work precisely, we need to take the infinite periodic continuation of U, or else identify the first and last sides of U to make an annulus. As it is, the reader needs to take special care in figuring out how the rightmost maximal dart fits together with the leftmost one. We have included a copy of Figure 2.2, except with the spines of the maximal darts drawn in black. See Figure 2.7.

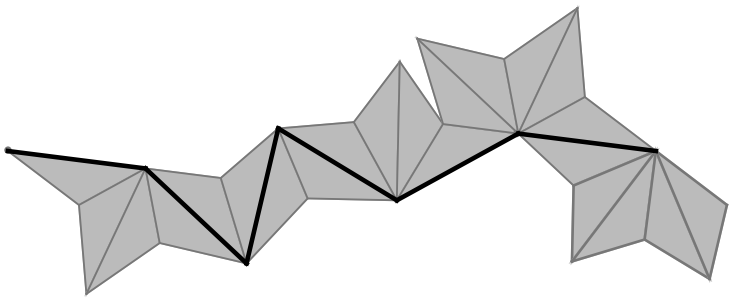

Figure 2.7: Dividing the unfolding into maximal darts.

We have taken a lot of trouble to describe the squarepath and its relation to the hexpath and the unfolding because we plan to specify all our words in terms of their squarepaths. Using the square path gives a very simple description of the word, and lets the reader best see the patterns which arise in our families.

2.4 Edge Labellings

We label each edge of $\mathcal{H}$ by the coordinates of its midpoint. This labelling is canonical, once we decide which point of $\boldsymbol{Z}^2$ gets labeled $(0, 0)$. The *McBilliards convention* is to assign the label $(0, 0)$ to the edge of $H(W)$ corresponding to the last digit of W. This edge is the leftmost edge of the unfolding $U(W, *)$. In Figure 2.8 we have labeled the origin and several nearby points.

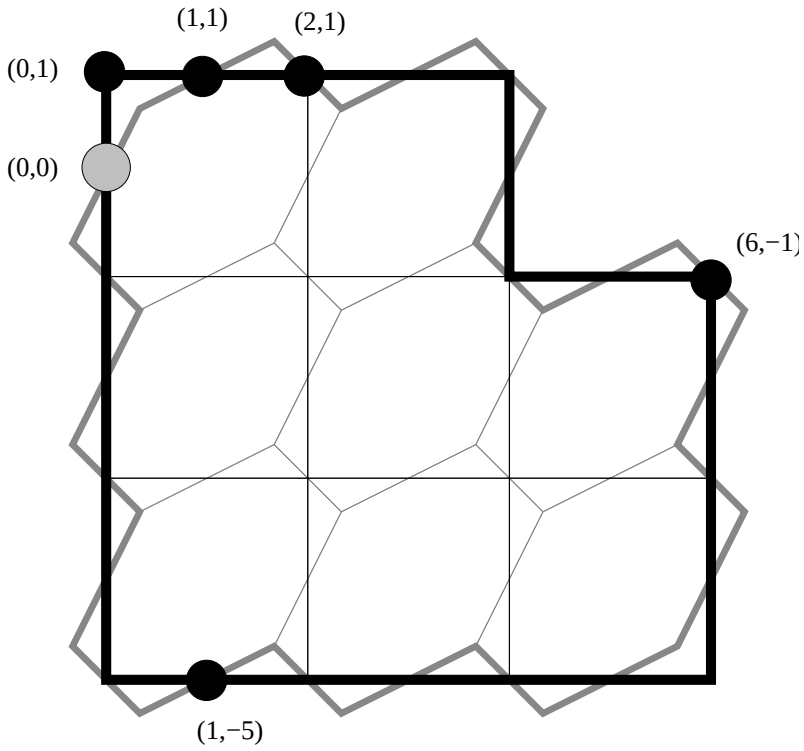

Figure 2.8: Some labellings.

We identify $\widehat{e}$ with its label. Our labelling has a geometric significance. Let $X = (x_1, x_2)$ be a parameter point and let T_X be the corresponding triangle. Let e_1 and e_2 be two edges of the unfolding $U(W, T_X)$. Let $\theta(e_1, e_2)$ be the counterclockwise angle through which we must rotate e_1 so as to produce an edge parallel to e_2. We take θ mod π, so that the orientations of e_1 and e_2 are irrelevant. Then, as is easily established by induction:

$$\theta(e_1, e_2) = X \cdot (\widehat{e}_2 - \widehat{e}_1). \tag{2.1}$$

2.5 Defining Functions

We frequently write

$$E(x) = \exp(i(x)) \tag{2.2}$$

for notational convenience.

Given two points $p, q \in \boldsymbol{R}^2$ we write

$$p \uparrow q; \qquad p \updownarrow q; \qquad p \downarrow q$$

iff the y coordinate respectively is greater than, equal, or less than the y coordinate of q. Suppose that p and q are two vertices of our unfolding. In this section we will give the formula for a function $F = F_{p,q}$ which has the property that $F = 0$ iff $p \updownarrow q$. These *defining functions* are computed purely from the word W. The orbit tile $O(W)$ can be described as the region where the defining functions corresponding to the (a_i, b_j) pairs are all positive. The edges of $O(W)$ is defined in terms of the 0-level sets of the defining functions.

For any $d \in \{1,2,3\}$ there is an infinite, periodic polygonal path made from type-d edges of the infinite periodic continuation of $U(W,T)$. The image of this path in $U(W,T)$ is what we call the *d-spine*. We have already encountered the 3-spine: It is the union of the 3-spines of the maximal darts of $U(W,*)$.

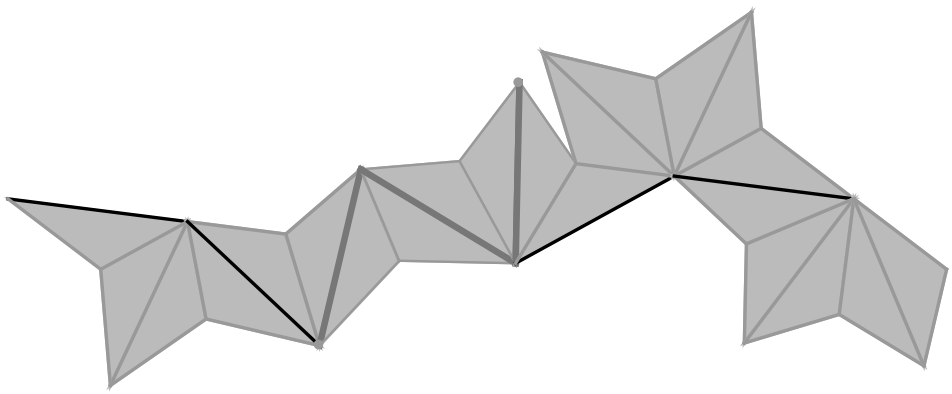

Figure 2.9: A 3-path and the 3-spine.

Let $e_0, ..., e_m$ denote the list of edges, ordered from left to right, which appear in the d-spine. We say that the vertices p and q are *d-connected* if there is a polygonal path of type-d edges connecting p to q. In this case, let $f_0, ..., f_n$ denote these edges, ordered from left to right. We order p and q so that p is the left endpoint of the d-path and q is the right endpoint. The 3 thick grey edges in Figure 2.9 show the 3-path connecting $p = b_4$ to $q = a_6$.

We define

$$P(X) = \pm \sum_{i=0}^{n} (-1)^i E(X \cdot \widehat{f_i}); \qquad Q(X) = \sum_{i=0}^{m} (-1)^i E(X \cdot \widehat{e_i}). \tag{2.3}$$

We will explain the global sign in front of P below. The reason for the general alternation of the signs is explained in [Sch06a]. Our functions have the following geometric interpretation: If we normalize so that the d edges have length 1 and rotate $U(W,T)$ so that the first edge is horizontal, then $\pm P(X)$ is the vector pointing from p to q and $Q(X)$ is the translation vector. Therefore,

$$F := \mathrm{Im}(\pm P\overline{Q}) = 0 \quad \Longleftrightarrow \quad p \updownarrow q. \tag{2.4}$$

For the above example the sign in front of P turns out to be a $(+)$. (See below.) We therefore have

$$P(X) = E(4x_1 - x_2) - E(6x_1 - x_2) + E(6x_1 - 3x_2).$$

$$Q(X) = E(x_2) - E(4x_1 + x_2) + E(4x_1 - x_2) - E(6x_1 - x_2) + E(6x_1 - 5x_2) + E(-5x_2).$$

Here is what we call the *function tableau* for P.

$$\begin{array}{cll} (+) & 4 & -1 \\ & 6 & -1 \\ & 6 & -3 \end{array}$$

When we reconstruct the function from its tableau, we use the convention that the signs of the terms alternate. The $(+)$ of $(-)$ indicates the global sign in front of P.

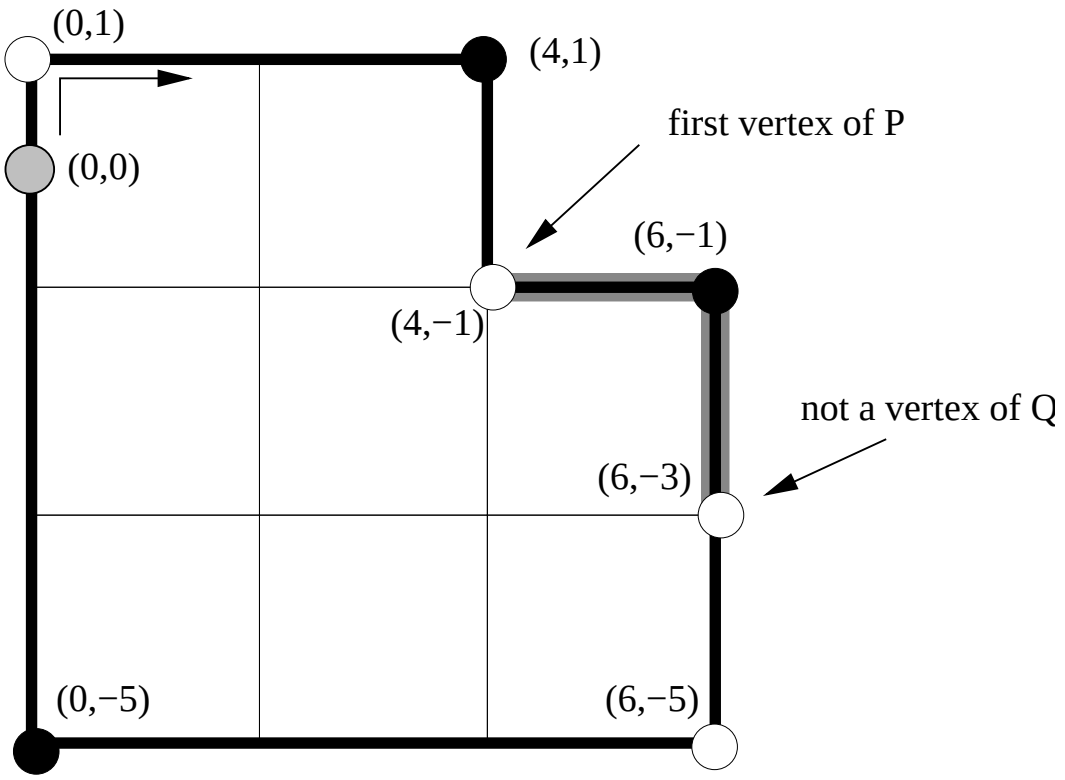

Figure 2.10 The paths $\widehat{P}$ (grey) and $\widehat{Q}$ (black)

When $d = 3$, we can represent both P and Q in terms of the squarepath. First of all, the list of vertices of $\widehat{Q}$ is precisely the function tableau for Q. The situation for P is more involved: The edges of $U(W, *)$ are in canonical bijection with the edges which emanate from the vertices of the hexpath. Say that a 3-edge of $\mathcal{Q}$ is a *starter* if it corresponds to an edge of $U(W, *)$ which is incident to p. Say that a 3-edge of $\mathcal{H}$ is a *finisher* if it corresponds to an edge of $U(W, *)$ which is incident to q. Let $\widehat{P}$ denote the shortest sub-path of $\widehat{Q}_d(W)$ whose initial endpoint is the midpoint of a starter and whose final endpoint is the midpoint of a finisher. Then the function tableau for P is just the list of coordinates of the vertices of $\widehat{P}$. Figure 2.10 shows the paths corresponding to $\widehat{P}$ and $\widehat{Q}$. The origin is marked with a grey dot.

We can interpret the path $\widehat{Q}$ as a function from $\boldsymbol{Z}^2$ to $\boldsymbol{Z}$, as follows. We alternately color the vertices encountered by Q black and white, starting with white. $\widehat{Q}$ assigns the value $x_1 - x_2$ to $X \in \boldsymbol{Z}^2$ if x_1 white vertices of $\widehat{Q}$ coincide with X and if x_2 black vertices of $\widehat{Q}$ coincide with X. We make the same definition for $\widehat{P}$, except that we have to take care whether or not to color the first vertex encountered by $\widehat{P}$ black or white. (See below.) With this interpretation, $\widehat{Q}$ is the Fourier series of Q.

$$Q(X) = \sum_{V \in \boldsymbol{Z}^2} \widehat{Q}(X) E(X \cdot V). \tag{2.5}$$

The same goes for P and $\widehat{P}$.

The Global Sign: This discussion supposes that $F > 0$ if $q \uparrow p$. (As above, p is on

the left.) We also suppose that the initial vertex of $\widehat{P}$ is also a vertex of $\widehat{Q}$. In this case, the sign in front of P is $(-1)^u$, where u is the number of vertices of $\widehat{Q}$ (starting with the first one) which lie before the first vertex of $\widehat{P}$. That is, the initial vertex of $\widehat{P}$ should get the same color whether it is considered a vertex of $\widehat{P}$ or a vertex of $\widehat{Q}$. For example, we can see from Figure 2.10 that $u = 2$ and so the sign is a $(+)$. This rule has a simple geometric proof: When p and q are the first and last vertices of the 3-spine of U, then $P = Q$ and so the sign definitely should be a $(+)$. If we move q along the 3-spine, the sign does not change, by "continuity": Moving either vertex by 1 "click" should produce a nearby value for P. However, moving the p vertex changes the global sign, given the form of Equation 2.3. In general the first vertex of $\widehat{P}$ need not be a vertex of $\widehat{Q}$. This irritating situation does not arise in this paper. McBilliards has a general algorithm which correctly determines the sign in every possible case.

2.6 The Dart Lemma

Figure 2.11 shows a typical dart. We say that the *inferior* vertices of D are the ones which are not adjacent to the 3-spine and not on the 3-spine. The inferior vertices are marked with white dots in Figure 2.11. We call the other vertices of the dart *superior*. In Figure 2.11 the superior vertices are in black or grey and the inferior vertices are in white.

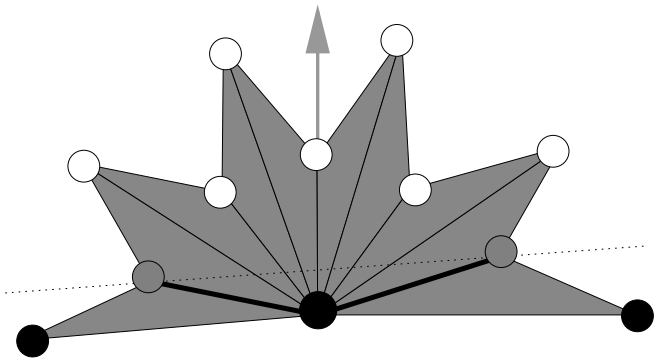

Figure 2.11: An Acute Dart

Recall that the unfolding U can be written as a union of maximal darts. We say that a vertex of U is *inferior* if it is an inferior vertex of one of the maximal darts. Let $\delta(W)$ denote the largest k such that $U(W, *)$ contains a k-dart. Here is the main result of this section:

Lemma 2.5 (Dart) *Let $X = (x_1, x_2)$. Suppose that*

$$\max(x_1, x_2) \leq \frac{2\pi}{\delta(W)}.$$

Suppose also that all the top superior vertices of $U(W, X)$ lie above all the bottom superior vertices of $U(W, X)$. Then $X \in O(W)$.

Remark: There is a more restrictive angle condition that almost immediately guarantees that the maximal darts are acute. This condition is given by

$$\max(x_1, x_2) \leq \frac{\pi}{2\delta(W) - 2}.$$

This is precisely the condition we will use in the proof of Theorem 1.2. Our condition is weaker than this and does not, in itself, guarantee that the maximal darts are acute. However, our weaker condition combines with the second hypothesis of the Dart Lemma to establish the acuteness. See the very end of our proof. We mention this because the discrepancy is likely to otherwise cause confusion.

We will prove the Dart Lemma in several stages. We say that the *base* of a dart is the vertex which is common to all the triangles. The base is denoted by a big black dot in Figure 2.11. We say that the *centerline* of the dart is the ray of bilateral symmetry, emanating from the base. The centerline is indicated by a ray in Figure 2.11. We say that the dart *points up* if the ray points upward, and *points down* if the ray points downward. Let D_V denote the union of outermost edges of D which are not the longest edges. This set is highlighted in Figure 2.11. We say that D is *acute* if D_V makes an acute angle towards the centerline of the dart. Figure 2.11 shows an acute dart.

Lemma 2.6 *If D is an up-pointing acute dart, then each inferior vertex of D lies above some superior vertex. Likewise, if D is down-pointing and acute, then each inferior vertex of D lies above some superior vertex of D.*

Proof: The short edges of D have the same length. Hence the line joining the two superior vertices separates all the inferior vertices from the base. ♠

We call U *controlled* if the following holds for all maximal darts D of U:

- D is acute.
- If the base of D is a bottom vertex of U then U points up
- If the base of D is a top vertex of U then U points down.

Lemma 2.7 *Suppose U is a controlled unfolding. Then the lowest top vertex of U and the highest bottom vertex of U are both superior vertices.*

Proof: We will prove this statement for the top vertices. The proof for the bottom vertices is the same. Let v be an inferior top vertex of U. Then there is some maximal dart D such that v is an inferior vertex of D. Each edge of D, except possibly the edges on the 3-spine, is an edge of reflection of U. Thus, the inferior vertices of D all have the opposite type (top or bottom) from the base. Likewise for the superior vertices of D. Hence, the inferior vertices and the superior vertices of D all have the same type. Since one inferior vertex of D is a top vertex, the base of D is a bottom vertex. Since U is controlled, D points up. Lemma 2.6 now implies that v is higher than one of the superior vertices v' of D. As we already mentioned, v' is also a top vertex of U. Hence, we have found another top vertex, v', which is lower than v. ♠

To finish the proof of the Dart Lemma, we just have to establish that $U = U(W, X)$ is a controlled unfolding. Let D be a maximal dart of U. Assume without loss of generality

that the basepoint of D is a bottom vertex. Each edge of D_V is an edge of reflection of U. Hence the endpoints of D_V are top vertices. All these vertices are superior vertices. Hence, the endpoints of D_V lie above the basepoint of D_V. Our restriction on X guarantees that the angle of D_V is at most 2π. Hence D_V must actually make an acute angle, since both its edges point up. The centerline lies between these two up-pointing edges. Hence D itself is up-pointing. Since D is arbitrary, we see that U is controlled. This completes the proof of the Dart Lemma.

2.7 Pseudo-Parallel Families

Suppose that e is an edge of the unfolding $U(W, *)$. When $U(W, X)$ is rotated so that it has horizontal holonomy, the line containing e is parallel to the complex number

$$E(\widehat{e} \cdot X)U_Q(X). \tag{2.6}$$

We say that the edges $\{e_0, ..., e_n\}$ form a *pseudo-parallel family* relative to the point X_0 if the dot product $e_j \cdot X_0$ is independent of j. In this case, the edges $e_0, ..., e_n$ are all parallel in $U(W, X_0)$. We assume that these edges have negative slope in $U(W, X_0)$. The points $\widehat{e}_0, ..., \widehat{e}_n$ must lie on a line segment in $\boldsymbol{R}^2$. In our examples in this paper, the line in question always has slope -1 because X_0 lies on the isosceles line. We order our edges so that $\widehat{e}_0, ..., \widehat{e}_n$ appear in order on the line.

Let $R'(e_j)$ denote the region in parameter space such that e_j has negative slope in the unfolding. Let $R(e_j)$ denote the path connected component of $R'(e_j)$ which contains X_0.

Lemma 2.8 (Convex Hull) *$R(e_0) \cap R(e_n) \subset R(e_j)$ for all j.*

Proof: We think of $\{X_t\}$ as a path in $R(e_0) \cap R(e_n)$ which connects X_0 to some other point X_1. Let S^1 denote the unit complex numbers and let $E : \boldsymbol{R} \to S^1$ be the universal covering map. For each object $z \in S^1$ we let $\widetilde{z}$ denote the lift to $\boldsymbol{R}$, so that $E(\widetilde{z}) = z$. In particular, we define

$$U(t) = U_Q(X_t); \qquad \widetilde{E}(t) = \widehat{e}_j \cdot X_t; \qquad E_j(t) = E(\widehat{x}_j \cdot X_t).$$

Let $\widetilde{I}_t \subset \boldsymbol{R}$ be the interval whose endpoints are $E_0(t)$ and $E_n(t)$. By convexity $\widetilde{E}_j(t) \subset \widetilde{I}_t$ for all t. The edges $e_0(t)$ and $e_n(t)$ have negative slope for all t. Hence $\widetilde{I}_t$ has length less than $\pi/2$ for any $t \in [0, 1]$. Hence $E_t(j)$ lies in the arc I_t, which has length less than $\pi/2$. If we rotate S^1 so that $U(t) = 1$ then the endpoints of I_t, namely $E_0(t)$ and $E_j(t)$, are both contained in the same negative quadrant of $\boldsymbol{R}^2$. (Either $(-+)$ or $(+-)$.) Hence I_t is contained in one of the negative quadrants. Hence $E_j(t)$ is also contained in one of these quadrants. That is, e_j has negative slope for any parameter value t. ♠

3 Proof of Theorem 1.2

Our proof of Theorem 1.2 is based on the 2 parameter family $Y_{m,n}$ of odd-length words.

$$Y_{n,m} = 1(W_n)^m 32; \qquad W_n = (31)^{n-1}(32)^{n-1} \tag{3.1}$$

Figure 1.4 of the introduction shows the orbit tiles for some of the words $Y_{n,m}$. The family W_n, which we call the *unstable family*, describes unstable periodic billiard paths in certain isosceles triangles of interest. The square words $Y_{m,n}^2$ are stable by Corollary 2.3. Theorem 1.2 is therefore a consequence of the following result.

Theorem 3.1 *For every integer $n \geq 2$ and real number x so that $\frac{\pi}{2n+2} < x < \frac{\pi}{2n}$, there is a periodic billiard path in T_x with combinatorial type $Y_{n,m}$ for some $m \in \mathbf{N}$.*

Here T_x denote the obtuse isosceles triangle corresponding to the point (x, x) in the plane. The two small angles of T_x have measure x-radians.

3.1 The Unstable Family

Proposition 3.2 *W_n describes a periodic billiard path in T_x for all $x < \frac{\pi}{2n-2}$.*

Proof: The unfolding for the word W_n consists of two maximal $n-1$ darts. Given our bounds on x, we satisfy the hypotheses given in the remark immediately following the statement of the Dart Lemma. Thus, it suffices to consider the superior vertices of the unfolding. There are 4 superior top vertices, labelled A, B, C, D. Likewise, there are 4 superior bottom vertices, labelled E, F, G, H. See Figure 3.1. Thus, by the Dart Lemma, it suffices to show that $X \uparrow Y$ for each $X \in \{A, B, C, D\}$ and $Y \in \{E, F, G, H\}$. We normalize coordinates so that $A = (0, 0)$, and the long side has length one. Then, we can compute the coordinates for the 3-spine.

$$E = (\sin(n-1)x, -\cos(n-1)x). \quad D = (2\sin(n-1)x, 0). \quad H = (3\sin(n-1)x, -\cos(n-1)x).$$

With this choice, the unfolding is horizontal as desired. (That is, $A \updownarrow D$.)

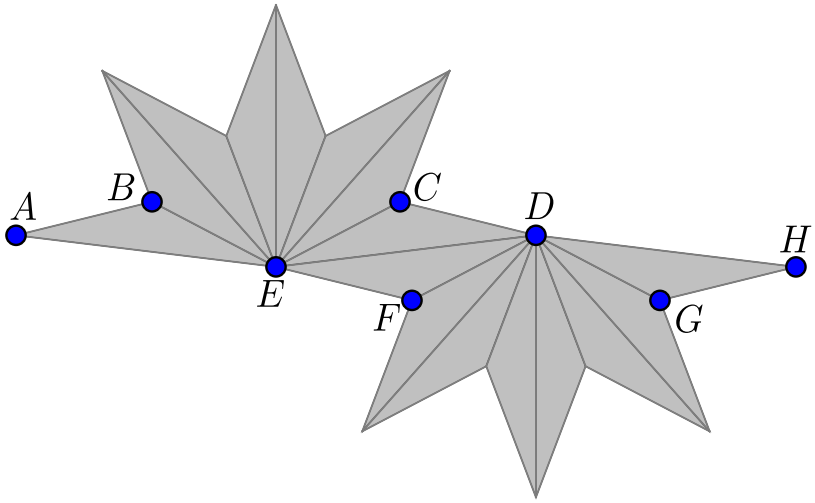

Figure 3.1: An unfolding for the word W_5. One period is shown, which begins at edge $\overline{AE}$ and ends at the parallel edge $\overline{DH}$.

By symmetry, each point has a partner-point at the same height:

$$A \updownarrow D \quad B \updownarrow C \quad E \updownarrow H \quad F \updownarrow G$$

Thus, it is sufficient to concentrate on the central rhombus, $CDFE$. Given a vector $\mathbf{v} \in \boldsymbol{R}^2$, we use $d(\mathbf{v})$ to denote the angle of the vector made with the horizontal. It is sufficient to check that the four vectors $\overrightarrow{EC}$, $\overrightarrow{ED}$, $\overrightarrow{FC}$, and $\overrightarrow{FD}$ point upward. That is, for $\mathbf{v}$ equal each of those four vectors, we must have $0 < d(\mathbf{v}) < \pi$. We compute

$$d(\overrightarrow{FC}) = d(\overrightarrow{EC}) = \frac{\pi}{2} - (n-2)x \quad d(\overrightarrow{ED}) = \frac{\pi}{2} - (n-1)x \quad d(\overrightarrow{FC}) = \pi - (n-1)x$$

In all cases, we have $0 < d(\mathbf{v}) < \pi$ for $0 < x < \frac{\pi}{2n-2}$. ♠

3.2 The stable family $Y_{n,m}$

The word $Y_{n,m}$ has an additional special symmetry. If you write $Y_{n,m}$ in reverse and swap the letters 1 and 2, you get $Y_{n,m}$ back. Given a word W, let $\widehat{W}$ denote W written in reverse with 1 swapped with 2. There is some word $W = W_{m,n}$ such that

$$Y_{m,n} = 1W3\widehat{W}2, \tag{3.2}$$

Remark: It is a consequence of work in [Hoo07] that every stable periodic billiard path in an isosceles triangle has an combinatorial type W with the symmetry $\widehat{W} = W$. This fact, however, is not necessary for our proof here.

We now record some special properties of words having the form given by the right hand side of Equation 3.2.

Proposition 3.3 *Let Y be a word of the form $Y = 1W3\widehat{W}2$, and T be an obtuse isosceles triangle. Consider the unfolding $U(Y^2, T)$ chosen so that the translation bringing the first edge to the last is horizontal. Then the long edge (edge 3) of the first triangle in the unfolding is horizontal.*

Proof: Consider the bi-infinite repeating word $\overline{Y}$. This word has some symmetry, which is revealed by expanding the word out.

$$\overline{Y} = \ldots 1W3\widehat{W}\ 21W3\widehat{W}2 \ \Big|\ 1W3\widehat{W}\ 21W3\widehat{W}$$

Reflection in the vertical line above swaps the letters 1 and 2 while preserving 3. This is precisely how the reflective symmetry of the isosceles triangles permutes the labeling of the sides. Thus, this symmetry extends to the bi-infinite unfolding $U(\overline{Y}, T)$. The direction of the holonomy of $U(Y^2, T)$ must be the eigenvector corresponding to eigenvalue -1 of the reflective symmetry of $U(\overline{Y}, T)$. But this reflection is just the reflective symmetry of the first triangle in the unfolding. So these two directions are parallel. ♠

We will use the following principle for detecting our billiard path. Recall that side 3 denotes the long side of an isosceles triangle.

Proposition 3.4 *Suppose that a billiard path in an obtuse isosceles triangle starts out parallel to side 3, and has initial combinatorial type $1W3$, where the final 3 corresponds to an edge which the path hits at the midpoint, M. Then the billiard path is closed and has combinatorial type $1W3\widehat{W}2$.*

See Figure 3.2 for a case when this proposition applies.

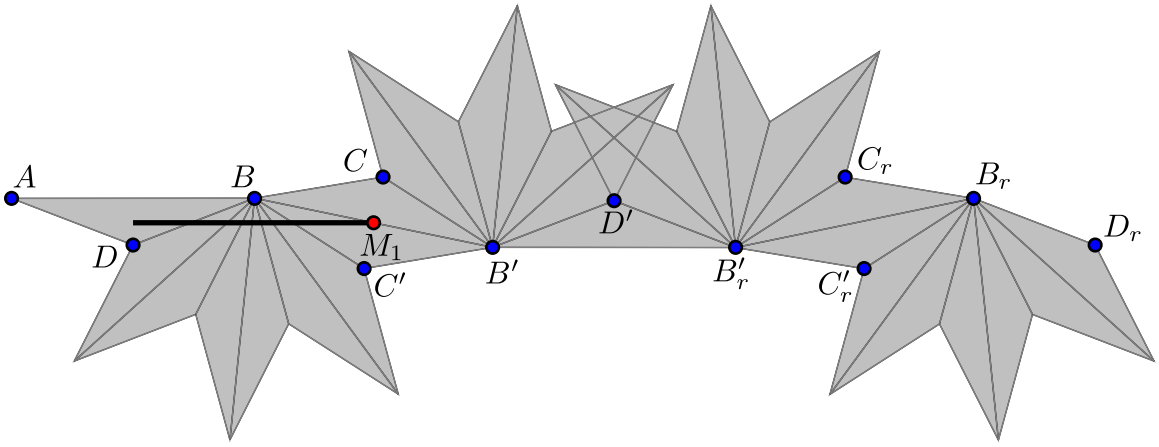

Figure 3.2: An unfolding for the square of the word $Y_{4,1}$.

Proof: The trajectory t_1 described in the proposition lies within the unfolding of the initial word $1W3$ and then hits M. The unfolding for the word $1W3\widehat{W}2$ has 180 degree rotational symmetry ϕ around the point M. Thus, the longer trajectory $t_2 = t_1 \cup \phi(t_1)$ lies within the unfolding of $1W3\widehat{W}2$. Now consider the unfolding of the even length word $(1W3\widehat{W}2)^2$. This unfolding has vertical reflective symmetry ρ which swaps the two halves of the word. (It is vertical assuming the trajectory is horizontal.) The trajectory $t_3 = t_2 \cup \rho(t_2)$ lies within the unfolding of $1W3\widehat{W}2$. ♠

We will break the proof of Theorem 3.1 into two cases. The first case is easiest.

Lemma 3.5 *For each x satisfying $\frac{\pi}{2n+1} \leq x < \frac{\pi}{2n}$ there is a periodic billiard path in T_x with combinatorial type $Y_{n,1}$.*

Proof: Given the triangle T_x, unfold the triangle according to the square of the word $Y_{n,1}$ as in Figure 3.2. Let M_1 be the midpoint we must hit. This is the first midpoint of a long side which is the fixed point of a 180 degree rotational symmetry of the the bi-infinite unfolding, $U(\overline{Y_{n,1}}, T_x)$.

We coordinatize the unfolding so that M_1 is given coordinates $(0, 0)$. We will show that all the top vertices have positive y-coordinate, and all the bottom vertices have negative y-coordinate. Regardless of n, the Dart Lemma tells us that most of the vertices are irrelevant. It is enough to prove this statement for those vertices, who are given names in Figure 3.2. We have named four vertices A, B, C and D. The other vertices are either images of these under the rotational symmetry about M_1 (denoted by $*'$), images under reflection in the

vertical line through D' (denoted by $*_r$), or images under the composition. So, it is enough to show that the statement is true for the vertices A, B, C and D.

The points A and B have the same y-coordinate by Proposition 3.3. M_1 lies below them, because angle $\angle ABM_1 = 2nx < \pi$. Also angle $\angle ABC = (2n+1)x \geq \pi$, so C has y-coordinate greater than or equal to the y-coordinates of A and B. Finally, M_1 lies closer to B then D. Furthermore, the vector $\overrightarrow{BM_1}$ is closer to horizontal than the vector $\overrightarrow{DB}$. ($\angle DBA = x = \angle M_1BC$, but the horizontal direction lies strictly between the directions of $\overrightarrow{BM_1}$ and $\overrightarrow{BC}$.) Thus the y-coordinate of D must be negative. ♠

Remark: The words $Y_{n,1}$ are the same as the words A_{n-1}, which appear in Figure 1.1 and play a prominent role in Theorem 1.3.

The second case is more complicated. While we could give a constructive proof, as above, we find that a non-constructive proof clarifies the situation. To illustrate this case, we consider the word $Y_{4,2}$ and the triangle T in Figure 3.3. The unfolding $U(Y_{4,2}, T)$ depicted in this Figure contains a horizontal segment joining the first triangle to the midpoint of the long side. This segment hits the sequence of sides $1(31)^4(32)^4 3$. Let $W = (31)^4(32)^4$. By Proposition 3.4, there is a periodic billiard path in T with combinatorial type $Y_{4,2} = 1W3\widehat{W}2$. The significant point is that by Proposition 3.4, we only need to consider the unfolding for an initial subword.

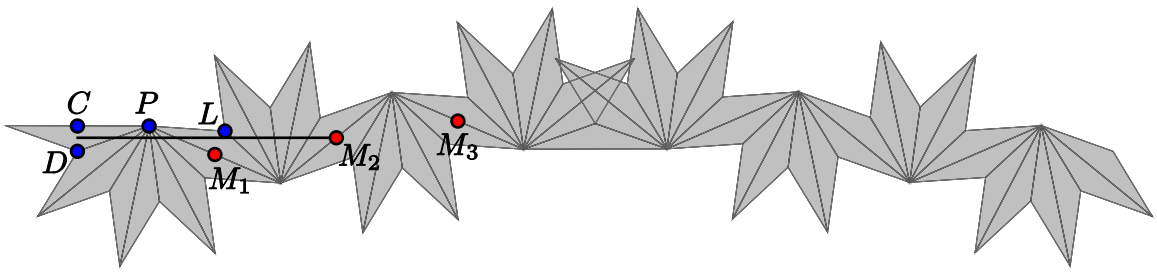

Figure 3.3: An unfolding of the square of the word $Y_{4,2}$.

Lemma 3.6 *For each x with $\frac{\pi}{2n+2} < x < \frac{\pi}{2n+1}$, there is a periodic billiard path in T_x with combinatorial type $Y_{n,m}$ for some $m \in \mathbf{N}$.*

Proof: Consider the unfolding of T_x according to the infinite word $1(W_n)^\infty$. See Figure 3.4. We normalize the unfolding so that the initial long side of T_x is horizontal.

We will show that there is some index m such that M_m lies below all preceding top vertices and above all preceding bottom vertices. Here the points $M_0, M_1, ...$ are the midpoints of some of the long segments. See Figure 3.4.

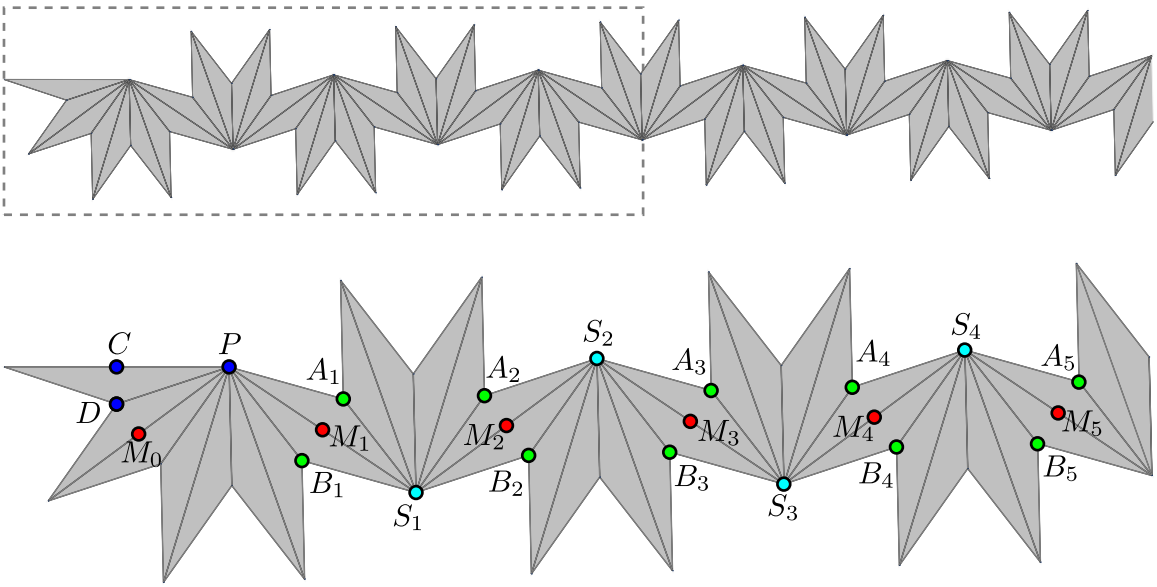

Figure 3.4: The top figure shows an unfolding for the word $1(W_4)^\infty$. The bottom figure shows a blow up of the unfolding with names of important vertices labeled.

Many of the vertices in Figure 3.4 are given names. The unlabelled vertices are inferior, and may be ignored by the Dart Lemma. Understanding this unfolding is made much easier by the fact that W_n is the combinatorial type of a periodic billiard path in T_x. See Proposition 3.2. We consider the vector $\mathbf{v} = \overrightarrow{M_1M_2}$. This vector points in the direction $(n+1)x - \frac{\pi}{2}$ (measured relative to the horizontal in polar coordinates). In particular, $\mathbf{v}$ has positive y-coordinate, since $x > \frac{\pi}{2n+2}$. To compute this direction, note that $\overrightarrow{S_1M_1}$ points in the direction $2nx$ and $\overrightarrow{S_1M_2}$ points in direction $2x$. We always normalize so that the long side has length 1. This gives us the formula

$$\mathbf{v} = \frac{1}{2}(\cos 2x, \sin 2x) - \frac{1}{2}(\cos 2nx, \sin 2nx).$$

Now we will eliminate some top vertices. The vector $\overrightarrow{PA_1}$ points in direction $\pi + 2nx < 2\pi$. So $A_1 \downarrow P$. Also $\overrightarrow{A_1A_k}$ is parallel to $\mathbf{v}$ for $k > 1$, so $A_1 \downarrow A_k$. And $\overrightarrow{A_{2k}S_{2k}}$ points in direction x, so $A_{2k} \downarrow S_{2k}$. It follows that A_1 has the least y-coordinate of any vertex in the unfolding $1(W_n)^\infty$.

Now we will eliminate some bottom vertices. $\overrightarrow{B_kB_{k+1}}$ points in the same direction as $\mathbf{v}$, so $B_{k+1} \uparrow B_k$. The vector $\overrightarrow{B_{2k+1}S_{2k+1}}$ points in direction $(2n+1)x - \pi < 0$, so $B_{2k+1} \uparrow S_{2k+1}$. It follows that the bottom vertex with greatest y-coordinate in the unfolding up to the appearance of M_m is either D or B_m. (We ignore the fact that when m is even B_m appears later in the unfolding than M_m.)

Letting P_y denote the y-coordinate of an arbitrary point P, we want to show that

$$(M_m)_y > (B_m)_y; \qquad D_y < (M_m)_y < (A_1)_y,$$

for some m. When m is even, $\overrightarrow{B_mM_m}$ points in the direction $2x + \frac{\pi}{2}$, so $M_m \uparrow B_m$. When m is odd, $\overrightarrow{B_mM_m}$ points in the direction $2nx - \frac{\pi}{2}$. So, for any choice of m, the first inequality

holds. The first endpoint M_0 lies below D since $\overrightarrow{M_0D}$ points in the direction $2x + \frac{\pi}{2}$. Let

$$f(x) = (A_1)_y - D_y. \qquad g(x) = (M_{i+1})_y - (M_i)_y. \tag{3.3}$$

Here $g(x)$ is independent of i. We compute

$$g(x) = \frac{1}{2}(\sin 2x - \sin 2nx); \qquad f(x) = \frac{1}{2\cos x}(\sin x - \sin(2n+1)x). \tag{3.4}$$

The formula for f follows from the fact that the length of the short side is $\frac{1}{2\cos x}$, and $\overrightarrow{PD}$ and $\overrightarrow{PA_1}$ point in directions $\pi + x$ and $\pi + (2n+1)x$ respectively.

A sufficient criterion for the second equation is that $g(x) < f(x)$. That this is true follows from some trigonometry. First we reduce $f(x)$ and $g(x)$ to more convenient forms.

$$\cos(x)f(x) = -\sin nx \cos(n+1)x \quad \text{and} \quad g(x) = -\sin(n-1)x \cos(n+1)x. \tag{3.5}$$

Thus,

$$\frac{f(x)}{g(x)} = \frac{\sin nx}{\cos x \sin(n-1)x} > \frac{1}{\cos x} > 1.$$

This completes the proof. ♠

4 Proof of Theorem 1.3

4.1 The A Family

Here we introduce the words $\{A_n\}$ for $n \geq 2$. These words already appear in [HH00], and their analysis is quite easy. A_n is the square of a word of odd length. Listing out the first few words explicitly and then writing the general pattern, we have:

$$A_2 = (2323131)^2; \quad A_3 = (23232313131)^2; \quad A_n = ((23)^n(13)^{n-1}1)^2 \tag{4.1}$$

The squarepath $\widehat{Q}(A_n)$ is a square of sidelength $2n$. Hence $U(A_n, *)$ is the union of 4 maximal n-darts. The 3-spine for $U(A_n, V_n)$ is contained in a straight line. There are two top vertices on this straight line and two bottom vertices. The top vertices are a_1 and a_2. The bottom vertices are b_{2n} and b_{2n+1}. Figures 4.1, 4.2, and 4.3 show the first few examples.

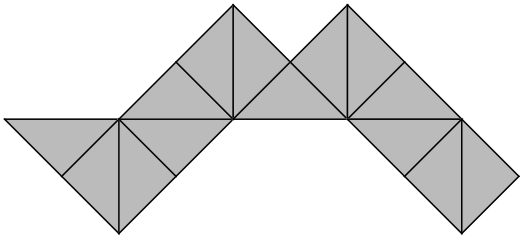

Figure 4.1 $U(A_2, V_2)$.

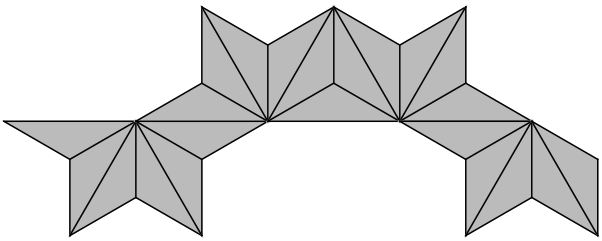

Figure 4.2 $U(A_3, V_3)$.

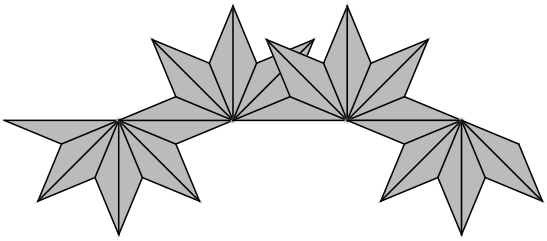

Figure 4.3 $U(A_4, V_4)$.

If X is a parameter point sufficiently close to V_n then the lowest top vertices of $U(A_n, X)$ remain a_1 and a_2 and the highest bottom vertices remain b_{2n} and b_{2n+1}. When $X \in N_{--}(n, \epsilon)$ the 3-spine for $U(A_n, X)$ is no longer a straight line segment, but rather makes a zig-zag. Both obtuse angles in the unfolding are slightly smaller, and this causes the 3 spine to make an acute angle in the directions of the centerlines of the maximal darts, as shown in Figures 4.4 and 4.5.

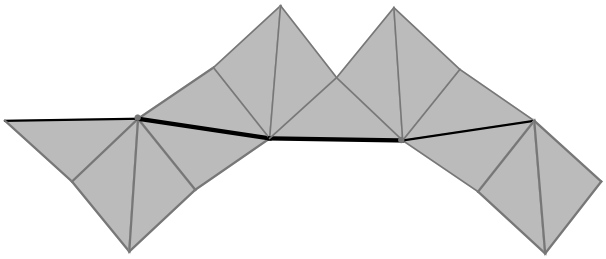

Figure 4.4: $U(A_2, X)$ for $X \in N_{--}$

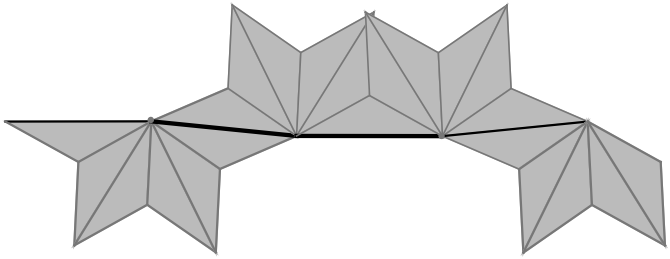

Figure 4.5 $U(A_3, X)$ for $X \in N_{--}$.

From this geometric picture we see easily that the a_1 and a_2 lie above b_{2n} and b_{2n+1} for points in $N_{--}(n, \epsilon_n)$.

As an alternate argument we note that, since A_n is an odd square, the unfolding $U(A_n, *)$ has glide-reflection symmetry. Thus, if a_i is the lowest top vertex then b_{2n+i-1} is the highest bottom vertex. Thus, it suffices to show that $a_1 \uparrow b_{2n}$ and $a_2 \uparrow b_{2n+1}$. We compute the defining function F for (a_1, b_{2n}) and find that

$$F(x_1, x_2) = -4\sin^2(nx)\sin(2nx). \tag{4.2}$$

For (x_1, x_2) near $V_n = (\pi/2n, \pi/2n)$, the above expression is negative iff $x_2 < \pi/2n$. That is, $a_1 \uparrow b_{2n}$ iff $x_2 < \pi/2n$ and x_2 is sufficiently close to $\pi/2n$. The calculation for the pair (a_2, b_{2n+1}) yields the same result, but with x_1 and x_2 interchanged.

This takes care of the first statement of Theorem 1.3.

4.2 The B Family

We will show that

$$N_{-+}(n, \epsilon_n) \subset O(B_n); \qquad n = 4, 5, 6... \tag{4.3}$$

By symmetry,

$$N_{+-}(n, \epsilon_n) \subset O(C_n); \qquad n = 4, 5, 6... \tag{4.4}$$

Our argument will show that the two segments bounding $N_{--}(n, \epsilon_n)$ (except for V_n itself) are respectively contained in $O(B_n)$ and $O(C_n)$. This takes care of the fourth statement of Theorem 1.3.

The word B_n has length $40n - 60$. This word is determined by its squarepath $\widehat{Q}_n := \widehat{Q}(B_n)$, which we now describe. We will draw $\widehat{Q}_4$ and $\widehat{Q}_5$, with the understanding that $\widehat{Q}_{n+1}$ is obtained from $\widehat{Q}_n$ by lengthening each edge by 2 units. The small grey squares in Figure 4.6 have edgelength 2. We have drawn some of the edges in grey to help the reader parse the loops. These loops are homeomorphic to figure 8 curves. The grey dot indicates the origin.

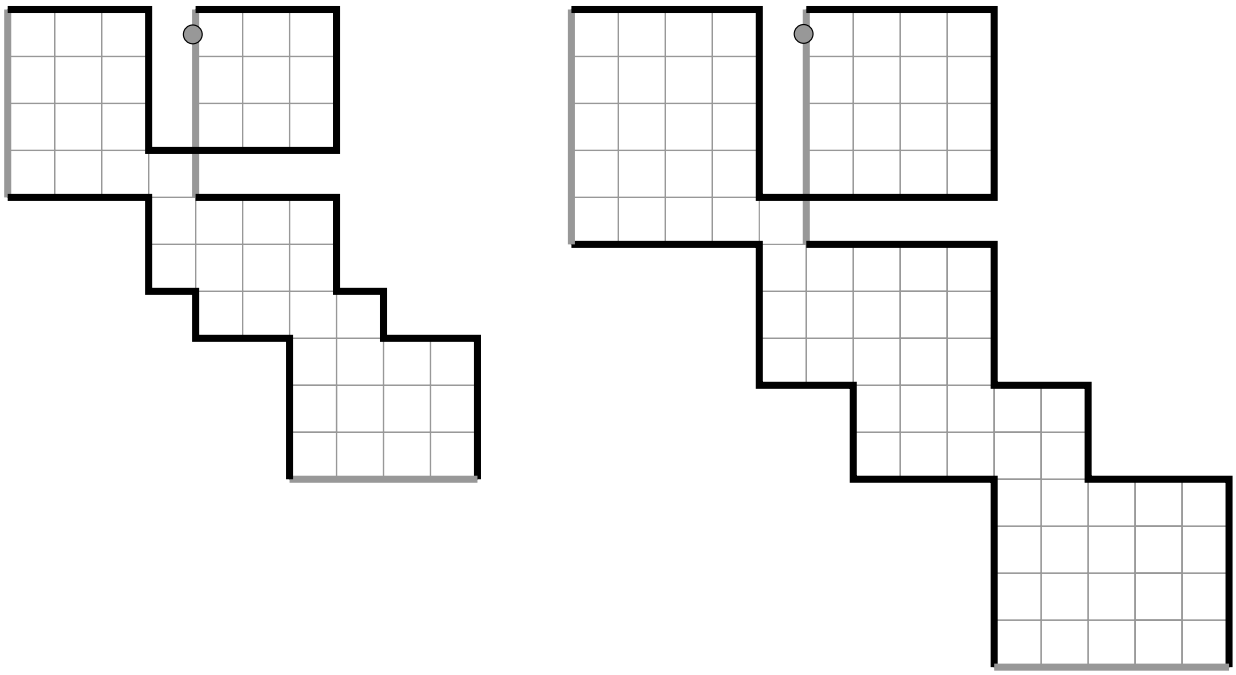

Figure 4.6: $\widehat{Q}_n$ for $n = 4, 5$.

The shortest unfolding $U(B_4, V_4)$ has 100 triangles in it. Here it is. We have highlighted the 3-spine.

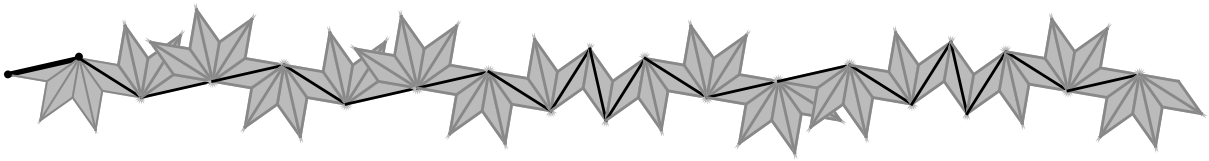

Figure 4.7: $U(B_4, V_4)$.

Equation 4.5 shows three lists. The list L_j is the list of jth coordinates of the successive vertices of the squarepath. The list L computes either $L_1 + L_2 \bmod 4n$ or $L_1 + L_2 + 2n \bmod 4n$ depending on the parity of the vertex.

$\mathbf{L}:$	$\mathbf{L_1}:$	$\mathbf{L_2}:$
1	$0n+0$	$0n+1$
-1	$2n-2$	$0n+1$
1	$2n-2$	$-2n+3$
1	$0n-2$	$-2n+3$
-1	$0n-2$	$0n+1$
1	$-2n+0$	$0n+1$
1	$-2n+0$	$-2n+1$
-1	$0n-2$	$-2n+1$
3	$0n-2$	$-4n+5$
-3	$2n-8$	$-4n+5$
3	$2n-8$	$-6n+11$
-1	$4n-12$	$-6n+11$
1	$4n-12$	$-8n+13$
1	$6n-12$	$-8n+13$
-1	$6n-12$	$-6n+11$
3	$4n-8$	$-6n+11$
-3	$4n-8$	$-4n+5$
3	$2n-2$	$-4n+5$
-1	$2n-2$	$-2n+1$
1	$0n+0$	$-2n+1$

(4.5)

Let

$$\omega_n = E(\frac{\pi}{2n}).; \qquad E(x) = \exp(ix). \tag{4.6}$$

We will often write $\omega = \omega_n$ when the dependence on n is clear. The holonomy of $U(B_n, V_n)$ is obtained as the alternating sum of the vertices of $\widehat{Q}$. Since we are evaluating this sum at V_n, each vertex contributes some power of ω to the sum. The list L above tells us which power. In deriving this list, we used the relation $\omega^{a+2n} = -\omega^a$. Note that L is independent of n. We have:

$$Q(V_n) = \sum_{i=1}^{20} \omega^{L(i)} = 8\omega + 4\omega^3 + 6\omega^{-1} + 2\omega^{-3}. \tag{4.7}$$

This agrees with the McBilliards Calculations. An easy calculus argument shows that $Q(V_n)$ lies between 1 and ω on the unit circle.

4.3 Reducing to Six Vertices

Any point X sufficiently near V_n satisfies the hypothesis of the Dart Lemma with respect to B_n. Hence, we just have to show that all the top superior vertices of $U(B_n, X)$ lie above all the bottom superior vertices of $U(B_n, X)$ for $X \in N_{-+}(n, \epsilon)$ when ϵ is sufficiently small. In this section we will reduce this problem to checking 6 superior vertices.

Since U_n decomposes into 20 maximal darts, there are at most 80 superior vertices, independent of n. Each maximal dart has 2 (O)uter superior vertices and 2 (I)nner superior vertices. The outer superior vertices lie on the 3-spine and the inner superior vertices do not.

The superior vertices in each maximal dart are naturally ordered from left to right. There are two superior vertices on the (L)eft and two on the (R)ight. We denote the 4 superior vertices of the Kth maximal dart (perhaps redundantly) by

$$(K, L, O); \quad (K, L, I); \quad (K, R, I); \quad (K, R, O). \tag{4.8}$$

Sometimes we will decorate our notation with an asterisk to indicate whether it is a top vertex $(\ )^*$ or a bottom vertex $(\ )_*$.

A *leader* is either a lowest top vertex or a highest bottom vertex. Here is the main result of this section:

Lemma 4.1 *For each n, the leaders of $U(B_n, V_n)$ are*

$$(1, L, I)_*; \quad (4, L, O)_*; \quad (16, L, I)_* \quad (5, R, I)^*; \quad (10, R, I)^*; \quad (12, R, O)^*.$$

Moreover, these points all have the same height.

Any top superior vertex a_2 which is not on our list should lie above $b_1 = (1, L, I)_*$. We will symbolically compute

$$F(V_n) = \mathrm{Im}(P(V_n)\overline{Q}(V_n))$$

for such pairs and show that the imaginary part of this function is positive. Hence $a_2 \uparrow b_1$. Likewise, if b_2 is a bottom superior vertex not on the list, we will show that $F(V_n) < 0$ where F is the function corresponding to (b_1, b_2). Finally we will show that the $P(V_n)$ is a real multiple of $Q(V_n)$ when P is defined relative to the pair (b_1, c) and c is on the list given in Lemma 4.1. The key to our calculations is a slick procedure for computing these points.

In computing our points we will slightly modify the method described in §2, so as to use the 3-spine as much as possible. Unfortunately, it is not possible to directly connect all the points of interest to us by a 3-path. The work-around we explain below works for every point except for $a_1 = (1, L, O)^*$, which we easily observe to lie above the points listed in Lemma 4.1. (The edge connecting $(1, L, O)$ to $(1, L, I)$ has negative slope.) For the rest of the superior vertices we do the following:

- Connect $(1, L, I)_*$ to $(1, L, O)^*$ using the common edge e_0.
- Connect $(I, L, O)_*$ to a point p' on the 3-spine which is adjacent to p, using the fewest number of edges $e_1, ..., e_s$ from the 3-spine.
- Connect p' to p by the edge e_{s+1} which is incident to both vertices.

Once p' is determined, there are either 2 or 3 choices for p. To use an analogy, the 3-spine is like the highway and the other edges we use are like the off and on ramps. Our first step is to get onto the highway using e_0. Then we drive along the highway using $e_1, ..., e_s$. At this point we can either take one of the off-ramps and stop the car or else go one more mile and stop the car, depending on our final destination. Figure 4.8 shows a fairly accurate picture for $s = 2$. The dotted lines indicated some of the triangles in the unfolding.

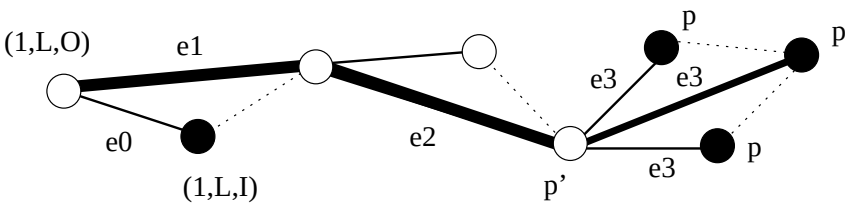

Figure 4.8: The Connecting Path

We normalize so that the type 3 (long) edges of our triangles have length 1. It follows from the Law of Sines that the short sides have length

$$\lambda = \frac{1}{\omega + \omega^{-1}}. \tag{4.9}$$

The vector that points from $(1, L, I)_*$ to p is

$$P(s, \delta) = -\lambda + \sum_{i=1}^{s} \omega^{L(i)} + \lambda^{|\delta|}\omega^{L(s+1)+\delta}. \tag{4.10}$$

Referring to Figure 4.8,, the number δ is -1 (bottom) or 0 (middle) or 1 (top) depending on which of the three choices we make for e_{s+1}. Here L refers to the labeling in Equation 4.5.

To demonstrate Equation 4.10, we note that the three paths suggested by Figure 4.8 lead to the three sums

$$-\lambda + \omega + \omega^{-1} + \lambda\omega^0; \qquad -\lambda + \omega + \omega^{-1} + \omega; \qquad -\lambda + \omega + \omega^{-1} + \lambda\omega^2.$$

Let's concentrate on the right sum. We will use the notation $x \to y$ to denote that $\mathrm{Im}(x)$ and $\mathrm{Im}(y)$ are positive multiples of each other. Our middle expression simplifies to

$$P = \frac{1 + \omega^2 + 2\omega^4}{\omega(1 + \omega^2)}.$$

Recalling our formula for the holonomy, we compute that

$$P\overline{Q} = \begin{bmatrix} 0 \\ 4 \\ 8 \\ 14 \\ 10 \\ 4 \\ 0 \end{bmatrix} \cdot \begin{bmatrix} \omega^{-6} \\ \omega^{-4} \\ \omega^{-2} \\ \omega^0 \\ \omega^2 \\ \omega^4 \\ \omega^6 \end{bmatrix} \to \begin{bmatrix} 10-8 \\ 4-4 \\ 0 \end{bmatrix} \cdot \begin{bmatrix} \omega^2 \\ \omega^4 \\ \omega^6 \end{bmatrix} = \begin{bmatrix} 2 \\ 0 \\ 0 \end{bmatrix} \cdot \begin{bmatrix} \omega^2 \\ \omega^4 \\ \omega^6 \end{bmatrix} \to \begin{bmatrix} 2 \\ 0 \\ 0 \end{bmatrix} \cdot \begin{bmatrix} \sin(1\pi/n) \\ \sin(2\pi/n) \\ \sin(3\pi/n) \end{bmatrix}.$$

Hence $\mathrm{Im}(F(V_n)) > 0$. The point of U_n corresponding to the third sum above is $(3, R, I)^*$, and this shows that $(3, R, I)^* \uparrow (1, L, I)_*$. It turns out that our sums always lead to the general expression

$$\begin{bmatrix} c_{-6} \\ c_{-4} \\ c_{-2} \\ c_0 \\ c_2 \\ c_4 \\ c_6 \end{bmatrix} \cdot \begin{bmatrix} \omega^{-6} \\ \omega^{-4} \\ \omega^{-2} \\ \omega^0 \\ \omega^2 \\ \omega^4 \\ \omega^6 \end{bmatrix} \to \begin{bmatrix} c_2 - c_{-2} \\ c_4 - c_{-4} \\ c_6 - c_{-6} \end{bmatrix} \cdot \begin{bmatrix} \omega^2 \\ \omega^4 \\ \omega^6 \end{bmatrix} \to \begin{bmatrix} a_1 \\ a_2 \\ a_3 \end{bmatrix} \cdot \begin{bmatrix} \sin(1\pi/n) \\ \sin(2\pi/n) \\ \sin(3\pi/n) \end{bmatrix} \qquad a_j, c_j \in \boldsymbol{Z}.$$

In listing the results of our calculations it suffices to list vector (a_1, a_2, a_3).

For each $\delta \in \{-1, 0, 1\}$ and each $\beta \in \{1, ..., 20\}$ we compute $P(\delta, s)\overline{Q}$ and extract the coefficient vector (a_1, a_2, a_3).

Here is the table for $\delta = -1$ and $\beta = 1, ..., 10$.

$$\begin{array}{cccccccccc} (0) & (-) & (-) & (-) & (-) & (-) & (-) & (-) & (-) & (-) \\ 0 & 0 & -4 & -2 & -2 & -6 & -4 & -4 & -2 & 0 \\ 0 & -2 & -2 & 0 & -2 & -2 & 0 & -2 & 0 & 0 \\ 0 & 0 & 0 & 0 & 0 & 0 & 0 & 0 & 0 & -2 \end{array} \tag{4.11}$$

Here is the table for $\delta = -1$ and $\beta = 1, ..., 10$.

$$\begin{array}{cccccccccc} (-) & (-) & (-) & (-) & (-) & (0) & (-) & (-) & (-) & (-) \\ 0 & 0 & -4 & -2 & -2 & 0 & 2 & 2 & 2 & -2 \\ -2 & -2 & -2 & 0 & -2 & 0 & 0 & -2 & -2 & -2 \\ -2 & 0 & 0 & 0 & 0 & 0 & -2 & -2 & 0 & 0 \end{array} \tag{4.12}$$

Here is the table for $\delta = 0$ and $\beta = 1, ..., 10$.

$$\begin{array}{cccccccccc} (+) & (-) & (0) & (+) & (-) & (-) & (+) & (-) & (+) & (-) \\ 4 & -2 & 0 & 2 & -4 & -2 & 0 & -6 & 2 & -4 \\ 2 & -2 & 0 & 2 & -2 & 0 & 2 & -2 & 4 & -4 \\ 0 & 0 & 0 & 0 & 0 & 0 & 0 & 0 & 2 & -2 \end{array} \tag{4.13}$$

Here is the table for $\delta = 0$ and $\beta = 11, ..., 20$.

$$\begin{array}{cccccccccc} (+) & (-) & (0) & (+) & (-) & (+) & (-) & (+) & (-) & (+) \\ 4 & -2 & 0 & 2 & -4 & 4 & -2 & 6 & 0 & 2 \\ 2 & -2 & 0 & 2 & -2 & 4 & -4 & 2 & -2 & 0 \\ 0 & 0 & 0 & 0 & 0 & 2 & -2 & 0 & 0 & 0 \end{array} \tag{4.14}$$

Here is the table for $\delta = 0$ and $\beta = 1, ..., 10$.

$$\begin{array}{cccccccccc} (+) & (+) & (+) & (+) & (+) & (0) & (+) & (+) & (+) & (+) \\ 6 & 2 & 2 & 4 & 0 & 0 & 2 & -2 & -2 & -2 \\ 2 & 2 & 0 & 2 & 2 & 0 & 2 & 2 & 2 & 0 \\ 0 & 0 & 0 & 0 & 0 & 0 & 0 & 0 & 2 & 2 \end{array} \tag{4.15}$$

Here is the table for $\delta = 0$ and $\beta = 11, ..., 20$.

$$\begin{array}{cccccccccc} (0) & (+) & (+) & (+) & (+) & (+) & (+) & (+) & (+) & (+) \\ 0 & 2 & 2 & 4 & 0 & 0 & 0 & 2 & 4 & 4 \\ 0 & 2 & 0 & 2 & 2 & 2 & 0 & 0 & 2 & 0 \\ 0 & 0 & 0 & 0 & 0 & 2 & 2 & 0 & 0 & 0 \end{array} \tag{4.16}$$

All the expressions on the first two tables correspond to bottom vertices. An inspection of Figure 4.7 shows that the expressions with $(+)$ signs correspond to top vertices and the expressions with $(-)$ signs correspond to bottom vertices. (We copy the figure above.) All the expressions on the bottom two tables correspond to top vertices. Finally, there are 6 expressions which are real, independent of n, and these correspond to the 6 vertices in Lemma 4.1. This completes the proof of Lemma 4.1.

4.4 The End of the Proof

Lemma 4.1 implies that $O(B_n)$ is determined by positions of the 6 vertices

$$\alpha_1 = (12, R, O)^*; \quad \alpha_2 = (5, R, I)^*; \quad \alpha_3 = (10, R, I)^*.$$

$$\beta_1 = (4, L, O)_*; \quad \beta_2 = (1, L, I)_*; \quad \beta_3 = (16, L, I)_*; \tag{4.17}$$

Let H_{ij} be the defining function which measures the height of α_i minus the height of β_j, when the unfolding is normalized to that the long edges have length 1. Below we will prove

Lemma 4.2 *For every relevant pair of indices, we have $\partial_1 H_{ij}(V_n) < 0$ and $\partial_2 H_{ij}(V_n) \geq 0$. There is equality in the second equation iff $(i,j) = (1,1)$.*

Note that $H_{ij}(V_n) = 0$. Lemma 4.2 therefore says that $H_{ij}(X) > 0$ provided that $(i,j) \neq (1,1)$ and $X \in N_{-+}(n, \epsilon_n)$ for sufficiently small ϵ_n. If we knew that H_{11} vanished identically on the line $x_1 = \pi/2n$ then we could conclude the same result for $(i,j) = (1,1)$. Before proving Lemma 4.2 we will take care of the exceptional pair of indices.

Lemma 4.3 *H_{11} vanishes identically on the line $x = \pi/2n$.*

Proof: We will draw the picture for the case $n = 4$, but the phenomenon we describe is completely general. Let P and Q and F be the defining functions associated to our two points. Figure 4.9 shows the paths $\widehat{Q}$ and $\widehat{P}$.

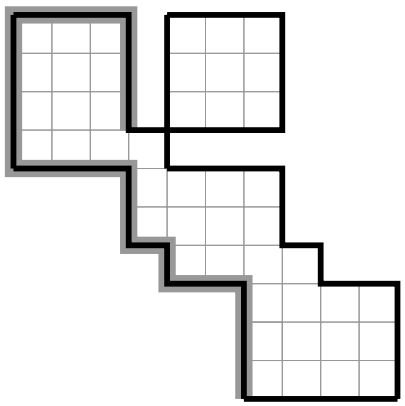

Figure 4.9: $\widehat{Q}$ in black and $\widehat{P}$ in grey.

Note that $\widehat{P}$ covers half the vertices of $\widehat{Q}$ and the vertices in the complement $\widehat{Q} - \widehat{P}$ are, as a subset of $\boldsymbol{Z}^2$, isometric to the vertices of $\widehat{P}$. The isometry is given by the translation $(x_1, x_2) \to (x_1 + 2n, x_2)$. Taking care to get the sign right, we see that $Q = P + P'$, where there is a bijection between the terms of P and the terms of P', having the form

$$E(ax_1 + bx_2) \to -E((a + 2n)x_1 + x_2).$$

When $x_1 = \pi/2n$ we see that corresponding terms take on the same value. Hence $Q = 2P$ when $x = \pi/2n$. But this means that $F(\frac{\pi}{2n}, x_2) = 0$. ♠

Equation 4.3 follows from Lemma 4.1, Lemma 4.2, and Lemma 4.3. It only remains to prove Lemma 4.2. The rest of the chapter is devoted to this.

4.5 Variation of Edgelength

In proving Lemma 4.2 we will connect various vertices of the unfolding together by the same sorts of paths we used in the proof of Lemma 4.1. These paths mainly involve the long edges, which all have unit length, but sometimes they involve a short edge as well. Even though we are evaluating the derivatives of our defining functions at V_n, we still need to understand how these short edges vary in length for points nearby V_n. In this section, we will deal with this issue.

Suppose T is a triangle with small angles x_1 and x_2, normalized so that the long side of T has unit length. Let l_j denote the length of the side of T which is opposite the x_j angle. Of course, l_j depends on the parameters x_1 and x_2. When $x_1 = x_2$ we have $l_1 = l_2$. When $x_1 = x_2 = \pi/2n$ we have

$$\lambda := l_1 = l_2 = \frac{\sin(x_1)}{\sin(x_1 + x_2)} = \frac{\sin(\pi/2n)}{\sin(\pi/n)} = \frac{1}{2\cos(\pi/2n)} = \frac{1}{\omega + \omega^{-1}}. \tag{4.18}$$

As usual, $\omega = E(\pi/2n)$. Here λ is as in Equation 4.10. Our calculations below require the quantities:

$$\begin{aligned}
\lambda_1 &:= \left.\frac{dl_2}{dx_2}\right|_{V_n} = \left.\frac{dl_1}{dx_1}\right|_{V_n} = \left.\frac{\sin(x_2)}{\sin^2(x_1+x_2)}\right|_{V_n} = \frac{2i\omega}{(\omega-\omega^{-1})(\omega+\omega^{-1})^2} \\
\lambda_2 &:= \left.\frac{dl_2}{dx_1}\right|_{V_n} = \left.\frac{dl_1}{dx_2}\right|_{V_n} = \left.\frac{-\cos(x_1+x_2)\sin(x_1)}{\sin^2(x_1+x_2)}\right|_{V_n} = \frac{-i\omega(\omega^2+\omega^{-2})}{(\omega-\omega^{-1})(\omega+\omega^{-1})^2}.
\end{aligned} \tag{4.19}$$

4.6 Proof of Lemma 4.2

We define

$$F_{\alpha,j} = \text{height}(\alpha_j) - \text{height}(a_1); \qquad F_{\beta,j} = \text{height}(\beta_j) - \text{height}(a_1). \tag{4.20}$$

here $a_1 = (1, L, O)^*$. Again, we measure these heights when the U_n is normalized so that the long edges are unit length. We have the obvious equation

$$H_{ij} = F_{\alpha,i} - F_{\beta_j}. \tag{4.21}$$

We will deduce Lemma 4.2 from our computations of $F_{\alpha,i}$ and $F_{\beta,j}$.

In our proof of Lemma 4.1 we constructed a path from $b_1 = (1, L, I)$ to and given point p. The first edge of this path joined b_1 to a_1. So, the path we use to connect a_1 to p is just the same one we used above, except with the first edge chopped off. In describing our paths, we let Y_k denote the path made from the first k edges of the 3-spine. We let $e_k^{\pm}$ denote the short edge such that

$$\widehat{e_k^{\pm}} = \widehat{e}_k + (\pm 1, 0).$$

Here e_k is the kth edge of the 3-spine. (The correspondence $e \to \widehat{e}$ is discussed in detail in §2.) The three edges e_k^-, e_k, e_k^+ correspond to 3 consecutive horizontal dots in Figure 4.8

With this notation, we have:

- The path connecting a_1 to α_1 is Y_{13}.

- The path connecting a_1 to α_2 is $Y_5 \cup e_6^+$. The short edge has type 2.
- The path connecting a_1 to α_3 is $Y_9 \cup e_{10}^+$. The short edge has type 2.
- The path connecting a_1 to β_1 is Y_3.
- The path connecting a_1 to β_2 is e_1^-. This (short) edge has type 1.
- The path connecting a_1 to β_3 is $Y_{15} \cup e_{16}^-$. This edge has type 2.

We will leave the details of our calculation to Mathematica, but here we outline the main points. In each case we $\widetilde{F} = P\overline{Q}$, so that $F = \mathrm{Im}(\widetilde{F})$. By the product rule we have

$$\partial_j \widetilde{F}(V_n) = P(V_n)\partial_j \overline{Q}(V_n) + \partial_j P(V_n)\overline{Q}(V_n). \tag{4.22}$$

We evaluate P and Q using Equation 4.10 (without the first term). We evaluate $\partial_j P$ and $\partial_j Q$ essentially by differentiating Equation 4.10 (without the first term.) We now explain how the differentiation works. Our calculations use the lists from Equation 4.5.

Let R be one of the expressions we want to differentiate. If Y_k appears in the definition of the path associated to R then we see a contribution of

$$\sum_{i=1}^{k} L_j(i)\omega^{L(i)}$$

in the expression for $\partial_j Y(V_n)$. In conjugating (for the case $R = Q$) we simply reverse the signs of the list of numbers in L. For instance

$$\partial_1 \overline{Q}(V_n) = \sum_{i=1}^{20} L_1(i)\omega^{-L(i)} =$$

$$\frac{2i}{\omega^3}[(-4 - 4\omega^2 - 7\omega^4 - 3\omega^6)n + (10 + 14\omega^2 + 16\omega^4 + 8\omega^6)]. \tag{4.23}$$

If we see $e_k^{\pm}$ in our expression, and this edge has type 1, then we see a contribution of

$$\lambda(L_1(k) \pm 1)\omega^{L(k)\pm 1} + \lambda_1 \omega^{L(k)\pm 1} \tag{4.24}$$

in the expression for $\partial_1 R(V_n)$ and a contribution of

$$\lambda(L_2(k) + 0)\omega^{L(k)+1} + \lambda_2 \omega^{L(k)\pm 1} \tag{4.25}$$

in the expressions for $\partial_2 R(V_n)$. If $e_k^{\pm 1}$ has type 2, then we see the same contributions, but with λ_1 and λ_2 switched.

These are the ingredients for our calculations. We let $\widetilde{H}_{ij} = \widetilde{F}_{\alpha,i} - \widetilde{F}_{\beta,j}$. When we compute these quantities using the expressions above, we find that the result always has the form

$$\partial_i \widetilde{H}_{jk} = \frac{f(n, \omega, \omega^{-1})}{\omega^a} \qquad \text{or} \qquad \frac{f(n, \omega, \omega^{-1})}{\omega^a(\omega^2 - \omega^{-2})}. \tag{4.26}$$

Here f is some polynomial in ω, ω^{-1} and n which is linear in n. (This polynomial, and the exponent a, both depend on the indices i, j, k.) The first case occurs 5 times and the second case occurs 13 times.

Since we only care about the sign of the imaginary part of $\partial_i \widetilde{H}_{jk}$ we clear denominators by multiplying the second form by the positive real expression

$$I(\omega^2 - \omega^{-2}). \tag{4.27}$$

Call the resulting expression $\widetilde{L}_{ijk}$. When $\partial_i \widetilde{H}_{jk}$ has the first form we simply set $\widetilde{L}_{ijk} = \partial_i \widetilde{H}_{jk}$.

In all cases we find that

$$\widetilde{L}_{ijk} = \begin{bmatrix} c_{-8} \\ c_{-6} \\ c_{-4} \\ c_{-2} \\ c_0 \\ c_2 \\ c_4 \\ c_6 \\ c_8 \end{bmatrix} \cdot \begin{bmatrix} \omega^{-8} \\ \omega^{-6} \\ \omega^{-4} \\ \omega^{-2} \\ \omega^0 \\ \omega^2 \\ \omega^4 \\ \omega^6 \\ \omega^8 \end{bmatrix} \to \begin{bmatrix} c_0 - \overline{c}_0 \\ c_2 - \overline{c}_{-2} \\ c_4 - \overline{c}_{-4} \\ c_6 - \overline{c}_{-6} \\ c_8 - \overline{c}_{-8} \end{bmatrix} \cdot \begin{bmatrix} 1 \\ \omega^2 \\ \omega^4 \\ \omega^6 \\ \omega^8 \end{bmatrix} = \begin{bmatrix} a_0 \\ a_1 \\ a_2 \\ a_3 \\ a_4 \end{bmatrix} \cdot \begin{bmatrix} 1 \\ \omega^2 \\ \omega^4 \\ \omega^6 \\ \omega^8 \end{bmatrix}. \tag{4.28}$$

This time c_j has the form

$$c_j = c_{j0} + c_{j1} n; \qquad c_{0j}, c_{j1} \in \boldsymbol{Z}[i]. \tag{4.29}$$

Again, the expression $x \to y$ means that the imaginary parts of these two expressions are positive multiples of each other.

In listing the results of our calculations, we just write out the coefficient vectors $(a_0, ..., a_5)$. Here are the 9 expressions for $-\widetilde{L}_{1jk}$:

$$\begin{array}{cccccc} * & 120in & 92in & 40in & 8in & 0 \\ & 0 & 68n-60 & 88n-72 & 48n-40 & 8n \\ & 0 & 124n-220 & 92n-168 & 24n-40 & 0 \\ & 0 & 44n-60 & 52n-72 & 24n-40 & 0 \\ & 0 & 32n-120 & 56n-144 & 32n-80 & 0 \\ & 0 & 88n-280 & 60n-240 & 8n-80 & -8n \\ & 0 & 140n-176 & 128n-168 & 56n-84 & 6n-12 \\ & 0 & 128n-236 & 132n-240 & 64n-124 & 6n-12 \\ * & i(224n-520) & i(134n-348) & i(40n-124) & i(-2n-12) & 0 \end{array} \tag{4.30}$$

(We have deliberately listed $-\widetilde{L}_{ijk}$.) Here are the 9 expressions for $\widetilde{L}_{2jk}$.

$$
\begin{array}{lccccc}
* & 0 & 0 & 0 & 0 & 0 \\
 & 0 & 52n-60 & 56n-72 & 32n-40 & 0 \\
 & 0 & 88n-176 & 92n-184 & 44n-84 & 0 \\
 & 0 & 52n-60 & 56n-72 & 32n-40 & 0 \\
 & 0 & 104n-120 & 112n-144 & 64n-80 & 0 \\
 & 0 & 140n-236 & 148n-256 & 76n-124 & 0 \\
 & 0 & 116n-220 & 88n-168 & 16n-40 & 0 \\
* & i(216n-360) & i(144n-240) & i(48n-80) & 0 & 0 \\
* & i(264n-520) & i(180n-352) & i(60n-124) & 0 & 0
\end{array}
\tag{4.31}
$$

The starred lines come from the first form in Equation 4.26 and the unstarred lines come from the second form. The first line in Equation 4.31 is $\widetilde{L}_{211}$, the quantity we expect to vanish in light of Lemma 4.3. For $n \geq 4$ the positive imaginary terms in the other starred lines dominate the negative imaginary terms, and the positive terms in the unstarred lines dominate the negative terms. Hence, with the exception of the one line which represents the quantity 0, all the other lines represent quantities with positive imaginary part. (To be sure, we checked this numerically for $n = 4, ..., 20$.)

This completes the proof of Lemma 4.2, and we are done.

5 The Words for Theorem 1.7

Theorem 1.7 is the most delicate of our existence results. Here we introduce the necessary words. In later chapters, we will analyze these words, as we did for the proofs of Theorems 1.2 and 1.3.

5.1 The Squarepaths

Theorem 1.7 involves the words $\{W_{nk}\}$ for $n = 3, 4, 5...$ and $k = 0, 1, 2....$ In this chapter we introduce these words and consider the corresponding unfoldings. It turns out that W_{nk} has length $24n + 30k^2 - 68k - 20$. The shortest word, W_{30}, has length 52. Rather than present W_{nk} as a long string of digits, we will draw the square path $\widehat{Q}_{nk} := \widehat{Q}_3(W_{nk})$. The path $\widehat{Q}_{nk}$ is not embedded, but is the union of two embedded halves. Reflection about a diagonal line swaps these two halves. We will draw one half of $\widehat{Q}_{nk}$, we well as the diagonal line.

$\widehat{Q}_{nk}$ is based an in $(n-1) \times n$ grid of squares, which we call an *n-stamp*. Each square in the stamp has edge-length 2, as in Figure 2.3.

Figure 5.1 shows 3 representations of the word W_{30}. The leftmost figure shows the squarepath $\widehat{Q}_{30}$. This closed path is composed of 2 halves that are swapped by reflection in a certain diagonal line of symmetry. The middle figure shows one half $\widehat{Q}_{30}$. This is the representation we will use in the other figures. We prefer this representation because the corresponding path is always embedded, and the full squarepath can be recovered in a straightforward way. Just reflect and concatenate. The right figure shows the corresponding half of the hexpath H_{30}.

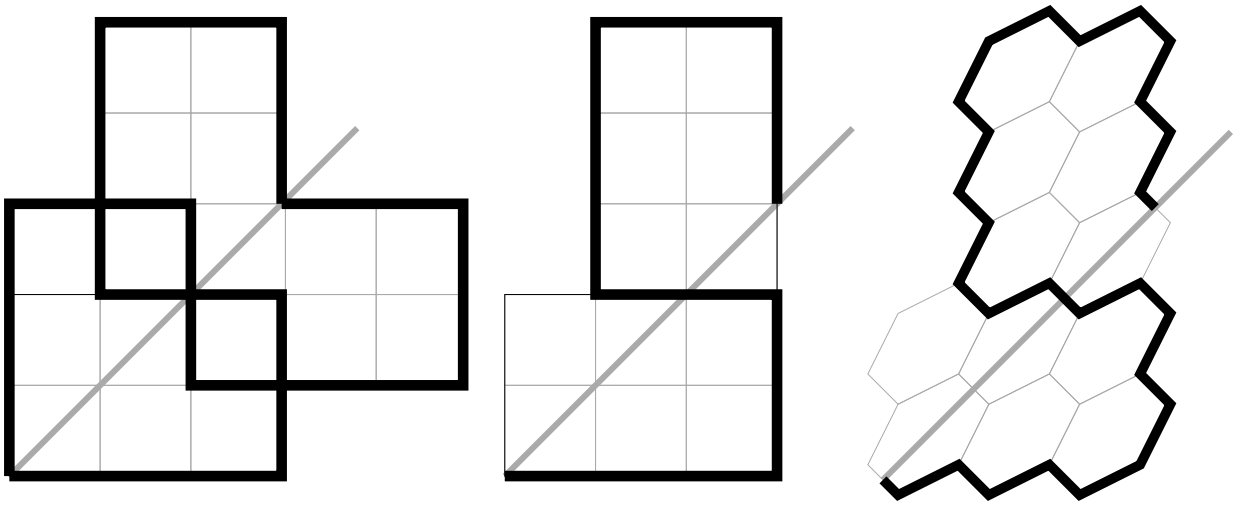

Figure 5.1: Half of $\widehat{Q}_{31}$.

Figure 5.1 is the beginning of an infinite pattern of paths. Figure 5.2 shows the corresponding halves of $\widehat{Q}_{3k}$ for $k = 1, 2, 3$. The small grid of squares has been erased in Figure 5.2.

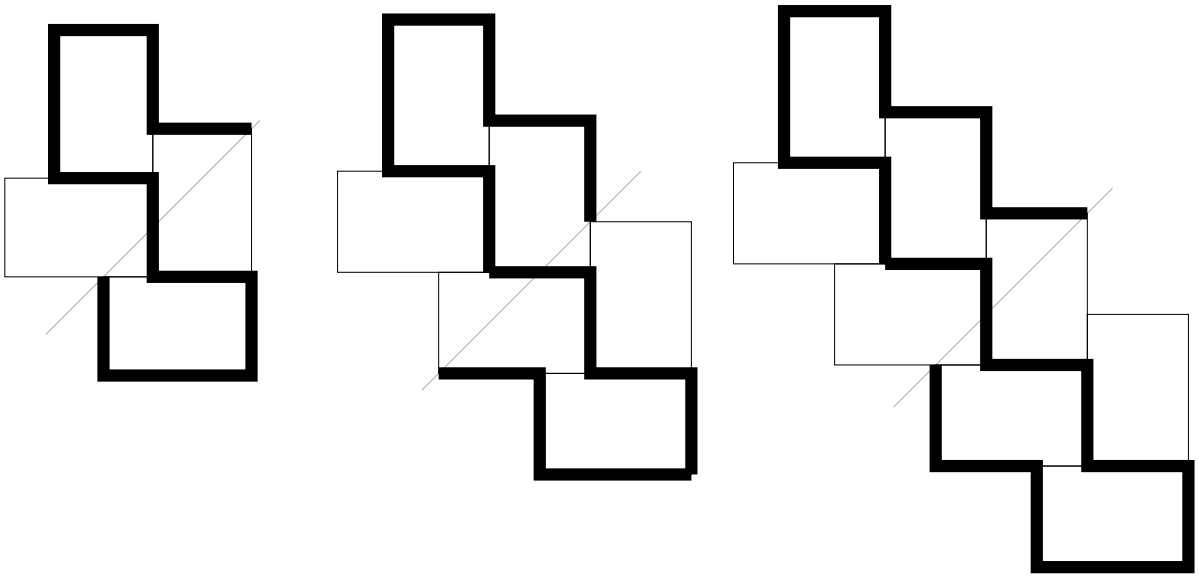

Figure 5.2: Half of $\widehat{Q}_{3k}$ for $k = 1, 2, 3$.

The path $\widehat{Q}_{n+1,k}$ is obtained by increasing the length of each edge of $\widehat{Q}_{nk}$ by 2 units. Figure 5.3 shows the left halves of $\widehat{Q}_{31}$, $\widehat{Q}_{41}$, and $\widehat{Q}_{51}$.

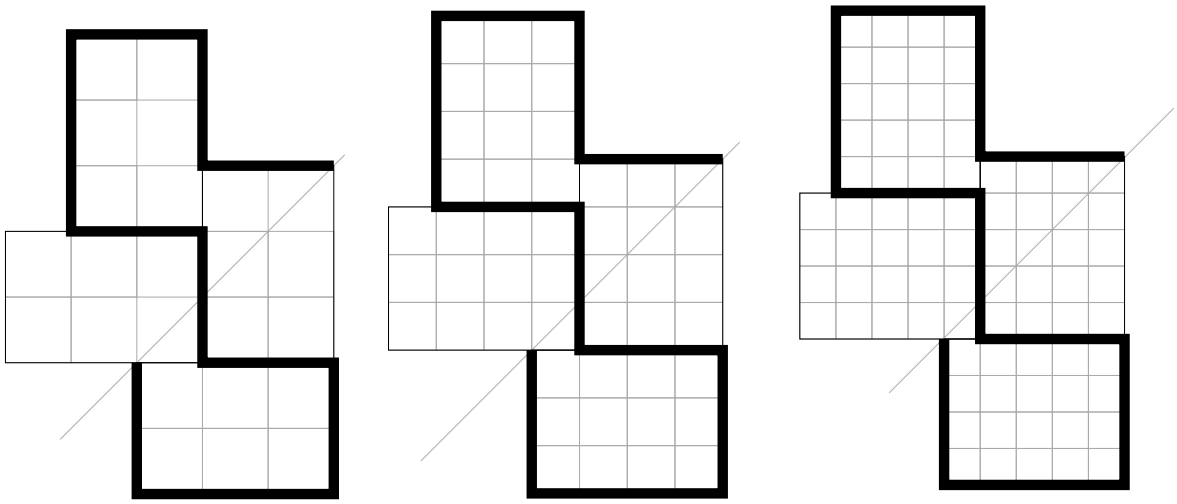

Figure 5.3: Half of the rectilinear paths for $\widehat{Q}_{30}$ and $\widehat{Q}_{40}$ and $\widehat{Q}_{50}$

5.2 The Unfoldings

We will see that U_{nk} consists of 4 "strips", attached along 4 "hinges". Figure 5.4 shows this structure.

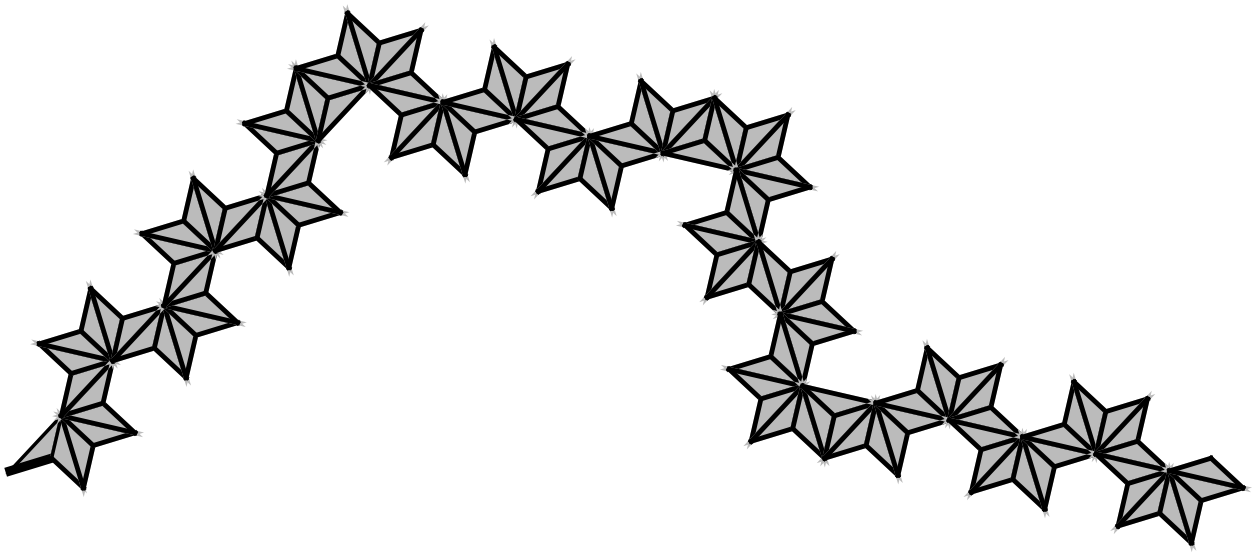

Figure 5.4: $U(W_{42}, V_3)$.

When we change the point relative to which we unfold, the strips do not change much and the hinges open and close, so to speak. For points in the orbit tiles, the hinges adjust so that the whole unfolding is practically a straight line. In Figure 4.4, we have chosen a point that is far from the relevant tile. Our remaining pictures show the unfoldings for points actually in the relevant orbit tile.

The strips are essentially composed of units that we call *blocks*. The left hand side of Figure 5.5 shows what we call a *block*. In general, a k-block is defined to be k blocks lined up in sequence. The right hand side of Figure 5.5 shows a 2-block. The triangles in a k-block all have the same shape, and this shape depends on the point in parameter space of interest to us. If we glue the opposite sides of a block together we get a space which is naturally the union of two 2-darts.

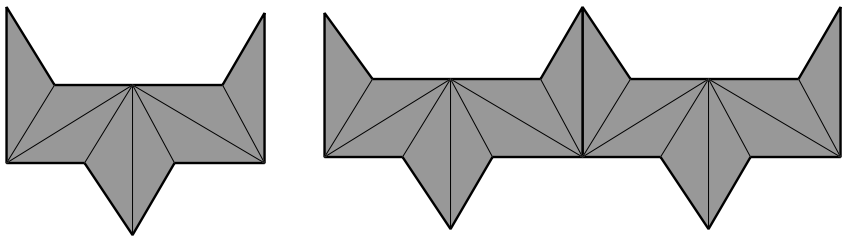

Figure 5.5: A 1-block and a 2-block

The strips are essentially composed of blocks. Once we describe U_{30}, we will describe U_{nk} as a modification which amounts to changing the combinatorial structure of each strip. Figure 5.6 shows $U(W_{30}, V_3)$.

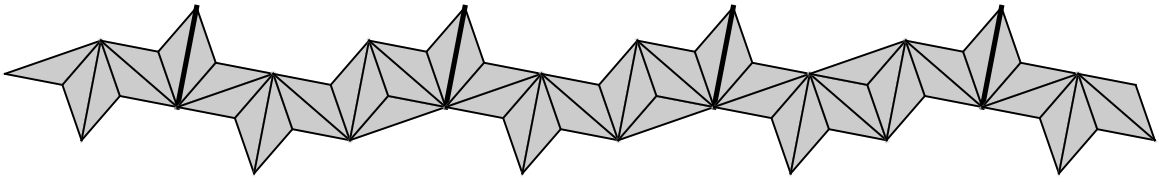

Figure 5.6: $U(W_{30}, V_3)$.

Note that $U(W_{30}, V_3)$ has 12 long edges which are all parallel and nearly vertical. We have highlighted 4 of these edges. The unfolding U_{3k} is obtained by cutting U_{30} open along each of the 4 highlighted edges and inserting a k-block. Figure 5.7 shows $U(W_{31}, V_3)$. The pattern continues in the obvious way. In describing our surgery, we have used the geometry of $U(W_{30}, V_3)$ to highlight 4 particular edges along which we cut. However, this surgery has a combinatorial meaning for any parameter.

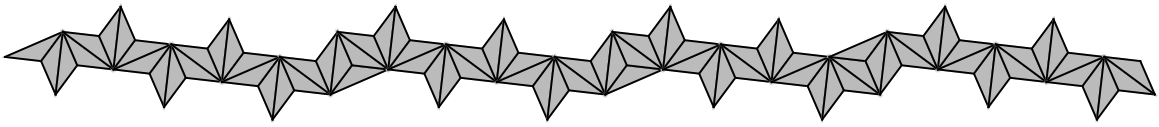

Figure 5.7: $U(W_{31}, V_3)$.

We obtain $U_{n,k}$ from U_{3k} by replacing each maximal m-dart with a maximal m'-dart, where

$$m' = m + (n-3).$$

This fits exactly with our description of $\widehat{Q}_{nk}$ as being obtained from $\widehat{Q}_{3k}$ by lengthening each edge by $2(n-3)$ units.

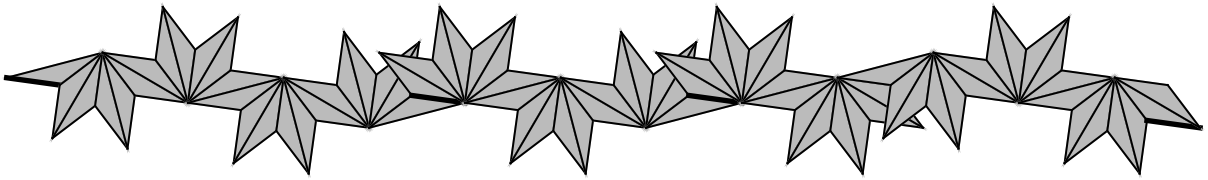

Figure 5.8: $U(W_{40}, V_4)$.

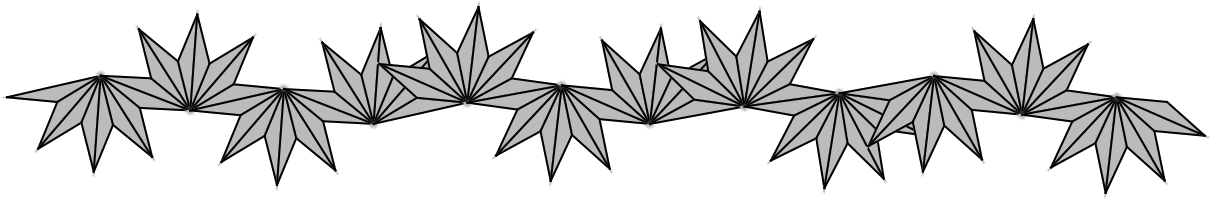

Figure 5.9: $U(W_{50}, V_5)$.

We end this section with a computation. The formulas in the next result will be useful when we make explicit computations in §6 and §7.

Lemma 5.1 *Let n be fixed and let e_k be the leftmost edge of $U(W_{nk}, V_n)$. As $k \to \infty$, the slope of e_k converges to 0.*

Proof: We normalize so that e_k has unit length. If we trim off the portions of the darts from the set $U := U(W_{nk}, V_n)$ we see that the resulting set is the union of 4 parallel annuli attached along 4 edges. We compute by elementary trigonometry and induction that the 4 strips have total length

$$\Psi_1 + \Psi^{\#} k; \qquad \Psi_1 = 12(1 + \cos(\frac{\pi}{n})); \qquad \Psi^{\#} = 8(1 + \cos(\frac{\pi}{n})). \tag{5.1}$$

Each annulus has width

$$\Psi_2 = \sin(\frac{\pi}{n}) \tag{5.2}$$

If we rotate U so that the first edge is horizontal then the holonomy has coordinates

$$\Psi_1 + i4\Psi_2 + \Psi^{\#}k. \tag{5.3}$$

The line determined by this complex number converges to a horizontal line as $k \to \infty$. Thus, if we rotate U so that the holonomy is horizontal, then the slope of the first edge tends to 0 as $k \to \infty$. ♠

Remark: In §7 we will give a more explicit and combinatorial derivation of the formulas in Lemma 5.1.

5.3 The Pivot Region

Here we isolate 4 basic features of the unfolding $U(W_{nk}, V_n)$.

- There is a family of $12 + 8k$ parallel and nearly vertical edges. We call these edges *quasi-vertical*, or QV for short.
- There is a family of $24 + 16k$ parallel and nearly horizontal edges. We call these edges *quasi-horizontal*, or QH for short.
- Each QV edge is *flanked* by two QH edges, in the sense that reflection in this QV edge swaps the two QH edges flanking it.
- There are exactly 4 QH edges which connect top to bottom vertices. We call these edges the *hinges*.

These facts are all established inductively. They hold true for the parameter $(3, 0)$, and then we check easily that they remain true when we perform one of the surgeries described above.

We have distinguished the above edges just for the unfoldings attached to specific parameters. However, we extend our definitions of QH and QV, using continuity, to the unfoldings attached to any point of parameter space. Of course, for points remote to the regions of interest to us, the QH edges need not be close to horizontal and the QV edges need not be close to vertical. Moreover, these edges need not be parallel to each other at other parameters. To talk precisely about the situation we make the following definition:

Definition: Let A_n denote the region $(x_1, x_2) \subset \Delta$ such that

$$x_j \in [\pi/2n, \pi/(2n-2)]; \qquad j = 1, 2.$$

The points V_n and V_{n-1} are two opposite corners of the little square defined by these conditions. Let $R'_{nk} \subset A_n$ denote the set of points such that all the QH edges have negative slope. Let R_{nk} denote the path connected component of R'_{nk} which contains V_n. We call R_{nk} the *pivot region*.

Lemma 5.2 *For any point in R_{nk} the QV edges all have positive slope.*

Proof: As we pointed out above, each QV edge V is flanked by two QH edges H_1 and H_2. That is, reflection in V swaps H_1 and H_2. This is a property that holds for all parameters: It is a combinatorial symmetry. Now, let $X \in R_{nk}$ be some point. We consider what happens as we vary the parameter continuously from V_n to X, staying inside R_{nk}. If the slope of V changes from positive to negative then V must be either vertical or horizontal at some point. But then it is impossible for H_1 and H_2 to both have negative slope at this point and still flank V. This is a contradiction. ♠

Referring to §2.6, we note that a vertex of U_{nk} is superior if and only if it is incident to a QH edge. This fact is seen by inspection for U_{30}, and then is unchanged by any of the surgeries we perform. We call a superior vertex a *pivot* if it is incident to one of the pivot edges. There are 4 top pivots and 4 botton pivots.

Lemma 5.3 *Let $X \in R_{nk}$ be any point. If all the top pivots lie above all the bottom pivots of $U(W_{nk}, X)$ then $X \in O(W_{nk})$.*

Proof: Let v be a top superior vertex of U_{nk} which is not a pivot. Inspecting our unfoldings, we see that v has one of two properties:

- v is the left vertex of a QH edge which is not a hinge.
- v lies to the left of another superior vertex v', and reflection in a QV edge swaps v and v'.

This property is easily seen, by inspection, for U_{30}, and our surgery operations do not destroy this property. In either of the above cases, our conditions on the slopes of the QV and QH edges forces v to lie above v'. Since this works for all superior vertices which are not pivots, we see that only a pivot can be the lowest top superior vertex. Likewise, only a pivot can be a bottom superior vertices. Hence, by hypothesis, all the top superior vertices lie above all the bottom superior vertices. Hence $X \in O(W_{nk})$ by the Dart Lemma. ♠

5.4 The Structure of the Quasi-Horizontal Edges

Say that a *QH point* in $\boldsymbol{Z}^2$ is a point $\widehat{e}$ which corresponds to a QH edge. Here we describe the pattern of QH points associated to our unfoldings.

We use the McBilliards labeling convention that the leftmost edge e_0 of U_{nk}, which happens to be a QH edge, corresponds to $(0,0) \in \boldsymbol{Z}^2$. If e is any other QH edge, then e is parallel to e_0 at the point $V_n = (\pi/2n, \pi/2n)$. But the angle between e and e_0 is given by $\widehat{e} \cdot (\pi/2n, \pi/2n)$. This angle must be an integer multiple of π. Hence

$$\widehat{e}_1 + \widehat{e}_2 \equiv 0 \mod 2n. \tag{5.4}$$

The map $(x,y) \to x+y$ maps the hexpath H_{nk} to a subset of $\boldsymbol{Z}$ having diameter less than $(4+\frac{1}{2})n$. Hence Equation 5.4 forces the QH points to lie along at most 4 lines of slope -1 in $\boldsymbol{Z}^2$. Hence the QH edges fall into at most 4 pseudo-parallel families, in the sense of §2.7.

After some trial and error we figured out how to draw the QH points. We find that these points fall into exactly 4 pseudo-parallel families, and we compute the extreme points of these families as follows: Setting

$$Z_{nk} = (2n-2)(k+2) - 1, \tag{5.5}$$

the coordinates for the extreme points, in each family, are given by

1. $(-3, -4n+3)$ and $(-4n+3, -3) + (Z_{nk}, -Z_{nk})$.
2. $(-2, -2n+2)$ and $(-2n+2, -2) + (Z_{nk}, -Z_{nk})$.
3. $(0,0)$ and $(0,0) + (Z_{nk}, -Z_{nk})$.
4. $(2n-2, 2)$ and $(2, 2n-2) + (Z_{nk}, -Z_{nk})$.

Actually, we don't care so much about these formulas. The main feature of the QH points we use is that the coordinates of the northwest extreme endpoints−the first ones listed in each line above−are independent of k. This property, together with symmetry, will tell us everything we want to know about these edges.

Figure 4,10 shows the first few examples of the QH points in $\boldsymbol{Z}^2$. The 8 larger dots are the extreme points. 4 of these dots are black and the other 4 are grey. The 4 grey dots in these figures correspond to the hinges. The northwest grey dot is labeled $(0,0)$. The southeast grey dot is $(A, -A)$. The black path is the path $\widehat{Q}$, discussed in §2.4, which corresponds to the 3-spine of the unfolding. This path is obtained by doubling the rectilinear paths discussed in §5.1.

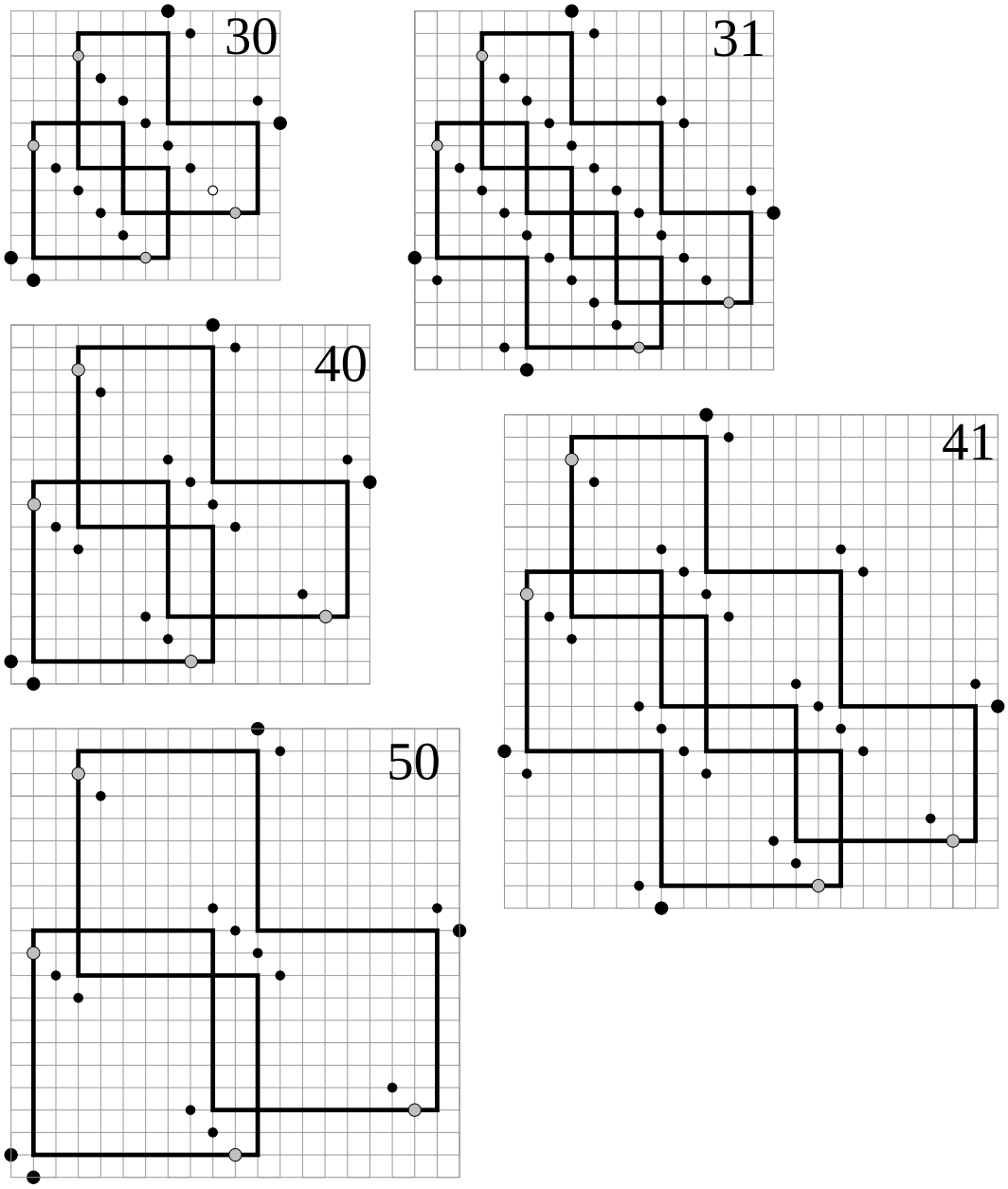

Figure 5.10: Points for the QH families.

6 The Quadratic Rescaling Theorem

6.1 Overview

We are interested in studying infinite sequences $\{W_{nk}\}$ of words introduced in the last chapter. We will hold n fixed and set $W_k = W_{nk}$. We wish to understand the asymptotic shape of the orbit tiles $O(W_k)$ as $k \to \infty$. Each $O(W_k)$ is a piecewise analytic polygon, whose sides are given as the 0-level sets of analytic functions. It turns out that $O(W_k)$ has a uniformly bounded number of sides, independent of both n and k, and we will be able to make sense of the notion of a *side* of $O(W_k)$ which is independent of k. This allows us to group the various defining functions involved into *families*. Our analysis is done one function-family at a time.

As we saw in §2, the function F_k has the special form

$$F_k(X) = \text{Im}(P_k(X - X_0)\overline{Q}_k(X - X_0)), \tag{6.1}$$

(The only difference between the set-up here and in §2 is that we take special care to translate F so that $(0,0)$, rather than X_0, is the main point of interest to us in the domain.) Here X_0 is the point in parameter space to which the orbit tiles converge. Summarizing the discussion in §2, P_k is the development image of a certain saddle connection associated to W_k, and Q_k is the holonomy of the unfolding.

We want to place conditions on $\{P_k\}$ and $\{Q_k\}$ so that the rescaled functions $\{G_k\}$ converges to a linear map (whose formula we can compute explicitly). Here

$$G_k(X) = F_k(Xk^{-2}). \tag{6.2}$$

The conditions we place on $\{P_k\}$ and $\{Q_k\}$ have to do with the growth patterns of the supports of their Fourier transforms. A few glances at the figures in §5 should be enough to convince the reader that the conditions we discuss are satisfied, in particular, by the functions associated to the words introduced in §5. We will state the Quadratic Rescaling Theorem in the next section and then spend the rest of the chapter proving it.

As in §2 we frequently let $E(x) = \exp(ix)$.

6.2 The Main Result

All our constructions are based on a translation $T : \boldsymbol{Z}^2 \to \boldsymbol{Z}^2$ and a point $X_0 \in \pi\boldsymbol{Q}^2$. More specifically, we have

$$T(x_1, x_2) = (x_1 + M_1, x_2 + M_2); \qquad X_0 = 2\pi\left(\frac{p_1}{q_1}, \frac{p_2}{q_2}\right). \tag{6.3}$$

There is a natural homomorphism associated to X_0:

$$\phi(x_1, x_2) = \left[\frac{p_1 q_2 x_1 + p_2 q_1 x_2}{\text{G.C.D.}(q_1, q_2)}\right] \in \boldsymbol{Z}/N; \qquad N = q_1 q_2/\text{G.C.D.}(q_1, q_2). \tag{6.4}$$

Here G.C.D. stands for *greatest common divisor*. We require that T is compatible with X_0 in the sense that $\phi(M_1, M_2) = 0$.

Remark: In this paper we will have $n = 3, 4, 5...$ and

$$T(x_1, x_2) = (x_1 + (2n-2), x_2 - (2n-2)); \qquad X_0 = 2\pi\left(\frac{1}{4n}, \frac{1}{4n}\right). \tag{6.5}$$

In this case, we have $\phi(x_1, x_2) = [x_1 + x_2] \in \boldsymbol{Z}/4n$, and $\phi(M_1, M_2) = 0$.

Going back to the general case, we let $\{R_k\}$ stand for either the sequence $\{P_k\}$ or $\{Q_k\}$. According to the theory developed in §2, we can write

$$R_k(X) = \sum_{V \in \boldsymbol{Z}^2} \widehat{R}_k(V) E(X \cdot V). \tag{6.6}$$

Here $\widehat{R}_k : \boldsymbol{Z}^2 \to \boldsymbol{Z}$ is the Fourier transform of $\boldsymbol{R}_k$. We say that $\widehat{R}_k$ has *linear growth* if there is some map $\widehat{R}^{\#} : \boldsymbol{Z}^2 \to \boldsymbol{Z}$ such that

$$\widehat{R}_{k+1} = \widehat{R}_k + \widehat{R}^{\#} \circ T^k; \qquad k = 0, 1, 2... \tag{6.7}$$

Here T is the translation above. We call $\widehat{R}^{\#}$ the *growth generator* for $\{R_k\}$. We require that both $\widehat{R}^{\#}$ and $\widehat{R}_0$ are supported on finitely many points of $\boldsymbol{Z}^2$. Intuitively, the support of $\widehat{R}_k$ grows linearly along the fibers of the homomorphism ϕ. As the notation suggestions, define

$$R_k^{\#}(X) = \sum_{V \in \boldsymbol{Z}^2} \widehat{R}_k^{\#}(V) E(X \cdot V). \tag{6.8}$$

Supposing that both $\{\widehat{P}_k\}$ and $\{\widehat{Q}_k\}$ have linear growth, we define

$$\delta = \det \begin{bmatrix} P^{\#}(X_0) & P_0(X_0) \\ Q^{\#}(X_0) & Q_0(X_0) \end{bmatrix};$$

$$\delta_j = \det \begin{bmatrix} P^{\#}(X_0) & \partial_j P^{\#}(X_0) \\ Q^{\#}(X_0) & \partial_j Q^{\#}(X_0) \end{bmatrix};$$

$$\Delta_j = \frac{M_j \delta}{2} + \mathrm{Im}(\delta_j). \tag{6.9}$$

Here ∂_j is the partial derivative with respect to x_j.

The rest of this chapter is devoted to proving:

Theorem 6.1 (Quadratic Rescaling) *Suppose that $\{\widehat{P}_k\}$ and $\{\widehat{Q}_k\}$ have linear growth with respect to T, and the quantities $P^{\#}(X_0)$ and $Q^{\#}(X_0)$ and δ are all real. Then $\{G_k\}$ converges in the C^∞-topology to G, whose equation is given by*

$$G(x_1.x_2) = F_0(0,0) - \Delta_1 x_1 - \Delta_2 x_2.$$

Remarks:
The C^∞ convergence means that each partial derivative of G_k converges, uniformly on compact subsets, to the corresponding partial derivative of G.

6.3 Quadratic Growth Conditions

Let $\mathcal{A}$ denote the set of all globally defined and analytic complex-valued functions on $\boldsymbol{R}^2$. Given a *multi-index* $I = (i_1, i_2)$ we define

$$X^I = x_1^{i_1} x_2^{i_2}; \qquad |I| = i_1 + i_2. \tag{6.10}$$

Given an infinite sequence $\{F_k\} \in \mathcal{A}$ we can write out the power series expansions

$$F_k(X) = \sum_I C_{k,I} X^I \tag{6.11}$$

We say that $\{F_k\}$ forms a *quadratic growth family* if $\{F_k(0,0)\}$ is a constant sequence we have the following finite limits for some $\epsilon > 0$.

$$\lim_{k\to\infty} C_{k,(1,0)} k^{-2} = C_1; \qquad \lim_{k\to\infty} C_{k,(0,1)} k^{-2} = C_2; \qquad \lim_{k\to\infty} \sum_{|I|\geq 2} |C_{k,I}|\ k^{(-2+\epsilon)|I|} = 0. \tag{6.12}$$

Note that ϵ only enters into the third equation.

Recall that $\{G_k\}$ is the rescaled version of $\{F_k\}$, as in Equation 6.2.

Lemma 6.2 (Convergence) *Suppose that $\{F_k\}$ is a quadratic growth family. Then $\{G_k\}$ converges in the C^∞ topology to the linear function G, whose formula is given by $G(x_1, x_2) = F_0(0,0) + C_1 x_1 + C_2 x_2$.*

Proof: From the chain rule, we get the following series expansion:

$$G_k(X) = \sum_I C_{k,I}\ k^{-2|I|}\ X^I. \tag{6.13}$$

Consider the difference

$$\widehat{G}(X) - G_k(X) = L_k(X) + R_k(X); \qquad R_k(X) = \sum_{|I|\geq 2} C_{k,I}\ k^{-2|I|}\ X^I.$$

Here $L_k(x)$ is a linear function whose coefficients vanish as $k \to \infty$, and R_k is everything else. It suffices to to show that R_k and all its derivatives tend to 0 uniformly on compact subsets.

Let ∂ stand for some partial derivative and let Ω be some big constant. Suppose $X = (x_1, x_2)$ is such that $|x_j| \leq \Omega$ for $j = 1, 2$. There is some constant N, depending on ∂, such that

$$|\partial R_k(X)| \leq \sum_{|I|\geq 2} |I|^N\ |C_{k,I}|\ k^{-2|I|}\ \Omega^{|I|} = \sum_{|I|\geq 2} \{|I|^N (\Omega/k^\epsilon)^{|I|}\}\ |C_{k,I}| k^{(-2+\epsilon)|I|}.$$

For

$$k > \left(\Omega N^N\right)^{1/\epsilon}$$

the term in braces is less than 1. Hence

$$|\partial R_k(X)| \leq \sum_{|I|\geq 2} |C_{k,I}|\ k^{(-2+\epsilon)|I|}.$$

By hypothesis, this last sum tends to 0 as $k \to \infty$. ♠

6.4 A Fact about the Fourier Transform

Now we begin to use the information about the sequences $\{P_k\}$ and $\{Q_k\}$ to establish the conditions on $\{F_k\}$ discussed in the Convergence Lemma above. Let X_0 be as in Equation 6.3 and let ϕ be the associated homomorphism, given in Equation 6.4. In particular, the value N is given by Equation 6.4. Consider a function of the form

$$R(X) = \sum_{V \in \boldsymbol{Z}^2} \widehat{R}(V) E(X \cdot V). \tag{6.14}$$

Choosing any residue class $k \in \boldsymbol{Z}/N$ we define the *modular transform*:

$$R_\phi(k) = \sum_{\phi^{-1}(k)} \widehat{R}(V). \tag{6.15}$$

In all cases of interest to us, the sum in Equation 6.14 is a finite sum. This sum defines a function $R_\phi : \boldsymbol{Z}/N \to \boldsymbol{C}$.

Lemma 6.3 (Modular Transform) *With the notation as above, we have*

$$R(X_0) = \sum_{j=1}^{N} R_\phi(j) E(2\pi j/N).$$

Proof: Let

$$N = \frac{q_1 q_2}{D}; \qquad D = \text{G.C.D.}(q_1, q_2).$$

We can write $R(X_0) = \sum_{j=1}^{N} R_j$, where

$$R_j = \sum_{(x_1,x_2) \in \phi^{-1}(j)} \widehat{R}(V) E\left(\frac{2\pi p_1 x_1}{q_1} + \frac{2\pi p_2 x_2}{q_2}\right) =$$

$$\sum_{(x_1,x_2) \in \phi^{-1}(j)} \widehat{R}(V) E\left(\frac{2\pi}{N}\left(\frac{x_1 p_1 q_2}{D} + \frac{x_2 p_2 q_1}{D}\right)\right) =$$

$$\sum_{(x_1,x_2) \in \phi^{-1}(j)} \widehat{R}(V) E\left(\frac{2\pi j}{N}\right) = R_\phi(j) E(2\pi j/N).$$

Summing over j we get the result. ♠

6.5 Growth Formulas

Let X_0 and T be as in Equation 6.3. In particular, recall that T represents translation by the vector $(M_1, M_2) \in \boldsymbol{Z}^2$. Let $\mathcal{V}$ denote the set of sequences of the form $\{R_k\}$ which have (M_1, M_2)-linear growth. We want to be clear that each individual *element* of $\mathcal{V}$ is a sequence

of functions. $\mathcal{V}$ is a vector space. The vector space laws on $\mathcal{V}$ are given by componentwise scaling and addition. That is

$$a \cdot \{R_k\} = \{aR_k\}; \qquad \{R_k\} + \{R'_k\} = \{R_k + R'_k\}. \tag{6.16}$$

Let $\mathcal{V}_0$ denote the subspace consisting of elements $\{R_k\}$ with $R_0 = 0$. There is a natural projection $\mathcal{V} \to \mathcal{V}_0$. The sequence $\{R_k\}$ is mapped to $\{S_k\}$ where $S_k = R_k - R_0$. We call $\{S_k\}$ the *pure projection* of $\{R_k\}$. We say that an element $\{R_k\}$ of $\mathcal{V}_0$ is *simple* if its growth generator $\widehat{R}^{\#}$ is the indicator function for a single lattice point. That is, there is some integral point A such that $\widehat{R}^{\#}(X) = 1$ iff $X = A$ and $\widehat{R}^{\#}(X) = 0$ otherwise. The simple elements of $\mathcal{V}_0$ form a basis for $\mathcal{V}_0$.

Lemma 6.4 *Let $\{R_k\}$ be any element of $\mathcal{V}$ and let $I = (i_1, i_2)$ be any multi-index. Then*

$$D_I R_k(X_0) = R^{\#}(X_0) \times \frac{i^{|I|} M_1^{i_1} M_2^{i_2}}{|I| + 1} \times k^{|I|+1} + O(k^{|I|}). \tag{6.17}$$

Proof: If $\{S_k\}$ is the pure projection of $\{R_k\}$ then

$$|D_I S_k(X_0)| - |D_I R_k(X_0)| = O(1)$$

Thus, it suffices to prove this lemma for elements of $\mathcal{V}_0$. Given the scaling and additivity properties of Equation 6.17, it suffices to establish Equation 6.17 for the simple elements of $\mathcal{V}_0$.

Suppose $\widehat{R}^{\#}$ is the indicator function for $(a_1, a_2) \in \boldsymbol{Z}^2$. Then

$$\widehat{D_I R_k}(x_1, x_2) = i^{|I|} x_1^{i_1} x_2^{i_2} \quad \iff \quad (x_1, x_2) \in \bigcup_{j=0}^{k-1} (a_1 + jM_1, b_1 + jM_2), \tag{6.18}$$

and otherwise this function vanishes. Let $\beta = \phi(a_1, a_2) \in \boldsymbol{Z}/N$. Note that $\beta = R^{\#}(X_0)$ for simple elements. All the points in Equation 6.18 lie in the same fiber of ϕ, namely $\phi^{-1}(\beta)$. From the Modular Transform Lemma we have

$$D_I R_k(X_0) = i^{|I|}\beta \times \sum_{j=0}^{k-1} (a_1 + jM_1)^{i_1} (a_2 + jM_2)^{i_2} =$$

$$i^{|I|}\beta M_1^{i_1} M_2^{i_2} \times \sum_{j=0}^{k-1} j^{|I|} + O(k^{|I|}) =$$

$$R^{\#}(X_0) \times \frac{i^{|I|} M_1^{i_1} M_2^{i_2}}{|I| + 1} k^{|I|+1} + O(k^{|I|}). \tag{6.19}$$

This completes the proof. ♠

One useful special case of Lemma 6.4, stated more precisely, is:

$$R_k(X_0) = R^{\#}(X_0)k + R_0(X_0). \tag{6.20}$$

Remark: We can relate Equation 6.20 to Lemma 5.1 as follows. In our examples we have $X_0 = V_n$, the Veech Point. If R is the holonomy function (the Q-function) associated to either the 1-spine or 2-spine of the unfolding U_{nk}, then $R_0(X_0) = \Psi_1 + i4\Psi_2$ and $R^{\#}(X_0) = \Psi^{\#}$.

Lemma 6.5 *Let $\{R_k\}$ be any element of $\mathcal{V}$. Then for $j = 1, 2$,*

$$\partial_j R_k(X_0) = \left(\frac{iM_j}{2} R^{\#}(X_0)\right)k^2 + \left(\partial_j R^{\#}(X_0) - \frac{iM_j}{2} R^{\#}(X_0)\right)k + \text{const.} \tag{6.21}$$

Proof: Let $\{S_k\}$ be the pure projection of $\{R_k\}$. Assuming for the moment that $\{S_k\}$ is a simple element, Equation 6.19, applied to $I = (1, 0)$, gives us

$$\partial_j S_k(X_0) - \frac{iM_1}{2} R^{\#}(X_0)k^2 = \partial_j S_k(X_0) + \frac{iM_1}{2}\beta k^2 =$$

$$\frac{i\beta M_1}{2}k + a_1 k = \left(\frac{iM_j}{2} S^{\#}(X_0)k + \partial_j S^{\#}(X_0)\right)k.$$

Hence Equation 6.21 holds, with zero constant term, for the simple elements. Both sides of Equation 6.17 (with zero constant term) can be interpreted as homomorphisms from $\mathcal{V}$ into $\boldsymbol{C}$. Hence, Equation 6.21 holds, with zero constant term, for all elements of $\mathcal{V}_0$. Finally we note that $\partial_j S_k(X_0)$ and $\partial_j R_k(X_0)$ differ by a constant. ♠

6.6 Consequences of the Growth Formulas

Now we assume that $\{P_k\}$ and $\{Q_k\}$ and $\{F_k\}$ are all as in the Quadratic Rescaling Theorem.

Lemma 6.6 $\{F_k(0,0)\}$ *is a constant sequence.*

Proof: Using Equation 6.20 we compute $F_k(0,0) = Xk^2 + Yk + F_0(0,0)$, where

$$X = \text{Im}(P^{\#}(X_0)\overline{Q^{\#}(X_0)}) = 0;$$

$$Y = \text{Im}[P_0(X_0)\overline{Q^{\#}(X_0)} + P^{\#}(X_0)\overline{Q_0(X_0)}] = \text{Im}(\delta) = 0.$$

This completes the proof. ♠

Lemma 6.7 $\partial_j F_k(0,0) = -\Delta_j k^2 + O(k)$.

Proof: For easy reference we repeat Equations 6.20 and 6.21. For ease of notation we write $\rho = \rho(X_0)$, understanding that all our functions ρ are evaluated at X_0 unless we explicitly indicate otherwise. We will also set $M = M_j$ and $\partial = \partial_j$.

$$R_k = R^{\#}k + R_0.$$

$$\partial R_k = \left(\frac{iM}{2}R^{\#}\right)k^2 + \left(\partial R^{\#} - \frac{iM}{2}R^{\#}\right)k + \text{const.}$$

Using these equations and the identity

$$\partial F_k(0,0) = \text{Im}\big[P_k\overline{\partial Q_k} + \partial P_k\overline{Q_k}\big],$$

we just expand everything out and cancel many terms in pairs. We find that

$$\partial F_k(0,0) = Xk^3 + k^2(Y_0 + Y_1 + Y_2) + O(k).$$

Here

$$X = \frac{M}{2}\text{Im}\big[-iP^{\#}\overline{Q^{\#}} + iP^{\#}\overline{Q^{\#}}\big] = 0;$$

$$Y_0 = \text{Im}\big[P^{\#}\frac{iM}{2}\overline{Q^{\#}} - \frac{iM}{2}P^{\#}\overline{Q^{\#}}\big] = 0;$$

Now we get to the nontrivial quantities. In our calculations we use the fact that $P^{\#}$ and $Q^{\#}$ are both real at X_0.

$$Y_1 = \text{Im}\big[P^{\#}\overline{\partial Q^{\#}} + \partial P^{\#}\overline{Q^{\#}})\big] = \text{Im}\big[-P^{\#}\partial Q^{\#} + (\partial P^{\#})Q^{\#}\big] = -\text{Im}(\delta);$$

$$Y_2 = \text{Im}\big[-\frac{iM}{2}P_0\overline{Q^{\#}} + \frac{iM}{2}P^{\#}\overline{Q_0}\big] =$$

$$\text{Re}\big[-\frac{M}{2}P_0\overline{Q^{\#}} + \frac{M}{2}P^{\#}\overline{Q_0}\big] =$$

$$\text{Re}\big[-\frac{M}{2}P_0Q^{\#} + \frac{M}{2}P^{\#}Q_0\big] = \frac{-M\delta}{2}.$$

This completes the proof. ♠

Now we turn to the task of establishing Equation 6.12.

Lemma 6.8 *There is some constant M such that*

$$|C_{k,I}| < (Mk)^{|I|+2}. \tag{6.22}$$

Proof: If follows from the linear growth of $\{\widehat{P}_k\}$ and $\{\widehat{Q}_k\}$ and Equation 6.1 that

$$F_k(x_1, x_2) = \sum_{j=1}^{N_k} J_{kj}\sin(A_{kj}x_1 + B_{kj}x_2), \tag{6.23}$$

Where, for some fixed constant M, we have

$$N_k < Mk^2; \quad \max_j(|J_{kj}|) < M \quad \max_j(|A_{kj}|) < Mk; \quad \max_j(|B_{kj}|) < Mk. \tag{6.24}$$

Let D be a differential operator of order α. We have

$$DF_k(x_1, x_2) = \sum_{j=1}^{N_k} J_{D,kj} \text{trig}(A_{kj} x_1 + B_{kj} x_2),$$

where trig stands for either the sine or the cosine function, depending on the parity of α. Equation 6.24 gives us $\max_j(|J_{D,kj}|) < M^{\alpha+1} k^\alpha$. Given that the sine and cosine functions lie between -1 and 1, and that there are at most Mk^2 terms in the sum for DF_k, we have

$$\sup |DF_k| \leq (Mk)^{\alpha+2}. \tag{6.25}$$

Let (n, k) stand for "n choose k". If $I = (i_1, i_2)$ is a multi-index, with $\alpha = |I|$, then we have

$$|C_{k,I}| \leq \frac{(\alpha, i_1) \sup |D_I F_k|}{\alpha!} = \frac{(\alpha, i_1)(Mk)^{\alpha+2}}{\alpha!}. \tag{6.26}$$

Summing over all multi-indices of weight α we get

$$\sum_{I:\ |I|=\alpha} |C_{k,I}| \leq \frac{2^\alpha (Mk)^{\alpha+2}}{\alpha!} \leq (Mk)^{\alpha+2}.$$

This is Equation 6.22. ♠

Here is an improvement on Equation 6.22, at least when $|I| = 2$.

Lemma 6.9 *There is some constant M such that*

$$|I| = 2 \qquad \Longrightarrow \qquad |C_I| < (Mk)^3 \tag{6.27}$$

Proof: To simplify our notation, an expression like $D_I P_k$ shall stand for $D_I P_k(X_0)$. The functions P_k and Q_k are always evaluated at X_0. We will consider $D_{2,0} F_k(0)$, the other partial derivatives of interest having a similar analysis. By the chain rule we have $D_{2,0} F_k(0) = A + B + C$, where

$$A = \text{Im}(D_{2,0} P_k \overline{D_{0,0} Q_k}); \quad B = \text{Im}(D_{1,0} P_k \overline{D_{1,0} Q_k}); \quad C = \text{Im}(D_{0,0} P_k \overline{D_{2,0} Q_k}).$$

From Lemma 6.17 and our assumptions, there are constants $a, b \in \boldsymbol{R}$ such that

$$D_{2,0} P_k = ak^2 D_{0,0} Q_k + O(k^2); \qquad D_{1,0} P_k = b D_{1,0} Q_k + O(k).$$

Hence

$$A = \text{Im}((ak^2 D_{0,0} Q_k \times \overline{D_{0,0} Q_k}) + O(k^2) \times O(k) = O(k^3),$$

and

$$B = \text{Im}((b D_{1,0} Q_k \times \overline{D_{1,0} Q_k}) + O(k) \times O(k) = O(k^2).$$

The term C has the same treatment as A. All in all, $|D_{2,0} F| = O(k^3)$. ♠

Lemma 6.10 *Equation 6.12 holds for* $\epsilon = 1/4$.

Proof: Without loss of generality, we may take $k > 2 + M^{100}$. Given Equations 6.22 and 6.27 we have

$$\sum_{|I|\geq 2} |C_{k,I}| k^{(-2+\epsilon)|I|} \leq \sum_{|I|=2} |C_{k,I}| k^{-4+1/2} + \sum_{\alpha=3}^{\infty} \sum_{|I|=\alpha} |C_{I,k}| k^{-7\alpha/4} \leq$$

$$3Mk^{-1/2} + \sum_{\alpha=3}^{\infty} M^{\alpha+2} k^{-(3\alpha/4)+2} \leq 3Mk^{-1/2} + \sum_{\alpha=3}^{\infty} k^{-(3\alpha/2)+2+(\alpha/200)+(1/100)} \leq$$

$$3Mk^{-1/2} + \sum_{k=3}^{10} k^{-1/8} + \sum_{\alpha=10}^{\infty} k^{-\alpha} \leq 3Mk^{-1/2} + 7k^{-1/8} + 2k^{-1}.$$

This last expression tends to 0 as $k \to \infty$. ♠

The Quadratic Rescaling Theorem is an immediate consequence of the Convergence Lemma, Lemma 6.6, Lemma 6.7, and Lemma 6.10.

7 Calculating the Pivot Region

7.1 The Main Result

We defined the pivot region R_{nk} in §5.3. (We will recall the definition in the next section.) In this section we compute the asymptotic shape of this region when n is fixed and $k \to \infty$. Let T_{nk} denote the dilation which maps V_n to $(0,0)$ and dilates by a factor of k^2. Define

$$C_n = \frac{s}{(2n-2)c}; \qquad c = \cos(\frac{\pi}{2n}) \qquad s = \sin(\frac{\pi}{2n}). \tag{7.1}$$

Lemma 7.1 (Pivot) *For any n, the set $T_{nk}(R_{nk})$ converges to the infinite strip Σ_n defined by the inequalities $|x-y| < C_n$.*

Remarks: (i) When we restrict to any bounded region of the plane, the convergence we have in mind is the same discussed in Theorem 1.7.
(ii) The Pivot Lemma is sharp. As we will see in the next chapter, the limit

$$\lim_{k\to\infty} T_{nk}(O(W_{nk}))$$

turns out to have vertices on both components of $\partial\Sigma_n$.,

The rest of the chapter is devoted to proving the Pivot Lemma.

7.2 Reducing to Defining Functions

Suppose for the moment that $e(t)$ is a continuously varying segment in $\boldsymbol{R}^2$ for $t \in [0,1]$. Suppose that $e(0)$ has negative slope. Let $f(t)$ denote the height of the left endpoint of $e(t)$ minus the height of the right endpoint of $e(t)$. Note that $f(0) > 0$. We would like to make the following statements, which we call the *slope statements:*

1. $e(t)$ has negative slope $\forall t \in [0,1]$ if $f(t) > 0$ $\forall t \in [0,1]$.

2. If $f(t) < 0$ for some parameter t then $e(t)$ has positive slope at t.

We would like the slope statements to be true because we would like to define the pivot region in terms of the defining functions associated to the endpoints of the QH edges. Unfortunately, the slope statements are not necessarily true. The problem is that $e(t)$ could become vertical at some point. However, the slope statements are true if $e(t)$ has finite slope for all $t \in [0,1]$. Most of this section is devoted to dealing with this irritating hitch in the slope statements. Once we have the kink worked out, we will proceed to define the pivot region in terms of defining functions.

Recall that R_{nk} is the path component of R'_{nk} which contains V_n; and R'_{nk} is the subset of A_n consisting of points where all the QH edges of U_{nk} have negative slope. (We defined A_n in §5.3; this set is about to be replaced so we will not bother to recall the definition here.) Let $A_{nk} \subset \Delta$ denote the subset consisting of points which are within $k^{-3/2}$ of P_n. For k sufficiently large, A_{nk} is a subset of A_n, the set defined in §5.3. Notice that $T_{nk}(A_{nk})$ is a

disk of radius $k^{1/2}$. Hence $\lim_{k\to\infty} T_{nk}(R'_{nk}) = \lim_{k\to\infty} T_{nk}(R'_{nk} \cap A_{nk})$. For this reason, we will always work within A_{nk} when we analyze R'_{nk} and R_{nk}.

For the next several results we choose two points $X_0, X_1 \in A_{nk}$. We might as well take $X_0 = V_n$. Let $U_j = U(W_{nk}, X_j)$ for $j = 0, 1$.

Lemma 7.2 *Let e_0 and e_1 be corresponding edges of U_0 and U_1, which are edges of the jth triangle from the left. If U_0 and U_1 are both rotated so that the leftmost edge is horizontal then the angle between e_1 and e_2 is at most $O(jk^{-3/2})$.*

Proof: The point $\widehat{e} \in \boldsymbol{Z}^2$ corresponding to e_0 and e_1 has norm $O(j)$. Also $|X_0 - X_1| = O(k^{-3/2})$ by hypothesis. But the angle between our two edges is $|\widehat{e} \cdot (X_0 - X_1)|$, a quantity which is $O(jk^{-3/2})$. ♠

Corollary 7.3 *If U_0 and U_1 are both rotated so that the leftmost edges are horizontal, then the angle between the holonomy of U_0 and the holonomy o U_1 is $O(k^{-1/2})$.*

Proof: Here we will use the fact that $X_0 = V_n$. Let L_0 denote the line which joins up the endpoints of the 3-spine S_0 of U_0. Given the structure of U_0 discussed in §5, we see that L has length which is linear in k. The holonomy of U_0 maps the left endpoint of L_0 to the right endpoint of L_0. Let S_1 be the 3-spine of U_1. If the left endpoints of corresponding jth edges of L_0 and L_1 are matched up, then the right endpoints differ by at most $O(jk^{-3/2})$. Hence, by vector addition, we see that the right endpoints of S_0 and S_1 differ by at most

$$\sum_{j=1}^{C_n k} O(jk^{-3/2}) = O(k^{1/2}),$$

assuming that the left endpoints have been matched up. Our notation in the last estimate is a bit informal. The constant C_n is present in the sum to indicate that there are at most $C_n k$ edges in U_{nk}. Hence L_1 also has length which is linear in k. It now follows from basic trigonometry that the angle between L_0 and L_1 is $O(k^{-1/2})$. ♠

Corollary 7.4 *If $X \in A_{nk}$ and k is sufficiently large then none of the QH edges in $U(W_{nk}, X)$ is vertical.*

Proof: If U_0 and U_1 are both rotated so as to have horizontal holonomy then the angle between corresponding edges of U_0 and U_1 is at most $O(k^{-1/2})$. This is an immediate consequence of the previous two results, and the fact that there are $O(k)$ triangles in U_0 and U_1. This lemma now follows from Lemma 5.1. The idea is that the QH edges are nearly horizontal for one point in A_{nk}, and then that cannot rotate much as we move around in A_{nk}. ♠

Now we can proceed with the analysis of the region R_{nk} by means of defining functions. For each QH edge e, let $F_{nk,e}$ denote the defining function which measures the height of the

right endpoint of e minus the height of the left endpoint of e. (We normalize so that e has length 1, as in §2.) In particular, let $e_1, ..., e_8$ be the Qh edges corresponding to the extreme QH points, as discussed in §5.4. Compare Figure 5.10. Let $\widetilde{R}_{nk} \subset A_{nk}$ denote those points X such that $F_{nk,a}(X) < 0$ for $a = 1, ..., 8$. Here is the main result of this section.

Lemma 7.5 *If* $\lim_{k\to\infty} T_{nk}(\widetilde{R}_{nk}) = \Sigma_n$, *then the Pivot Lemma is true.*

Proof: As above, we use the convention that our defining functions measure the height of the left vertex minus the height of the right vertex. Let $X \in \widetilde{R}_{nk}$. The Convex Hull Lemma says that $F_{nk,e}(X) > 0$ for all QH edges e. Given Corollary 7.4 we now know that all the QH edges have negative slope. Hence $\widetilde{R}_{nk} \subset R'_{nk}$ for k sufficiently large. If $T_{nk}(\widetilde{R}_{nk})$ converges to Σ_n then the connected component U_k of $T_{nk}(\widetilde{R}_{nk})$ containing $(0,0)$ also converges to Σ_n. Since $\widetilde{R}_{nk} \subset R'_{nk}$, we see that U_k is a connected subset of R'_{nk} which contains V_n. Hence $U_k \subset T_{nk}(R_{nk})$. In summary, some subset U_k of $T_{nk}(R_{nk})$ converges to Σ_n.

Suppose we could find a sequence $\{X_k\}$ of points such that $X_k \in R_{nk}$ but $T_{nk}(X_k)$ converges to some point of $\boldsymbol{R}^2 - \Sigma_n$. Then some defining function $F_{nk,a}$ would be negative at X_k. But then, by the second slope statement and Corollary 7.4, some QH edge would have positive slope at X_k. This is a contradiction. Hence $T_{nk}(R_{nk})$ itself converges to Σ_n. ♠

7.3 Bilateral Symmetry

Now we will focus our attention on the 8 extreme QH points, the ones listed in §5.4. The important fact for us is that the coordinates of the 4 *northwest* extreme points are independent of k and the 4 *southwest* extreme points are, in a geometric sense, symmetrically located with respect to the northwest extreme points. Each pseudo-parallel family is bounded by a northwest point and a southeast point. We call two such extreme points *partners*.

Lemma 7.6 *Suppose that* F_1 *and* F_2 *are the defining functions associated to a pair of partner extreme points. Then* $F_1(x,y) = F_2(y,x)$.

Proof: The hexpath H_{nk} has bilateral symmetry across a diagonal line. If we reflect H_{nk} in its line of symmetry and trace it backwards we get the same path. Correspondingly, if we rotate U_{nk} by 180 degrees and trace it backwards we get a cyclic permutation of U_{nk}, except with the edges of type 1 and 2 reversed. From this symmetry we see that *partner extreme points correspond to edges of different types*. We label so that the extreme point corresponding to F_j has type j.

Consider the effect of changing the origin in $\boldsymbol{Z}^2$. This amounts to adding some vector V_0 to all the lattice points. If we compute our defining functions with the new labeling at X we simply multiply both P and Q by the same quantity $E(X \cdot V_0)$. Hence F is unchanged. For the duration of the lemma, we change the origin so that it lies on the line of bilateral symmetry for the hexpath H_{nk}. In this case we have $P_1(x,y) = P_2(y,x)$ by symmetry. Reflection in the main diagonal interchanges the two sets $\widehat{Q}_1$ and $\widehat{Q}_2$. Hence $Q_1(x,y) = Q_2(y,x)$. From Equation 6.1 we see that $F_1(x,y) = F_2(y,x)$. ♠

7.4 The Computation

According to the symmetry above, we just have to analyze the defining functions associated to the 4 northwest extreme points. Let $\{P_k\}$ and $\{Q_k\}$ and $\{F_k\}$ be the functions associated to one of these points. We use the convention that F_k measures the height of the right vertex minus the height of the left vertex. Referring to the setup for the Q.R.T., we have the basic constants

$$X_0 = V_n = (\frac{\pi}{2n}, \frac{\pi}{2n}) \qquad M_1 = 2n-2; \qquad M_2 = -2n+2. \tag{7.2}$$

The fundamental translation T moves points $2n-2$ units south and east. Inspecting the figures in §5.1, we see that the hexpath H_{nk}, interpreted as a function from $\boldsymbol{Z}^2$ into $\boldsymbol{Z}$ has T-linear growth. The same therefore is true of the path $\widehat{Q}$, which is derived from H_{nk} as discussed in §§2.4. By Lemma 5.1 we have $Q^{\#}(V_n) = \Psi^{\#} \in \boldsymbol{R}$. (We will give a second derivation of this fact in §8, based on the combinatorics of the 3-spine of the unfolding.)

Note that $\widehat{P}_k$ is the indicator function for a single point whose coordinates do not change with P. Hence $P^{\#}$ is the 0-function. The value of $P_k(V_n)$ is independent of both k and the choice of northwest extreme point. For the point $(0,0)$ we can see that $P_k(V_n) = \pm 1$. Our convention of the position of the left vertex minus the position of the right vertex leads to $P_k(V_n) = -1$. All in all, we have

$$P_0(V_n) = -1; \qquad P^{\#}(V_n) = \partial_i P^{\#}(V_n) = 0; \qquad \delta = Q^{\#}(V_n); \qquad \delta_j = 0. \tag{7.3}$$

From Lemma 5.1, we have $\delta = \Psi^{\#} \in \boldsymbol{R}$. Hence $\{F_k\}$ satisfies the conclusions of the Q.R.T.

Define

$$c' = \cos(\frac{\pi}{n}); \qquad s' = \sin(\frac{\pi}{n}). \tag{7.4}$$

We have $s' = 2cs$ and $c' = 2c^2 - 1$. From Lemma 5.1 we have

$$Q_0(V_n) = \Psi_1 + i4\Psi_2 = 12(1+c') + 4is' = 24c^2 + 8ics. \tag{7.5}$$

$$Q^{\#}(V_n) = \Psi^{\#} = 8(1+c') = 16c^2. \tag{7.6}$$

(We will give another derivation of this in §8. See Equation 8.1.) Combining Equation 7.3 with Equation 7.6 we see that

$$F_0(0,0) = \mathrm{Im}(P_0(V_0)\overline{Q_0(V_n)}) = 8cs; \qquad \delta = 16c^2;$$

$$-\Delta_2 = \Delta_1 = -\frac{M_1}{2}\delta + 0 = -(16n-16)(c^2) = -\frac{8cs}{C_n}. \tag{7.7}$$

According to the Q.R.T, the family of functions $\{G_k\}$ converges in the smooth topology to the function

$$G(x_1,x_2) = 8cs - \Delta_1 x_1 - \Delta_2 x_2 =$$

$$8cs + (16n-16)c^2 x_1 - (16n-16)x_2 =$$

$$8cs \times (1 + \frac{x_1}{C_n} - \frac{x_2}{C_n}). \tag{7.8}$$

This calculation agrees, for small n, with the automatic computations done by McBilliards. We now see that G is one of the two linear functions defining Σ_n. The other function comes from symmetry, as we have discussed above. This completes the proof of the Pivot Lemma.

8 Rescaling The Orbit Tiles

8.1 Overview

We continue using the notation from previous chapters. In particular, T_{nk} is the dilation which maps V_n to 0 and expands by k^2. We are interested in understanding the limits, as $k \to \infty$, of the sets

$$T_{nk}(O(W_{nk})).$$

Let a_1, a_2, a_3, a_4 be the top pivot vertices of U_{nk}, labeled from left to right. Likewise let b_1, b_2, b_3, b_4 be the bottom pivot vertices of U_{nk}, labeled from left to right. For any pair (p, q) of vertices amongst these, let $F_k[p, q]$ be the corresponding defining function. We are suppressing n from our notation. If we want to evaluate our function at a point X, we write it as $F_k[p, q](X)$. In computing these functions we will use the following sign conventions

- $F_k[a_i, b_j] > 0$ iff $a_i \uparrow b_j$.
- $F_k[a_i, a_j] > 0$ iff $a_j \uparrow a_i$.
- $F_k[b_i, b_j] > 0$ iff $b_j \uparrow b_i$.

Assuming that $\{F_k[p, q]\}$ satisfies the $G[p, q]$ denote the rescaled limit of the sequence $\{F_k[p, q]\}$. Below we will prove

Lemma 8.1 *Each of the* 3 *families*

$$\{F_k[a_1, b_2]\}; \qquad \{F_k[b_2, b_3]\}; \qquad \{F_k[b_3, a_4]\}$$

satisfies the hypotheses of the Q.R.T. for $j = 2, 3, 4$.

We will compute the scaling limits of these functions explicitly below. The work in §7 shows that each of the function families $\{F_k[a_i, b_i]\}$ satisfies the hypotheses (and hence the conclusion) of the Q.R.T. Any other function $F_k[p, q]$ can be written as a linear combination of the functions $F_k[a_i, b_i]$ and the functions from Lemma 8.1. (We will find these linear combinations explicitly below.) Hence, all our function families satisfy the conclusions of the Q.R.T.

Let $\Omega_n \subset \boldsymbol{R}^2$ denote the convex set on which all the functions $G[a_i, b_j]$ are positive. By the Q.R.T. Ω_n is a convex polygon−possibly empty or infinite−with at most 16 sides. By the same symmetry as discussed in §7, we know that Ω_n is symmetric with respect to reflection in the line $x_1 = x_2$. We also know that $\Omega_n \subset \Sigma_n$, because the defining functions for Σ_n, namely $G[a_i, b_i]$, are by definition positive on Ω_n.

Lemma 8.2 *Assume that* Ω_n *is bounded. Then* $T_{nk}(O(W_{nk}))$ *converges to* Ω_n*, in the sense mentioned in the introduction.*

Proof: Let U be any open set whose closure is contained in the interior of Ω_n. Let X be any point of $T_{nk}^{-1}(U)$. By the Pivot Lemma, $X \in R_{nk}$ for k sufficiently large. Lemma 5.3 now says that the lowest top vertex of $U(W_{nk}, X)$ is one of the a_i and the highest bottom

vertex is one of the b_j. Once k is sufficiently large, the functions $G_k[a_i, b_j]$ will all be positive on U. Hence $F_k[a_i, b_j](X) > 0$ provided that k is sufficiently large. But now we know that all the top vertices of $U(W_{nk}, X)$ lie above all the bottom vertex. Hence $X \in O(W)$. Hence $U \subset T_{nk}(O(W))$. This is Property 1 of our definition of convergence.

Suppose that we can find points $X_k \in O(W_{nk})$ such that $T_{nk}(X_k)$ converges to a point in $\boldsymbol{R}^2$ which is not contained in the closure of Ω_n. Then, for k sufficiently large, at least one of the functions $F_k[a_i, b_j]$ is negative on X_k. But then some bottom vertex of $U(W_{nk}, X_k)$ lies above some top vertex. Hence $X_k \notin O(W_{nk})$. This is a contradiction. This contradiction, establishes Property 2 of our convergence. ♠

During our proof of Lemma 8.1 we will gather enough information to compute all the functions defining Ω exactly. It is then a simple matter to check that these functions cut out precisely the region advertised in Theorem 1.7.

8.2 Asymptotic Limit Calculations

Here will prove Lemma 8.1 and compute the rescaled limits for the relevant families of functions. For each of the 3 function families of interest to us, the corresponding vertices can be connected to each other using part of the 3-spine. Figure 8.1 shows by example the general pattern for the paths $\widehat{P}$ and $\widehat{Q}$. The example corresponds to U_{41}, but every picture has the same combinatorial structure. In our figures in this chapter, the grids have edgelength 1 rather than 2, as in §5. We make the change because we want to point out integer coordinates of various points in the squarepath, and some of these coordinates might be odd.

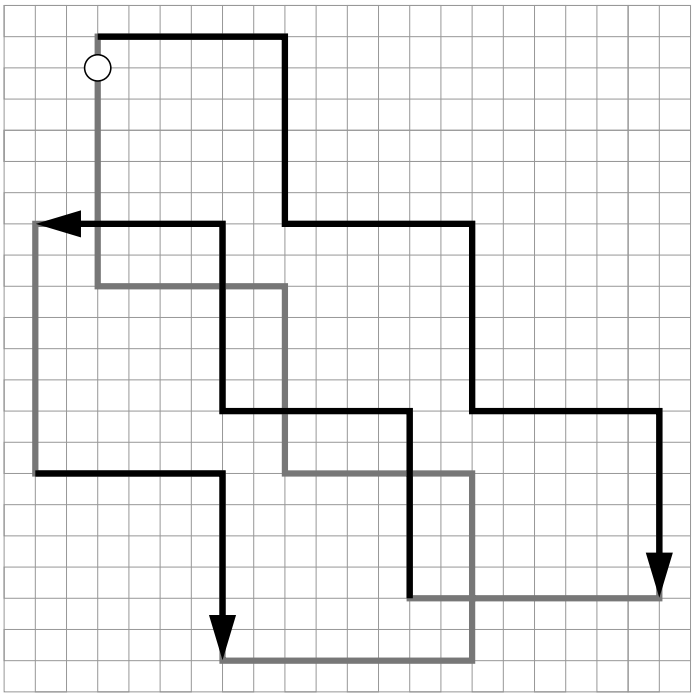

Figure 8.1: Paths in $\boldsymbol{Z}^2$.

The whole path represents $\widehat{Q}$. The white dot denotes the origin. Each of the three black paths corresponds to a different one of our function families. Tracing the path around clockwise, starting at the origin, we encounter the paths in the same order that the function families are listed. From this picture we see clearly that both $\widehat{P}$ and $\widehat{Q}$ have T linear growth, where T is as in §7. It remains to compute all the quantities relevant to the Q.R.T., for each of the three families. We will do this in a step by step fashion. To keep our pictures concrete, we will draw the case $n = 4$, though the general case is extremely similar.

8.2.1 The Holonomy Calculation

Here we compute the quantities associated to the family $\{Q_k\}$. Just by scaling we get

$$Q_0(X_0) = \lambda_n \Psi; \qquad Q^{\#}(X_0) = \lambda_n \Psi^{\#}; \qquad \lambda_n = \frac{1}{2c}. \tag{8.1}$$

We explain the constant λ_n in §8.3 below. Unfortunately, the geometric method used in the proof of Lemma 5.1 does not readily shed light on the derivatives of $Q^{\#}$. So, here we will use the combinatorial method explained in §2. At any rate, our calculations here serve as a second proof of Lemma 5.1.

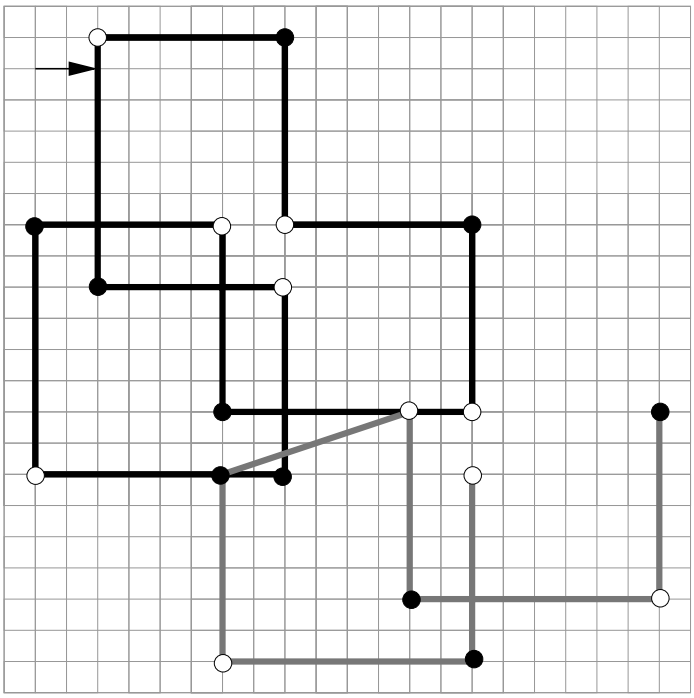

Figure 8.2: Fourier Transform of the Holonomy

Figure 8.2 shows $\widehat{Q}_0$, using the representation we discussed in §2. The big grey dot is the origin. The dots connected by the grey path are not part of $\widehat{Q}_0$. These dots are the support of $\widehat{Q}^{\#}$.

Let

$$M = 2n - 2 \tag{8.2}$$

we arrive at the following tableaux for Q_0 and $Q^{\#}$.

$$\begin{array}{cccc|cccc}
(+) & 0 & 1 & & (+) & & & \\
 & M & 1 & & . & & & \\
 & M & 1-M & & . & & & \\
 & 2M & 1-M & & & 3M & 1-2M & \\
 & 2M & 1-2M & & & 3M & 1-3M & \\
 & M-2 & 1-2M & & & 2M-2 & 1-3M & \\
 & M-2 & 1-M & & & 2M-2 & 1-2M & \\
 & -2 & 1-M & & & -2+M & 1-2M & \\
 & -2 & -1-2M & & & -2+M & -1-3M & \\
 & M & -1-2M & & & 2M & -1-3M & \\
 & M & -1-M & & & 2M & -1-2M & \\
 & 0 & -1-M & & . & & &
\end{array} \tag{8.3}$$

We determined the sign for the second tableaux by trial and error: We expect $Q^{\#}(X_0)$ to be positive real rather than negative real because our unfoldings grow in the positive direction. To help show the pattern we have staggered the entries in the tableau for $\widehat{Q}^{\#}$ to indicate their corresponding lines in the tableau for $\widehat{Q}_0$.

we use the notation

$$c = \cos(\frac{\pi}{2n}); \qquad s = \sin(\frac{\pi}{2n}). \tag{8.4}$$

as in §7. We could use the Modular Transform Lemma from §6 to evaluate the above functions and their derivatives at X_0. However, we will do the calculations symbolically in Mathematica. From Equation 8.3 we get:

$$\begin{aligned}
Q_0(X_0) &= 12c + 4is; \\
Q^{\#}(X_0) &= 8c. \\
\partial_1 Q^{\#}(X_0) &= 8i(4n-5)c; \\
\partial_2 Q^{\#}(X_0) &= 8(n-1)s - 40i(n-1)c.
\end{aligned} \tag{8.5}$$

In particular, using the double angle formulas we see that Equation 8.1 is indeed true.

8.2.2 The First Function Family

Here we compute the quantities associated to $\{P_k\}$, for $P_k[a_1, b_2]$. Figure 8.3 shows $\widehat{P}_0$ and $\widehat{P}^{\#}$.

The bottom two dots represent $\widehat{P}^{\#}$. Setting $M = 2n-2$ we read off the following function tableaux for P and $P^{\#}$.

$$\begin{array}{cccc|ccc}
(-) & 0 & 1 & & (+) & 3M & (1-2M) \\
 & M & 1 & & & 3M & (1-3M) \\
 & M & 1-M & & & & \\
 & 2M & 1-M & & & & \\
 & 2M & 1-2M & & & &
\end{array} \tag{8.6}$$

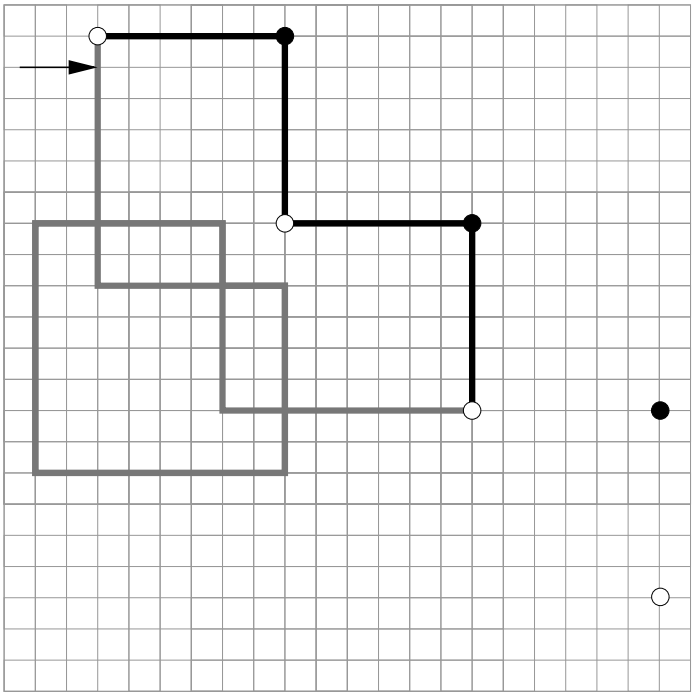

Figure 8.3: Fourier Transform for the First Path

Remarks: (i) The tableau for $\widehat{P}_0$ consists of the first 5 lines of the tableau for $\widehat{Q}_0$, and the tableau for $\widehat{P}^{\#}$ consists of the first 2 lines of the tableau for $\widehat{Q}^{\#}$. In this sense, the tableaux for $\widehat{Q}_0$ and $\widehat{Q}^{\#}$ form a kind of master list.
(ii) The fact that (by inspection) $F_0(0,0) > 0$ determines the global signs for our tableaux.

We compute symbolically from Equation 8.6 that

$$P_0(X_0) = -5c - is; \qquad P^{\#}(X_0) = -2c. \tag{8.7}$$

Next, we compute that:

$$\partial_1 P^{\#}(X_0) = 12i(n-1)c; \qquad \partial_2 P^{\#}(X_0) = 2(n-1)s - 2i(5n-6)c. \tag{8.8}$$

Equations 8.2.1 and 8.7 tells us, in particular, that $Q^{\#}(X_0)$ and $P^{\#}(X_0)$ are both real. (We could also deduce this geometrically. Combining Equations 8.2.1 and 8.7 we compute that

$$F_0(0,0) = \mathrm{Im}(-5c - is)(\overline{12c + 4is}) = 8cs = 4\sin(\frac{\pi}{n}). \tag{8.9}$$

This is the same value we got for the family considered in §7 in connection with the Pivot Lemma. We don't have an explanation for this agreement.

Next, we compute

$$\delta = \det \begin{bmatrix} -5c - is & -2c \\ 12c + 4is & 8c \end{bmatrix} = -16c^2 \in \boldsymbol{R}. \tag{8.10}$$

All the relevant quantities are real, and so the associated family $\{F_k\}$ satisfies the hypotheses of the Quadratic Rescaling Theorem. Using the formulas above we compute

$$\mathrm{Im}(\delta_1) = \mathrm{Im}\det \begin{bmatrix} -2c & -12i(n-1)c \\ 8c & 8i(4n-5)c \end{bmatrix} = 16(2n-1)c^2.$$

Similarly

$$\delta_2 = 16c^2.$$

Finally

$$\Delta_1 = \frac{2n-2}{2}\delta + \delta_1 = 16nc^2; \qquad \Delta_2 = \frac{2-2n}{2}\delta + \delta_2 = 16nc^2. \tag{8.11}$$

By the Q.R.T., the rescaled limit of the sequence $\{F_k\}$ is

$$G(x_1, x_2) = 8cs - 16nc^2x_1 - 16nc^2x_2. \tag{8.12}$$

The result agrees with the automatic computations done by McBilliards for small values of n. Note the similarity to the middle line of Equation 7.8.

8.2.3 The Second Function Family

Here we compute the quantities associated to $\{P_k\}$, for $P_k[b_2, b_3]$. Comparing Figures 8.1 and 8.2 we find that the tableau for $\widehat{P}_0$ consists of lines $6, 7, 8$ of the tableau for $\widehat{Q}_0$ and the tableau for $\widehat{P}^{\#}$ consists of lines $3, 4$ of the tableau for $\widehat{Q}^{\#}$. Here are these tableaux:

$$\begin{array}{cccc} (-) & M-2 & 1-2M \\ & M-2 & 1-M \\ & -2 & 1-M \end{array} \qquad \begin{array}{cccc} (+) & 2M-2 & 1-3M \\ & 2M-2 & 1-2M \end{array} \tag{8.13}$$

From these tableaux we compute that

$$P_0(X_0) = 3cis; \qquad P^{\#}(X_0) = 2c;$$

$$\partial_1 P^{\#}(X_0) = 4i(2n-3)c; \qquad \partial_2 P^{\#}(X_0) = 2(n-1)s - 2i(5n-6)c. \tag{8.14}$$

Using these equations, and the ones above for Q, we compute that

$$F(0,0) = 0; \quad \delta = 0; \quad \Delta_1 = \mathrm{Im}(\delta_1) = 16c^2; \quad \delta_2 = \mathrm{Im}(\delta_2) = -16c^2. \tag{8.15}$$

There $\{F_k\}$ satisfies the hypotheses of the Q.R.T. and the rescaled limit is

$$G(x_1, x_2) = -16c^2x_1 + 16c^2x_2. \tag{8.16}$$

Remark: For small values of n this agrees with the calculations made by McBilliards. For this example, it took many tries before we got the sign right. The problem is that the constant term vanishes, making it much trickier to deduce the correct sign without making an error.

8.2.4 The Third Function Family

Here we compute the quantities associated to $\{P_k\}$, for $P_k[b_3, a_4]$. Comparing Figures 8.1 and 8.2 we find that the tableau for $\widehat{P}_0$ consists of line 9 of the tableau for $\widehat{Q}_0$ and the tableau for $\widehat{P}^{\#}$ consists of lines $5, 6$ of the tableau for $\widehat{Q}^{\#}$. Here are these tableaux:

$$-2 \quad -1-2M \qquad\qquad (+) \quad \begin{matrix} -2+M & 1-2M \\ -2+M & -1-3M \end{matrix} \tag{8.17}$$

From these tableaux we compute that

$$P_0(X_0) = c + is; \qquad P^{\#}(X_0) = 2c;$$

$$\partial_1 P^{\#}(X_0) = 4i(n-2)c; \qquad \partial_2 P^{\#}(X_0) = 2(n-1)s - 2i(5n-4)c. \tag{8.18}$$

Using these equations, and the ones above for Q, we compute that

$$F(0,0) = 8cs; \quad \delta = -16c^2; \quad \delta_1 = (16+32n)c^2; \quad \delta_2 = 16c^2;$$

$$\Delta_1 = 16nc^2; \quad \Delta_2 = 16nc^2. \tag{8.19}$$

Therefore $\{F_k\}$ satisfies the hypotheses of the Q.R.T, and the rescaled limit is

$$G(x_1, x_2) = 8cs - 16nc^2 x_1 - 16nc^2 x_2. \tag{8.20}$$

For small values of n this agrees with the calculations made by McBilliards.

8.3 The Fudge Factor

Suppose that p_1, p_2, p_3 are three vertices on our unfolding. Let F_{ij} be the defining function which computes (up to scale) the height difference between p_i and p_j. Here we refer to the function defined in §2. We would like to say that $F_{13} = F_{12} + F_{23}$ but there is a catch. The functions might not all be computed with respect to the same spine of the unfolding, and thus the function values might represent differences in heights measured at different scales. This explains the fudge factor λ_n in Equation 8.1. In this section we will address this issue systematically.

Let $\theta_d(X)$ denote the sine of the angle of the triangle T_X which is opposite the dth edge. Supposing that F has been computed in terms of the d-spine, we define

$$\widetilde{F}(X) = \sin^2(\theta_d) F. \tag{8.21}$$

Then $\widetilde{F}$ measures the height difference between the relevant points when the edge of type d is scaled to have length $\sin(\theta_d)$. the exponent 2 appears in the definition because the functions P and Q both scale linearly with the edge length, and F is the imaginary part of their product.

It follows from the Law of Sines that a triangle may be scaled, with a single scale, so that its type d edge has length $\sin(\theta_d)$. Therefore, the functions $\widetilde{F}$ is computed at the same scale, independent of which spine it uses. Thus we really do have

$$\widetilde{F}_{13} = \widetilde{F}_{12} + \widetilde{F}_{23}. \tag{8.22}$$

Our modification works well with the Q.R.T. The set of functions that satisfy the conclusion of the Q.R.T. with respect to the same point X_0 forms an algebra. That is, they can be added, scaled, and multiplied together. Letting $A_k(X) = \sin(\theta_d(X))$, a function which is actually independent of the parameter k. We see easily that the sequence $\{A_k\}$ satisfies the conclusions of the Q.R.T. and has rescaled limit function $\sin_d(X_0)$. Therefore, if $\{F_k\}$ satisfies the conclusions of the Q.R.T. and has rescaled limit G, then $\{\widetilde{F}_k\}$ also satisfies the conclusions of the Q.R.T. and has rescaled limit

$$\widetilde{G} = \sin(\theta_d(X_0)G. \tag{8.23}$$

In the examples of interest to us, we have the following conversions: If G is based on the 3-spine then

$$\widetilde{G} = (s')^2 G = 4c^2 s^2 G. \tag{8.24}$$

If G is based on either the 1-spine or the 2-spine then

$$\widetilde{G} = s^2 G. \tag{8.25}$$

Working with the $\widetilde{G}$ limits instead of the G limits, we can add and subtract with impunity.

8.4 The Shapes of the Tiles

In this section we compute the region Ω_n, using the explicit formulas for the functions defining Ω_n. Our first task is to write down all these functions. To make our notation simpler, we will understand that our functions are always evaluated at the point (x_1, x_2). We will also use the notation

$$\begin{bmatrix} A \\ B \\ C \end{bmatrix} = A + Bx_1 + Cx_2. \tag{8.26}$$

In the language of §7.3, the first and third hinges of the unfolding U_{nk} correspond to northwest extreme points, and the second and fourth hinges correspond to southeast extreme points. Combining Lemma 7.6 and Equation 7.8 we see that

$$\widetilde{G}[a_1, b_1] = \widetilde{G}[a_3, b_3] = \begin{bmatrix} 8cs^3 \\ 16(n-1)c^2s^2 \\ -16(n-1)c^2s^2 \end{bmatrix} \tag{8.27}$$

$$\widetilde{G}[a_2, b_2] = \widetilde{G}[a_4, b_4] = \begin{bmatrix} 8cs^3 \\ -16(n-1)c^2s^2 \\ 16(n-1)c^2s^2 \end{bmatrix} \tag{8.28}$$

Again, these are the functions which define the strip Σ_n from the Pivot Lemma. Summarizing the calculations we made in this chapter, we have

$$\widetilde{G}[a_1, b_2] = \widetilde{G}[a_4, b_3] = \begin{bmatrix} 32c^3s^3 \\ -64nc^4s^2 \\ -64nc^4s^2 \end{bmatrix}; \qquad \widetilde{G}[b_2, b_3] = \begin{bmatrix} 0 \\ -64c^4s^2 \\ +64c^4s^2 \end{bmatrix}. \tag{8.29}$$

To explain the rules we use to compute the rest of the defining functions, we simplify our notation. We let $[a_i b_j]$ stand for $\widetilde{G}[a_i, b_j]$. Using our sign conventions above (and checking the signs against the output from McBilliards) we find that

- $[a_1 b_3] = [a_1 b_2] - [b_2 b_3]$
- $[a_4 b_2] = [a_4 b_3] + [b_2 b_3]$
- $[a_1 b_4] = [a_1 b_3] - [a_4 b_3] + [a_4 b_4]$
- $[a_2 b_1] = [a_2 b_2] - [a_1 b_2] + [a_1 b_1]$
- $[a_2 b_3] = [a_2 b_2] - [b_2 b_3]$
- $[a_2 b_4] = [a_2 b_3] - [a_4 b_3] + [a_4 b_4]$
- $[a_3 b_1] = -[a_1 b_3] + [a_3 b_3] + [a_1 b_1]$
- $[a_3 b_2] = [a_3 b_3] + [b_2 b_3]$
- $[a_3 b_4] = -[a_4 b_3] + [a_3 b_3] + [a_4 b_4]$
- $[a_4 b_1] = [a_4 b_4] + [a_1 b_1] - [a_1 b_4]$

Since we are only interested in pairs of the form $[a_i b_j]$ we further compress our notation and write $[ij] = [a_i b_j] = \widetilde{G}[a_i, b_j]$. We computed all the above quantities symbolically and noticed a lot of symmetry. To help express this symmetry we write $[i_1 j_1] \sim [i_2 j_2]$ if the map $(x_1, x_2) \to (x_2, x_1)$ conjugates the one function to the other. We compute the following relations:

1. $[13] \sim [42]$.
2. $[24] \sim [31]$.
3. $\frac{1}{2} \times [13] + \frac{1}{2} \times [42] = [12] = [43]$.
4. $\frac{1}{2} \times [24] + \frac{1}{2} \times [31] = [21] = [34]$.
5. $\frac{1}{2} \times [13] + \frac{1}{2} \times [31] = [11] = [33] \sim [22] = [44]$.
6. $t \times [11] + (1-t) \times [44] = [14] = [32] \sim [23] = [41]$, where $t = 2c^2/(n-1)$.

(We recall that $c = \cos(\pi/2n)$.)

The above relations easily imply that all the defining functions are convex combinations of

$$[13] \sim [42]; \quad [24] \sim [31]$$

Hence Ω_n is defined by these 4 alone. Now that we are done adding these functions together, we can replace them by positive multiples and still define the same region in the plane. Setting

$$\sigma = \sec(\pi/n) = \frac{1}{2c^2 - 1} \tag{8.30}$$

we compute

$$[13] \propto \begin{bmatrix} 1 \\ -2(n-1)(c/s) \\ -2(n+1)(c/s) \end{bmatrix}; \qquad [24] \propto \begin{bmatrix} -1 \\ 2(c/s)(n+1+\sigma) \\ 2(n-1)(c/s)(1+2\sigma) \end{bmatrix}. \tag{8.31}$$

Now we dilate the plane by

$$\zeta_n := 2(n-1)(c/s).$$

The region $\zeta_n \Omega_n$ is the region cut out by the defining functions obtained from the ones above (and their symmetric conjugates) by dividing all the second and third coordinate entries by ζ_n. That is, $\zeta_n \Omega_n$ is defined by the functions:

$$\begin{bmatrix} 1 \\ -\frac{n+1}{n-1} \\ -1 \end{bmatrix}; \qquad \begin{bmatrix} -1 \\ \frac{1+n+2\sigma}{n-1} \\ 1+2\sigma \end{bmatrix}; \qquad \begin{bmatrix} -1 \\ 1+2\sigma \\ \frac{1+n+2\sigma}{n-1} \end{bmatrix}; \qquad \begin{bmatrix} 1 \\ -1 \\ -\frac{n+1}{n-1} \end{bmatrix}. \tag{8.32}$$

Setting

$$\mu_n = \frac{1}{2} - \frac{\tan^2(\pi/2n)}{2} \tag{8.33}$$

we now list the vertices from Theorem 1.7, modified so that their first coordinate is padded with a 1.

$$\begin{bmatrix} 1 \\ -\frac{1}{n} \\ 1-\frac{1}{n} \end{bmatrix}; \qquad \begin{bmatrix} 1 \\ \frac{1}{2}-\frac{1}{2n} \\ \frac{1}{2}-\frac{1}{2n} \end{bmatrix}; \qquad \begin{bmatrix} 1 \\ 1-\frac{1}{n} \\ -\frac{1}{n} \end{bmatrix}; \qquad \begin{bmatrix} 1 \\ \mu_n(\frac{1}{2}-\frac{1}{2n}) \\ \mu_n(\frac{1}{2}-\frac{1}{2n}) \end{bmatrix}; \tag{8.34}$$

We claim that $\zeta_n \Omega$ is the convex hull of the vertices from Theorem 1.7. To see this, it suffices to show that the matrix of dot products between the vectors in Equation 8.32 and the vectors in Equation 8.34 is non-negative, and has two zeros in each row and column. Here is the matrix

$$\begin{bmatrix} \frac{2}{n-1} & \beta & 0 & 0 \\ 0 & \sigma & \sigma & 0 \\ 0 & 0 & \beta & \frac{2}{n-1} \\ \frac{1}{2c^2} & 0 & 0 & \frac{1}{2c^2} \end{bmatrix}; \qquad \beta = \frac{2\sigma(n-2-\cos(\pi/n))}{n-1} \tag{8.35}$$

This completes our verification that $\zeta_n \Omega_n$ is the convex hull of the above mentioned vertices.

We got Ω_n as the limit of rescaling by a quadratic family $\{T_{nk}\}$ of dilations. If we had used the quadratic family $\{\zeta_n T_{nk}\}$ instead, we would get $\zeta_n \Omega$ right on the nose. This is the family $\{S_{nk}\}$ we use for the proof of Theorem 1.7. This completes our proof of Theorem 1.7.

As a final remark, we calculate that both functions [13] and [31] vanish at a common vertex of Ω_n. Hence the function [11], one of the defining functions for Σ_n, also vanishes at this vertex. Hence Ω_n has a vertex on $\partial\Sigma_n$. By symmetry, Ω_n intersects both components of $\partial\Sigma_n$ in a vertex. This justifies our comment, in §7, that the Pivot Lemma is sharp.

9 Stability questions

In this section, we prove Theorem 1.5. Recall that V_n for $n \geq 3$ is the obtuse isosceles triangle with two angles of measure $\pi/(2n)$. We will prove that if n is a power of two, then V_n has no stable periodic billiard paths. For n not a power of two, we will construct a stable periodic billiard path.

Remarks 9.1 (Errors Corrected) *This version of the paper corrects errors in the published version of the document, [HS09]. These errors occurred in sections 9.3 and 9.5. Namely, Lemma 2.2 is corrected and clarified from the corresponding statement in the published document. More fundamentally, the homology classes corresponding to stable periodic billiard paths in the published version of section 9.5 were incorrect. This version contains corrected formulas for these classes, and more detailed proofs. The authors would like to thank Yilong Yang for pointing out the errors in [HS09].*

9.1 A Homological Condition for Stability

Given a triangle T, let $\mathcal{D}T$ denote its double with the vertices removed. (The double of a polygon can be thought of a pillowcase for a pillow made in the shape of the polygon.) See Figure 9.1. There is a natural folding map $f : \mathcal{D}T \to T$ which sends each of the two triangles making up $\mathcal{D}T$ isometrically to T. (This map folds in the sense that is 2-1 except on the edges of the triangle, where it is 1-1.) If $\tilde{p}$ is a closed geodesic on $\mathcal{D}T$, then $f(\tilde{p})$ is a periodic billiard path. Conversely, if p is a periodic billiard path in T (which hits an even number of sides in a period), then there is a closed geodesic lift $\tilde{p}$ with $f(\tilde{p}) = p$. The lift $\tilde{p}$ is unique up to the single non-trivial automorphism of the folding map f, which preserves the labeling of edges and swaps the two triangles.

Lemma 9.2 *A periodic billiard path p in a triangle T is stable if and only if its lift $\tilde{p}$ to the double $\mathcal{D}T$ is null homologous (equivalent to zero in $H_1(\mathcal{D}T, \boldsymbol{Z})$).*

Remark: Because we removed the vertices of the triangles from $\mathcal{D}T$, $\mathcal{D}T$ is topologically a 3-punctured sphere. Thus, $H_1(\mathcal{D}T, \boldsymbol{Z}) \cong \boldsymbol{Z}^2$

Proof: This is formally a restatement of Lemma 2.2. The total sign counted for the edge labeled 1 in Lemma 2.2 is equivalent to computing the algebraic sign of the intersection of $\tilde{p}$ with the lift of the edge labeled 1 to $\mathcal{D}T$. Having zero algebraic intersection number with each of the lifts of an edge to $\mathcal{D}T$ is equivalent to being null homologous. ♠

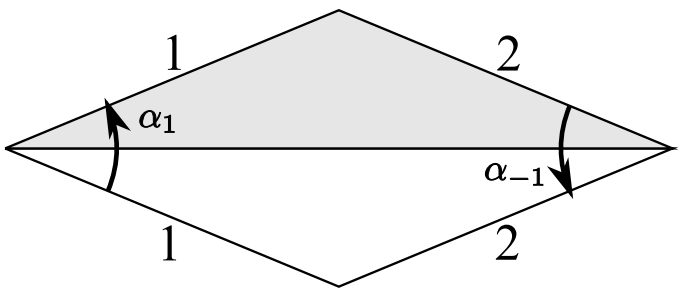

Figure 9.1 The double $\mathcal{D}T$ of the triangle $T = V_4$. The numerals indicate pairs of edges which are glued together by an orientation preserving isometry of the plane.

9.2 Translation surfaces and Veech's lattice property

We will need to understand some of the implications of work of Veech [Vee89]. For this, we introduce some of the ideas appearing in the study of translation surfaces. See [MT02] for a more thorough introduction.

A *translation surface* is a union of polygonal subsets of the plane with edges glued together pairwise by translation. There is a natural translation surface associated to every triangle T. Let $G = \langle r_1, r_2, r_3 \rangle$ denote the subgroup of $Isom(\boldsymbol{R}^2)$ generated by the reflections in the sides of the triangle T. The translation surface $S(T)$ is the disjoint union of the triangles $g(T)$ with $g \in G$ with some identifications. Two triangles $g_1(T)$ and $g_2(T)$ are identified by translation if $g_1 \circ g_2^{-1}$ is a translation. Also, we identify two triangles $g_1(T)$ and $g_2(T)$ along the i-th edge by translation if $g_1 \circ g_2^{-1}$ can be written as a composition of r_i and a translation.

The resulting surface $S(T)$ is the smallest translation surface cover of $\mathcal{D}T$. The covering map is the map which sends each triangle in $S(T)$ isometrically to the triangle in $\mathcal{D}T$ with the same orientation. In this section, we follow the convention that the vertices of the triangles making up $S(T)$ are removed. (These points are really cone points, we only remove them to make our topological notation simpler.)

Since a translation surface is built from polygonal subsets of the plane glued together by translations, the surface inherits a notion of the *direction* of a unit tangent vector. This notion of direction is just the measure of angle compared to a horizontal vector. This notion of direction is a fibration from the unit tangent bundle $T_1S(T)$ to the circle $\boldsymbol{R}/2\pi\boldsymbol{Z}$.

There is a natural action of the affine group $SL(2, \boldsymbol{R})$ on the space of translation surfaces. Suppose $A \in SL(2, \boldsymbol{R})$ and S is a translation surface, then we will define $A(S)$. Suppose S is the disjoint union of the polygonal subsets of the plane P_i with $i \in \Lambda$ with edges identified pairwise by translation. Let $A(S)$ be the disjoint union of the polygons $A(P_i)$ with A acting linearly on the plane with the same edge identifications. The new edge identifications are also by translation. This is possible because A sends parallel lines to parallel lines and preserves the ratio's of lengths of pairs of parallel segments.

The *Veech group* $\Gamma(S)$ is the subgroup of elements $A \in SL(2, \boldsymbol{R})$ such that there is a direction preserving isometry $\varphi_A : A(S) \to S$. We abuse notation by using A to denote the natural map from $S \to A(S)$ given by the restriction of the action of A on the plane to the polygonal subsets of the plane making up S. The map $\varphi_A \circ A : S \to S$ is known as an affine automorphism of S. The set of such maps forms a group known as the *affine automorphism group* of S.

The Veech group $\Gamma(S)$ is always discrete. We say S has the *lattice property* if $\Gamma(S)$ is a lattice in $SL(2, \boldsymbol{R})$. We will utilize the following consequence of Veech's work. If a translation surface has the lattice property, then the collection of closed geodesics on S can be well understood.

A direction $\theta \in \boldsymbol{R}/2\pi\boldsymbol{Z}$ is called a *completely periodic direction* for a translation surface S if every bi-infinite geodesic in this direction is closed.

Theorem 9.3 (Veech Dichotomy) *Suppose S has the lattice property. Let $\theta \in \boldsymbol{R}/2\pi\boldsymbol{Z}$ be a direction. Then either θ is a completely periodic direction for S or the geodesic flow in the direction θ is uniquely ergodic. Moreover, θ is completely periodic if and only if there is a parabolic $A \in \Gamma(S)$ for which θ is an eigendirection.*

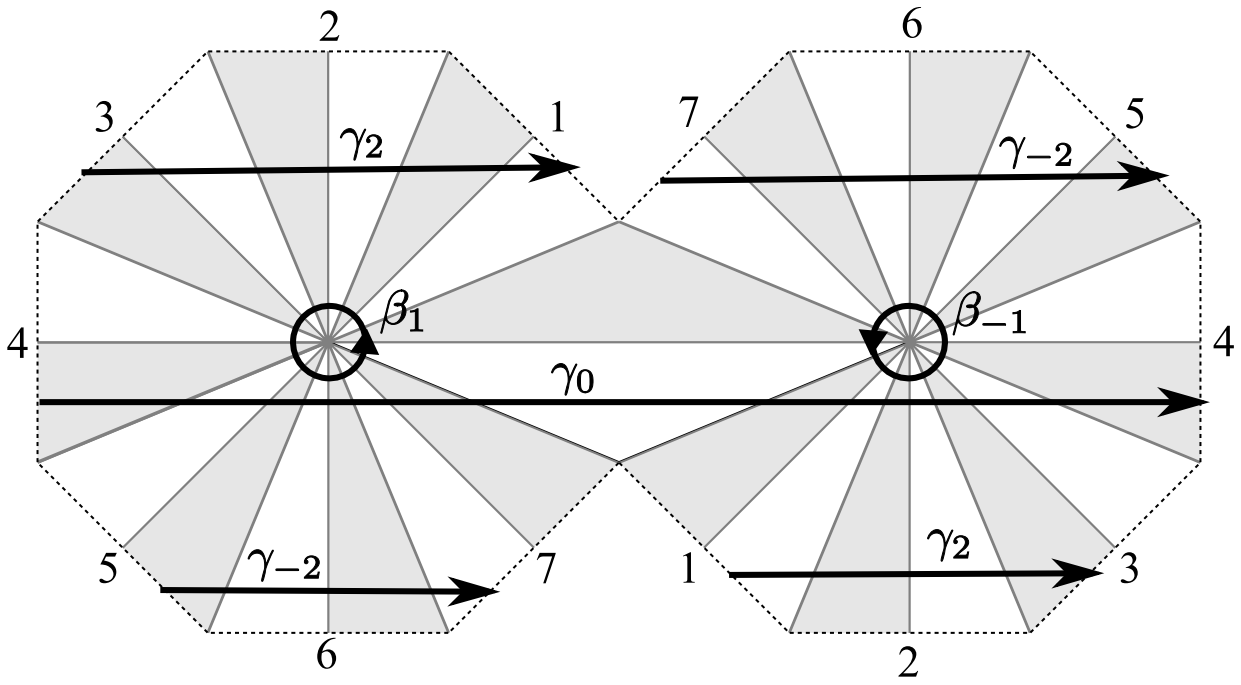

Figure 9.2: The translation surface $S(V_4)$. All but two of the obtuse isosceles triangles have been split along their axes of symmetries. Numbers indicate edge identifications by translations. Curves in the homology classes β_{-1}, β_1, γ_{-2}, γ_0 and γ_2 are shown.

Veech showed that $S(V_n)$ has the lattice property.

We will now carefully describe $S(V_n)$, so that we can explicitly use Veech's property. See Figure 9.2 for visual guidance. To build $S(V_n)$, start with a copy of V_n oriented in the plane so that longest side lies on the x-axis. Cut this triangle in two along the axis of symmetry. Reflecting each half repeated along the edges it shares with V_n yields two regular $2n$-gons. The halves can then be reassembled by gluing according to appropriate translations. This amounts to gluing each edge of the left regular $2n$-gon to the opposite side of the right $2n$-gon by translation. We remove the center point of each $2n$-gon and also the vertices of the $2n$-gon, since these points correspond to vertices of lifts of our triangle V_n. (This removal of vertices will make our homological notation simpler.)

Theorem 9.4 (Veech) *Let $n \geq 3$. The Veech group $\Gamma\big(S(V_n)\big)$ is a hyperbolic (n, ∞, ∞) triangle group. The group $\Gamma\big(S(V_n)\big) = \langle A, B \ : \ (A \circ B^{-1})^n = e \rangle$ is generated by parabolics which fix the directions of angle 0 or $\frac{\pi}{2n}$. The corresponding affine automorphisms act as single right Dehn twists in each maximal cylinder in the respective eigendirection.*

We enjoy the following consequence.

Lemma 9.5 (Enumeration) *If p_1 is a closed geodesic on $S(V_n)$ then there is a closed geodesic p_0 in the directions 0 or $\frac{\pi}{2n}$ and an affine automorphism $\varphi_D \circ D$ which maps p_1 onto p_0.*

Proof: The direction of p_1 is not uniquely ergodic. Thus by Veech dichotomy, this direction must be an eigendirection for a parabolic $C \in \Gamma\big(S(V_n)\big)$. Because of the structure of the group, there must be an $D \in \Gamma\big(S(V_n)\big)$ and an integer $k \neq 0$ such that either $D \circ C \circ D^{-1} = \pm A^k$ or $D \circ C \circ D^{-1} = \pm B^k$. Then D maps the direction of p_1 onto either the direction 0 or $\frac{\pi}{2n}$. It follows that the affine automorphism corresponding to D sends the geodesic p_1 to a geodesic which travels in either the direction 0 or $\frac{\pi}{2n}$. This image is our p_0. ♠

9.3 Generators for the Affine Automorphism Group

In this subsection, we combine the idea of Lemma 9.2 with Veech's lattice property to yield necessary and sufficient conditions for stability of a periodic billiard path in V_n constructed via the affine automorphism group of $S(V_n)$.

Topologically, $\mathcal{D}V_n$ is a 3-punctured sphere. We choose generators α_1 and α_{-1} for $H_1(\mathcal{D}V_n, \boldsymbol{Z}) \cong \boldsymbol{Z}^2$. See Figure 9.1.

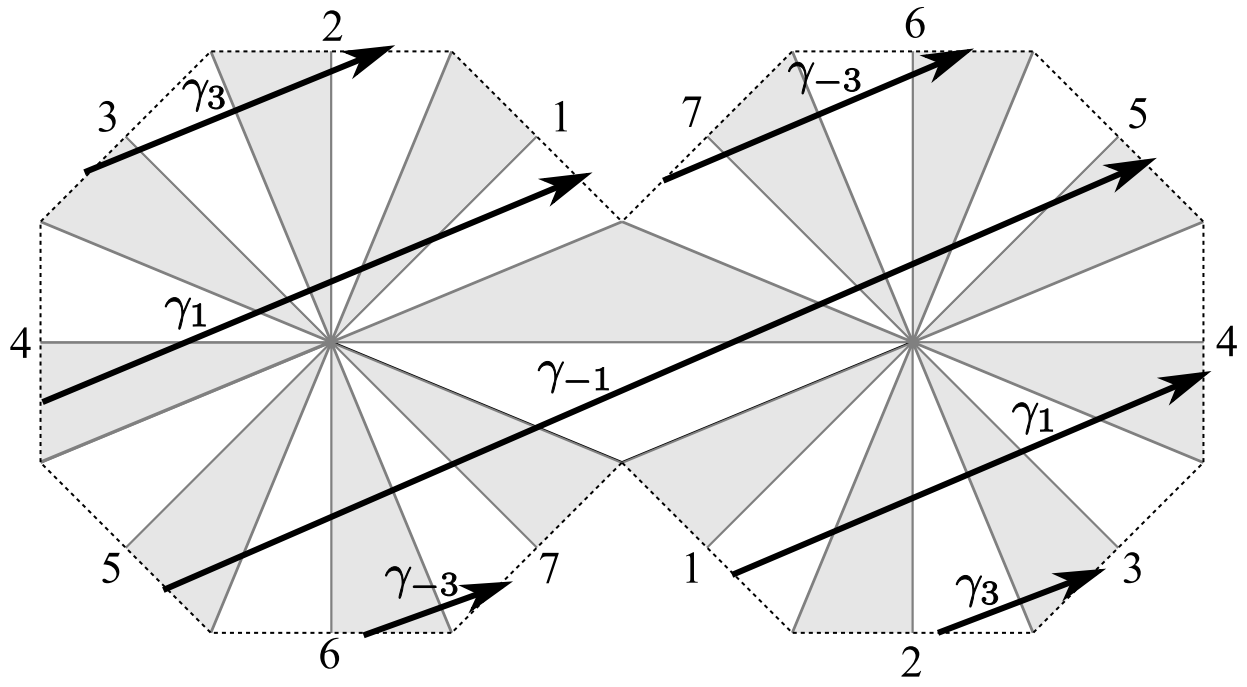

Figure 9.3: The translation surface $S(V_4)$. Curves in the homology classes γ_{-3}, γ_{-1}, γ_1 and γ_3 are shown

We choose a basis for the homology group $H_1\big(S(V_n), \boldsymbol{Z}\big) \cong \boldsymbol{Z}^{2n+1}$. Our basis is the homology classes of the collection of curves

$$\mathcal{B} = \{\beta_1, \beta_{-1}, \gamma_{1-n}, \ldots, \gamma_{n-1}\}$$

depicted in Figures 9.2 and 9.3. The homology classes γ_k with k even all contain horizontal geodesics. We order them so that the portions of these geodesics in the left polygon increase in y coordinate as the index k increases. The homology class γ_0 is chosen so that a geodesic

in this class travels below the centers of the two $2n$-gons. The homology classes γ_k with k odd all contain geodesics which travel in the direction of angle $\frac{\pi}{2n}$. With the correct choice of indices, we have algebraic intersection numbers $\gamma_{2i} \cap \gamma_{2i+1} = 1$ and $\gamma_{2i} \cap \gamma_{2i-1} = 1$, but no other pairs of curves intersect.

We think of first cohomology, $H^1\big(S(V_n), \boldsymbol{Z}\big)$, as the dual space to homology. Let

$$\mathcal{B}^* = \{\beta_1^*, \beta_{-1}^*, \gamma_{1-n}^*, \ldots, \gamma_{n-1}^*\}$$

denote the dual basis for $H^1\big(S(V_n), \boldsymbol{Z}\big)$.

Consider the natural covering map $\phi : S(V_n) \to \mathcal{D}T$. Let $\phi : H_1\big(S(V_n), \boldsymbol{Z}\big) \to H_1(\mathcal{D}T, \boldsymbol{Z})$ be the induced map on homology. This satisfies the following properties:

- $\phi(\beta_i) = 2n\alpha_i$ for $i \in \{1, -1\}$.
- $\phi(\gamma_k) = \begin{cases} (n+k)\alpha_1 - (n+k)\alpha_{-1} & \text{if } k < 0 \\ n\alpha_1 + n\alpha_{-1} & \text{if } k = 0 \\ (k-n)\alpha_1 + (n-k)\alpha_{-1} & \text{if } k > 0 \end{cases}$

Using ϕ, we get elements of the cohomology group $H^1\big(S(V_n), \boldsymbol{Z}\big)$, given by the coefficients of α_1 and α_{-1}. Denote these elements by ϕ_1^* and ϕ_{-1}^*. We think of these as maps of the form $H_1\big(S(V_n), \boldsymbol{Z}\big) \to \boldsymbol{Z}$. They satisfy $\phi(x) = \phi_1^*(x)\alpha_1 + \phi_{-1}^*(x)\alpha_{-1}$. We have

$$\begin{aligned} \phi_1^* &= 2n\beta_1^* + \gamma_{1-n}^* + 2\gamma_{2-n}^* + \ldots + n\gamma_0^* - (n-1)\gamma_1^* - (n-2)\gamma_2^* - \ldots - \gamma_{n-1}^* \\ \phi_{-1}^* &= 2n\beta_{-1}^* - \gamma_{1-n}^* - 2\gamma_{2-n}^* - \ldots - (n-1)\gamma_{-1}^* + n\gamma_0^* + (n-1)\gamma_1^* + \ldots + \gamma_{n-1}^*. \end{aligned} \tag{9.1}$$

We now describe the action of the affine automorphism group on $S(V_n)$. If g is an element of this affine automorphism group, we also use g to denote the induced action on homology, and use g^* to denote the pullback action. That is, if $\eta^* \in H^1\big(S(V_n), \boldsymbol{Z}\big)$ and g is an affine automorphism of $S(V_n)$ acting on homology, then

$$\big(g^*(\eta^*)\big)(x) = \eta^*\big(g^{-1}(x)\big) \quad \text{for all } x \in H_1\big(S(V_n), \boldsymbol{Z}\big).$$

(So, viewed as matrices acting on our bases, g^* is the inverse transpose of g.) For the formulas that follow, we follow the convention $\gamma_{-n} = \gamma_n = 0$ and $\gamma_{-n}^* = \gamma_n^* = 0$. The affine automorphism group of $S(V_n)$ is generated by the following elements:

- The involution which swaps the two regular $2n$-gons. The actions on homology and cohomology are given by

$$\sigma : \ \beta_i \mapsto \beta_{-i} \ : \ \gamma_k \mapsto \gamma_{-k} \tag{9.2}$$

$$\sigma^* : \ \beta_i^* \mapsto \beta_{-i}^* \ : \ \gamma_k^* \mapsto \gamma_{-k}^*. \tag{9.3}$$

- The right Dehn twists in the odd cylinders. The actions on homology and cohomology are given by

$$\tau_o : \ \beta_i \mapsto \beta_i \ : \ \gamma_k \mapsto \begin{cases} \gamma_k & \text{if } k \text{ is odd} \\ \gamma_{k-1} + \gamma_k + \gamma_{k+1} & \text{if } k \text{ is even} \end{cases} \tag{9.4}$$

$$\tau_o^* : \ \beta_i^* \mapsto \beta_i^* \ : \ \gamma_k^* \mapsto \begin{cases} -\gamma_{k-1}^* + \gamma_k^* - \gamma_{k+1}^* & \text{if } k \text{ is odd} \\ \gamma_k^* & \text{if } k \text{ is even} \end{cases} \tag{9.5}$$

- The right Dehn twists in the even cylinders. The actions on homology and cohomology are given by

$$\tau_e:\ \beta_i \mapsto \beta_{-i}\ :\ \gamma_k \mapsto \begin{cases} \gamma_k & \text{if } k \text{ is even} \\ -\beta_{-k}+\gamma_{k-1}+\gamma_k+\gamma_{k+1} & \text{if } k \in \{-1,1\} \\ \gamma_{k-1}+\gamma_k+\gamma_{k+1} & \text{if } k \text{ is odd and } k \notin \{-1,1\} \end{cases} \tag{9.6}$$

$$\tau_e^*:\ \beta_i^* \mapsto \beta_{-i}^*+\gamma_i^*\ :\ \gamma_k^* \mapsto \begin{cases} \gamma_k^* & \text{if } k \text{ is odd} \\ -\gamma_{k-1}^*+\gamma_k^*-\gamma_{k+1}^* & \text{if } k \text{ is even} \end{cases} \tag{9.7}$$

We also record the action of $(\tau_e^*)^{-1}$:

$$(\tau_e^*)^{-1}:\ \beta_i^* \mapsto \beta_{-i}^*-\gamma_{-i}^*\ :\ \gamma_k^* \mapsto \begin{cases} \gamma_k^* & \text{if } k \text{ is odd} \\ \gamma_{k-1}^*+\gamma_k^*+\gamma_{k+1}^* & \text{if } k \text{ is even} \end{cases}$$

The work above gives us an method to prove the existence or non-existence of a stable periodic billiard path. By the Enumeration Lemma, every closed geodesic $S(V_n)$ is the image of one of the geodesics in one of the homology classes $\gamma_{1-n},\ldots,\gamma_{n-1}$ under an affine automorphism in $\langle \sigma, \tau_o, \tau_e \rangle$. Let $x \in H_1\big(S(V_n), \boldsymbol{Z}\big)$ be the homology class of a closed geodesic on $S(V_n)$. Then there is a $w \in \langle \sigma, \tau_o, \tau_e \rangle$ such that $x = w(\gamma_k)$. For x to be stable, we must have $\phi(x) = 0 \in H_1(\mathcal{D}T, \boldsymbol{Z})$. This is equivalent to saying that $\phi_i^*(x) = 0$ for each $i \in \{-1,1\}$. Since w^* denotes the pullback action on cohomology, observe that for $i \in \{-1,1\}$, we have

$$\phi_i^*(x) = \phi_i^*\big(w(\gamma_k)\big) = \big((w^*)^{-1}(\phi_i^*)\big)(\gamma_k).$$

In particular, the geodesic in the homology class x is stable if and only if for each $i \in \{-1,1\}$, when $(w^*)^{-1}(\phi_i^*)$ is written in the basis $\mathcal{B}^*$, the coefficient of γ_k^* is zero. We summarize these conclusions in the proposition below.

Proposition 9.6 *Let $x = w(\gamma_k) \in H_1\big(S(V_n), \boldsymbol{Z}\big)$ be the homology class of a geodesic in $S(V_n)$. The corresponding billiard path in V_n is stable if and only if for each $i \in \{-1,1\}$, when $(w^*)^{-1}(\phi_i^*)$ is written in the basis $\mathcal{B}^*$, the coefficient of γ_k^* is zero.*

We simplify this proposition by noting the following:

Proposition 9.7 *The cohomology class $\phi_1^*+\phi_{-1}^* = 2n\beta_1+2n\beta_{-1}+2n\gamma_0^*$ is invariant under the group action $\langle \sigma^*, \tau_o^*, \tau_e^* \rangle$.*

Proof: We check the least trivial case of the action of τ_e^*, and leave the other cases to the reader:

$$\begin{aligned} \tau_e^*(2n\beta_1^*+2n\beta_{-1}^*+2n\gamma_0^*) &= 2n(\beta_{-1}^*+\gamma_1^*)+2n(\beta_1^*+\gamma_{-1}^*)+2n(-\gamma_{-1}^*+\gamma_0^*-\gamma_1^*) \\ &= 2n\beta_1^*+2n\beta_{-1}^*+2n\gamma_0^*. \end{aligned}$$

♠

We give a more careful statement of our final conclusions below:

Lemma 9.8 (Stability) *Suppose p is a periodic billiard path in V_n. Then, there is a lift to a closed geodesic $\tilde{p}$ in $S(V_n)$. Let x be the homology class of $\tilde{p}$. By the Enumeration Lemma, $x = w(\gamma_k)$ for some affine automorphism w in the group $\langle \sigma, \tau_o, \tau_e \rangle$ and some $k \in \{1-n, \ldots, n-1\}$. Then, p is stable if and only if $k \neq 0$ and when $(w^*)^{-1}(\phi_1^*)$ is written in the basis $\mathcal{B}^*$, the coefficient of γ_k^* is zero.*

Proof: This Lemma is essentially the same as Proposition 9.6. We observe that stability is equivalent to the statement that the coefficients of γ_k^* is zero for the cohomology class $(w^{-1})^*(\phi_1^*)$ and the invariant cohomology class $(w^{-1})^*(\phi_1^* + \phi_{-1}^*) = \phi_1^* + \phi_{-1}^*$. The coefficient of γ_k^* of $\phi_1^* + \phi_{-1}^*$ is zero if and only if $k \neq 0$. ♠

9.4 Instability

Suppose that $n = 2^m$ for an integer $m \geq 2$. We will use the Stability Lemma to show that V_n has no stable periodic billiard paths. We will show that the condition for stability given in the Stability Lemma can not hold modulo $2n = 2^{m+1}$; i.e. for the corresponding cohomology classes in $H^1\big(S(V_n), \boldsymbol{Z}/2n\boldsymbol{Z}\big)$.

The following holds for all n, though we will only use it for powers of two.

Proposition 9.9 *Let $w^* \in \langle \sigma^*, \tau_o^*, \tau_e^* \rangle$. There exist odd integers r, s such that*

$$w^*(\phi_1^*) \equiv \sum_{i=1-n}^{n-1} c(i)\gamma_i^* \pmod{2n}$$

with coefficients given by

$$c(i) = \begin{cases} r(i+n) & \text{if } i \text{ is odd} \\ s(i+n) & \text{if } i \text{ is even.} \end{cases}$$

Proof of part 1 of Theorem 1.5: We assume $n = 2^m$. Our numbers i lie within the set $\{1-n, \ldots, n-1\}$ in particular $i+n$ is never equivalent to zero modulo $2n$. Multiplication by an odd number permutes the classes of $\boldsymbol{Z}/2n\boldsymbol{Z} = \boldsymbol{Z}/2^{m+1}\boldsymbol{Z}$ and preserves zero. Thus, $r(i+n)$ is never equivalent to zero modulo 2^{m+1}. Therefore, the Stability Lemma implies that there can be no stable periodic billiard paths in V_n. ♠

Proof of Proposition 9.9: The proof is by induction in the group $\langle \sigma, \tau_o, \tau_e \rangle$. The statement is true for the identity element with $r = s = 1$. See Equation 9.1.

We set up some notation. Let $\mathbf{E}$ and $\mathbf{O}$ denote the even and odd integers in $\{1-n, \ldots, n-1\}$. We find it convenient (as before) to let γ_n^* and γ_{-n}^* represent the zero cohomology class.

Now suppose that the statement is true for the group element w_0^* for the odd numbers r and s. That is, suppose that in $H^1(S(V_n), \boldsymbol{Z}/2n\boldsymbol{Z})$,

$$w_0^*(\phi_1^*) = \sum_{i \in \mathbf{O}} r(i+n)\gamma_i^* + \sum_{i \in \mathbf{E}} s(i+n)\gamma_i^*.$$

By Equation 9.3, applying the involution σ^* yields:

$$\begin{aligned}\sigma^* \circ w_0^*(\phi_1^*) &= \textstyle\sum_{i\in\mathbf{O}} r(i+n)\gamma_{-i}^* + \sum_{i\in\mathbf{E}} s(i+n)\gamma_{-i}^* \\ &= \textstyle\sum_{i\in\mathbf{O}} r(n-i)\gamma_i^* + \sum_{i\in\mathbf{E}} s(n-i)\gamma_i^* \\ &= \textstyle\sum_{i\in\mathbf{O}} -r(n+i)\gamma_i^* + \sum_{i\in\mathbf{E}} -s(n+i)\gamma_i^*.\end{aligned}$$

So, the equation holds for $w^* = \sigma^* \circ w_0^*$ for the choice of odds $-r$ and $-s$. Now consider the action of τ_o^*. We have

$$\begin{aligned}\tau_o^* \circ w_0^*(\phi_1^*) &= \textstyle\sum_{i\in\mathbf{O}} r(i+n)(-\gamma_{i-1}^* + \gamma_i^* - \gamma_{i+1}^*) + \sum_{i\in\mathbf{E}} s(i+n)\gamma_i^* \\ &= \textstyle\sum_{i\in\mathbf{O}} r(i+n)\gamma_i^* + \sum_{i\in\mathbf{E}} \big(-r(i-1+n) - r(i+1+n) + s(i+n)\big)\gamma_i^* \\ &= \textstyle\sum_{i\in\mathbf{O}} r(i+n)\gamma_i^* + \sum_{i\in\mathbf{E}} (s-2r)(i+n)\gamma_i^*.\end{aligned}$$

So, the equation holds for $w^* = \tau_o^* \circ w_0^*$ with the choice of odds r and $s-2r$. Similarly, the equation holds when $w^* = (\tau_o^*)^{-1} \circ w_0^*$ with the choice of odds r and $s+2r$. We need to be slightly more careful with the even twist because of the role of the zero cohomology classes γ_{-n}^* and γ_n^*. Working modulo $2n$, we have:

$$\begin{aligned}\tau_e^* \circ w_0^*(\phi_1^*) &= \textstyle\sum_{i\in\mathbf{O}} r(i+n)\gamma_i^* + \sum_{i\in\mathbf{E}} s(i+n)(-\gamma_{i-1}^* + \gamma_i^* - \gamma_{i+1}^*) \\ &= \big(r-2s\big)\gamma_{1-n}^* + \big(-r-(2n-2)s\big)\gamma_{n-1}^* + \\ &\quad \textstyle\sum_{i\in\mathbf{O}\smallsetminus\{1-n,n-1\}} \big(-s(i-1+n) - s(i+1+n) + r(i+n)\big)\gamma_i^* + \\ &\quad \textstyle\sum_{i\in\mathbf{E}} s(i+n)\gamma_i^* \\ &= \textstyle\sum_{i\in\mathbf{O}} (r-2s)(i+n)\gamma_i^* + \sum_{i\in\mathbf{E}} s(i+n)\gamma_i^*.\end{aligned}$$

So, the equation holds when $w^* = \tau_e^* \circ w_0^*$ for the choice of odds $r-2s$ and s. Similarly, when $w^* = (\tau_e^*)^{-1} \circ w_0^*$, we use the odds $r+2s$ and s. ♠

9.5 Existence of Stable Trajectories

Suppose that $n \geq 3$ is not a power of two. We will show the second part of Theorem 1.5; V_n has a stable periodic billiard path. We prove this by establishing homology classes of geodesics on $S(V_n)$ which project to stable geodesics. These homology classes are provided by the following two theorems.

Theorem 9.10 (Odd case) *Suppose $n \geq 3$ is odd. Then a closed geodesic in the homology class $(\tau_e \circ \tau_o^{-1})^{\frac{n-1}{2}} \circ \tau_e^{\frac{3-n}{2}}(\gamma_{n-2})$ in $S(V_n)$ projects to a stable periodic billiard path in V_n via the folding map $S(V_n) \to V_n$.*

Theorem 9.11 (Even case) *Suppose n is even and not a power of two. Then $n = 2^a b$ for an odd integer $b \geq 3$ and an integer $a \geq 1$. Let $w = (\tau_e \circ \tau_o^{-1})^{\frac{n}{2}} \circ \tau_o^{\frac{b-1}{2}}$. Then, a closed geodesic in the homology class $w(\gamma_{n-2^{a+1}})$ projects to a stable periodic billiard path in V_n via the folding map $S(V_n) \to V_n$.*

Remarks 9.12 *The above formulas correct the incorrect formulas in [HS09]. The proofs were wrong due in large part to calculation errors. For this reason, we make the calculations very explicit below. Also, work in this section was checked with Mathematica.*

To prove these theorems, we investigate the action of $(w^*)^{-1}$ on ϕ_1^* in order to apply the Stability Lemma. The w provided by each theorem begins with a power of $\tau_e \circ \tau_o^{-1}$, which is conjugate but not equal to a rotation of $S(V_n)$. The following is the main formula necessary in the proofs of the above results.

Lemma 9.13 (Elliptic orbit) *Let $n \geq 3$ be an integer and let k be an integer with $0 \leq k \leq \frac{n}{2}$. Then,*

$$\begin{aligned}\big(\tau_o^* \circ (\tau_e^*)^{-1}\big)^k(\phi_1^*) &= n\big(1+(-1)^k\big)\beta_1^* + n\big(1-(-1)^k\big)\beta_{-1}^* + n\gamma_0^* + \\ &\quad (-1)^k \textstyle\sum_{j=1}^{\min\{2k,n-1\}} \big(j+(-1)^j(4jk-2jn+n)\big)(\gamma_j^* - \gamma_{-j}^*) + \\ &\quad (-1)^k \textstyle\sum_{j=2k+1}^{n-1}(j-n)\big(1+(-1)^j 4k\big)(\gamma_j^* - \gamma_{-j}^*).\end{aligned}$$

To simplify the computations required to prove the lemma, we find it useful to break ϕ_1^* into pieces. Namely, ϕ_1^* is the sum of

$$\Phi_A^* = 2n\beta_1^* + n\gamma_0^* \quad \text{and} \quad \Phi_B^* = \sum_{j=1}^{n-1}(j-n)(\gamma_j^* - \gamma_{-j}^*).$$

The following two propositions give formulas for the image of each under $\big(\tau_o^* \circ (\tau_e^*)^{-1}\big)^k$. Combining them gives the proof of the lemma above.

Proposition 9.14 *Let $n \geq 3$ be an integer and suppose $0 \leq k \leq \frac{n}{2}$. Then, we have*

$$\begin{aligned}\big(\tau_o^* \circ (\tau_e^*)^{-1}\big)^k(\Phi_A^*) &= n\big(1+(-1)^k\big)\beta_1^* + n\big(1-(-1)^k\big)\beta_{-1}^* + n\gamma_0^* + \\ &\quad n(-1)^k \textstyle\sum_{j=1}^{2k}(-1)^j(\gamma_j^* - \gamma_{-j}^*).\end{aligned}$$

To make sense of the case when $k = \frac{n}{2}$, recall that we assigned γ_n^* and γ_{-n}^* to be zero.

Proof: We prove this by induction in k. The statement is true when $k = 0$ by definition of Φ_A^*. Now we will prove it when $k = 1$. We have

$$\begin{aligned}(\tau_e^*)^{-1}(\Phi_A^*) &= (\tau_e^*)^{-1}(2n\beta_1^* + n\gamma_0^*) \\ &= 2n(\beta_{-1}^* - \gamma_{-1}^*) + n(\gamma_{-1}^* + \gamma_0^* + \gamma_1^*) \\ &= 2n\beta_{-1}^* - n\gamma_{-1}^* + n\gamma_0^* + n\gamma_1^*.\end{aligned}$$

Then applying τ_o^* to the above yields:

$$\begin{aligned}\tau_o^* \circ (\tau_e^*)^{-1}(\Phi_A^*) &= \tau_o^*(2n\beta_{-1}^* - n\gamma_{-1}^* + n\gamma_0^* + n\gamma_1^*) \\ &= 2n\beta_1^* - n(-\gamma_{-2}^* + \gamma_{-1}^* - \gamma_0^*) + n\gamma_0^* + n(-\gamma_0^* + \gamma_1^* - \gamma_2^*) \\ &= 2n\beta_1^* + n\gamma_{-2}^* - n\gamma_{-1}^* + n\gamma_0^* + n\gamma_1^* - n\gamma_2^*\end{aligned}$$

This is equivalent to the formula given in the proposition when $k = 1$.

We continue by induction. Assume that the statement is true for k with $1 \leq k < \frac{n}{2}$. We will prove the statement for $k+1$. For conciseness let $\Psi_k^* = \big(\tau_o^* \circ (\tau_e^*)^{-1}\big)^k(\Phi_A^*)$. Let $\mathbf{E}$ and

$\mathbf{O}$ denote the even and odd integers non-strictly between 1 and $2k$. By inductive hypothesis, we have

$$\begin{aligned}(\tau_e^*)^{-1}(\Psi_k^*) &= (\tau_e^*)^{-1}\Big(n\big(1+(-1)^k\big)\beta_1^* + n\big(1-(-1)^k\big)\beta_{-1}^* + n\gamma_0^* + \\ &\quad n(-1)^k\textstyle\sum_{j=1}^{2k}(-1)^j(\gamma_j^*-\gamma_{-j}^*)\Big) \\ &= n\big(1+(-1)^k\big)(\beta_{-1}^*-\gamma_{-1}^*) + n\big(1-(-1)^k\big)(\beta_1^*-\gamma_1^*) + n(\gamma_{-1}^*+\gamma_0^*+\gamma_1^*) + \\ &\quad n(-1)^k\textstyle\sum_{j\in\mathbf{E}}(\gamma_{j-1}^*+\gamma_j^*+\gamma_{j+1}^*-\gamma_{-j-1}^*-\gamma_{-j}^*-\gamma_{1-j}^*) - \\ &\quad n(-1)^k\textstyle\sum_{j\in\mathbf{O}}(\gamma_j^*-\gamma_{-j}^*) \\ &= n\big(1+(-1)^{k+1}\big)\beta_1^* + n\big(1-(-1)^{k+1}\big)\beta_{-1}^* + n\gamma_0^* + n(-1)^k\textstyle\sum_{j=1}^{2k+1}(\gamma_j^*-\gamma_{-j}^*).\end{aligned}$$

We now let $\mathbf{O}'$ be the odds non-strictly between 1 and $2k+1$. We apply τ_o^* to the result from the above:

$$\begin{aligned}\Psi_{k+1}^* &= \tau_o^*\Big(n\big(1+(-1)^{k+1}\big)\beta_1^* + n\big(1-(-1)^{k+1}\big)\beta_{-1}^* + n\gamma_0^* + \\ &\quad n(-1)^k\textstyle\sum_{j\in\mathbf{O}'}\tau_o^*(\gamma_j^*-\gamma_{-j}^*) + n(-1)^k\sum_{j\in\mathbf{E}}\tau_o^*(\gamma_j^*-\gamma_{-j}^*)\Big) \\ &= n\big(1+(-1)^{k+1}\big)\beta_1^* + n\big(1-(-1)^{k+1}\big)\beta_{-1}^* + n\gamma_0^* + \\ &\quad n(-1)^k\textstyle\sum_{j\in\mathbf{O}'}(-\gamma_{j-1}^*+\gamma_j^*-\gamma_{j+1}^*+\gamma_{-j-1}^*-\gamma_{-j}^*+\gamma_{1-j}^*) + \\ &\quad n(-1)^k\textstyle\sum_{j\in\mathbf{E}}(\gamma_j-\gamma_{-j}) \\ &= n\big(1+(-1)^{k+1}\big)\beta_1^* + n\big(1-(-1)^{k+1}\big)\beta_{-1}^* + n\gamma_0^* + \\ &\quad n(-1)^{k+1}\textstyle\sum_{j=1}^{2k+2}(-1)^j(\gamma_j^*-\gamma_{-j}^*).\end{aligned}$$

This proves the proposition. ♠

Proposition 9.15 *For an integer $n \geq 3$ and an integer k satisfying $0 \leq k \leq \frac{n}{2}$, we have*

$$\begin{aligned}\big(\tau_o^* \circ (\tau_e^*)^{-1}\big)^k(\Phi_B^*) &= (-1)^k\textstyle\sum_{j=1}^{\min\{2k,n-1\}}\big(j+(-1)^j(4jk-2jn)\big)(\gamma_j^*-\gamma_{-j}^*) + \\ &\quad (-1)^k\textstyle\sum_{j=2k+1}^{n-1}(j-n)\big(1+(-1)^j 4k\big)(\gamma_j^*-\gamma_{-j}^*).\end{aligned}$$

Proof: First we setup some notation. We let $\eta_j^* = \gamma_j^* - \gamma_{-j}^*$. If $j = 0$ or $j = n$, then η_j is zero.

We will prove this proposition by induction in k. We observe the statement is true when $k = 0$. Now suppose it holds for k with $0 \leq k < \frac{n}{2}$. We define $\mathcal{A}$ and $\mathcal{B}$ so that they sum to $\big(\tau_o^* \circ (\tau_e^*)^{-1}\big)^k(\Phi_B^*)$:

$$\mathcal{A} = (-1)^k\sum_{j=1}^{2k} j\big(1+(-1)^j(4k-2n)\big)\eta_j^*.$$

$$\mathcal{B} = (-1)^k\sum_{j=2k+1}^{n-1}(j-n)\big(1+(-1)^j 4k\big)\eta_j^*.$$

We first consider the action of $(\tau_e^*)^{-1}$ on $\mathcal{A}$. For each integer $i > 0$ define the collections of even and odd integers:

$$\mathbf{E}(2i) = \{2, 4, \ldots, 2i\} \quad \text{and} \quad \mathbf{O}(2i-1) = \{1, 3, \ldots, 2i-1\}.$$

We have:

$$\begin{aligned}(\tau_e^*)^{-1}(\mathcal{A}) &= (-1)^k(\tau_e^*)^{-1}\Big(\textstyle\sum_{j\in\mathbf{O}(2k-1)} j(1-4k+2n)\eta_j^* + \sum_{j\in\mathbf{E}(2k)} j(1+4k-2n)\eta_j^*\Big)\\ &= (-1)^k\Big(\textstyle\sum_{j\in\mathbf{O}(2k-1)} j(1-4k+2n)\eta_j^* +\\ &\quad \textstyle\sum_{j\in\mathbf{E}(2k)} j(1+4k-2n)(\eta_{j-1}^*+\eta_j^*+\eta_{j+1}^*)\Big)\\ &= (-1)^k\Big(2k(1+4k-2n)\eta_{2k+1}^* + \textstyle\sum_{j\in\mathbf{O}(2k-1)} j(3+4k-2n)\eta_j^* +\\ &\quad \textstyle\sum_{j\in\mathbf{E}(2k)} j(1+4k-2n)\eta_j^*\Big).\end{aligned}$$

Now we apply τ_o^* to the end of the above formula:

$$\begin{aligned}\tau_o^*\circ(\tau_e^*)^{-1}(\mathcal{A}) &= (-1)^k\Big(2k(1+4k-2n)(-\eta_{2k}^*+\eta_{2k+1}^*-\eta_{2k+2}^*)+\\ &\quad \textstyle\sum_{j\in\mathbf{O}(2k-1)} j(3+4k-2n)(-\eta_{j-1}^*+\eta_j^*-\eta_{j+1}^*)+\\ &\quad \textstyle\sum_{j\in\mathbf{E}(2k)} j(1+4k-2n)\eta_j^*\Big)\\ &= (-1)^k\Big(-(2k-1)(3+4k-2n)\eta_{2k}^* + 2k(1+4k-2n)(\eta_{2k+1}^*-\eta_{2k+2}^*)+\\ &\quad \textstyle\sum_{j\in\mathbf{O}(2k-1)} j(3+4k-2n)\eta_j^* + \sum_{j\in\mathbf{E}(2k-2)} j(-5-4k+2n)\eta_j^*\Big).\end{aligned}$$

One can observe that the coefficients for η_j with $j\in\{1,\ldots,2k-1\}$ agree with our formula for $\big(\tau_o^*\circ(\tau_e^*)^{-1}\big)^{k+1}(\Phi_B^*)$ given in the proposition. (Note that the sign difference comes from the fact that in the proposition, we begin with $(-1)^{k+1}$.)

Now we will do a similar calculation for $\mathcal{B}$. Let $\mathbf{O}$ and $\mathbf{E}$ denote the odds and evens satisfying $1\le i\le n-1$. We have:

$$\begin{aligned}(\tau_e^*)^{-1}(\mathcal{B}) &= (-1)^k(\tau_e^*)^{-1}\Big(\textstyle\sum_{j\in\mathbf{O}\setminus\mathbf{O}(2k-1)}(j-n)(1-4k)\eta_j^* +\\ &\quad \textstyle\sum_{j\in\mathbf{E}\setminus\mathbf{E}(2k)}(j-n)(1+4k)\eta_j^*\Big)\\ &= (-1)^k\Big(\textstyle\sum_{j\in\mathbf{O}\setminus\mathbf{O}(2k-1)}(j-n)(1-4k)\eta_j^* +\\ &\quad \textstyle\sum_{j\in\mathbf{E}\setminus\mathbf{E}(2k)}(j-n)(1+4k)(\eta_{j-1}^*+\eta_j^*+\eta_{j+1}^*)\Big)\\ &= (-1)^k\Big((3+8k-2n)\eta_{2k+1}^* + \textstyle\sum_{j\in\mathbf{O}\setminus\mathbf{O}(2k+1)}(j-n)(3+4k)\eta_j^*\\ &\quad \textstyle\sum_{j\in\mathbf{E}\setminus\mathbf{E}(2k)}(j-n)(1+4k)\eta_j^*\Big)\end{aligned}$$

We apply τ_o^* to the end of the above formula:

$$\begin{aligned}\tau_o^*\circ(\tau_e^*)^{-1}(\mathcal{B}) &= (-1)^k\Big((3+8k-2n)(-\eta_{2k}^*+\eta_{2k+1}^*-\eta_{2k+2}^*)+\\ &\quad \textstyle\sum_{j\in\mathbf{O}\setminus\mathbf{O}(2k+1)}(j-n)(3+4k)(-\eta_{j-1}^*+\eta_j^*-\eta_{j+1}^*)\\ &\quad \textstyle\sum_{j\in\mathbf{E}\setminus\mathbf{E}(2k)}(j-n)(1+4k)\eta_j^*\Big)\\ &= (-1)^k\Big((3+8k-2n)(-\eta_{2k}^*+\eta_{2k+1}^*)+\\ &\quad (-10-16k+4n)\eta_{2k+2}^*+\\ &\quad \textstyle\sum_{j\in\mathbf{O}\setminus\mathbf{O}(2k+1)}(j-n)(3+4k)\eta_j^* + \sum_{j\in\mathbf{E}\setminus\mathbf{E}(2k+2)}(j-n)(-5-4k)\eta_j^*\Big).\end{aligned}$$

The coefficients match with our formula for $\big(\tau_o^* \circ (\tau_e^*)^{-1}\big)^{k+1}(\Phi_B^*)$ so long as $j \geq 2k+3$.

We now check the coefficients of η_j^* for $2k \leq j \leq 2k+2$. The coefficient of η_{2k}^* of the sum $(\tau_e^*)^{-1}(\mathcal{A}+\mathcal{B})$ is given by

$$(-1)^k\big(-(2k-1)(3+4k-2n)-(3+8k-2n)\big) = (-1)^{k+1}(2k+2-n)\big(1+4(k+1)\big),$$

as required by the proposition. The coefficient of η_{2k+1}^* is given by:

$$(-1)^k\big(2k(1+4k-2n)+(3+8k-2n)\big) = (-1)^{k+1}(2k+1)(1-4(k+1)+2n)$$

as required. The coefficient of η_{2k+2}^* is given by:

$$(-1)^k\big(-2k(1+4k-2n)-2(5+8k-2n))\big) = (-1)^{k+1}(2k+2)\big(1+4(k+1)-2n\big).$$

This also coincides with the formula in the proposition. We have now checked all coefficients. ♠

Proof of Theorem 9.10 (The odd case): By the Stability Lemma, it is equivalent to show that the coefficient of γ_{n-2}^* is zero in $(\tau_e^*)^{\frac{n-3}{2}} \circ \big(\tau_o^* \circ (\tau_e^*)^{-1}\big)^{\frac{n-1}{2}}(\phi_1^*)$. Let $\mathcal{A} = \big(\tau_o^* \circ (\tau_e^*)^{-1}\big)^{\frac{n-1}{2}}(\phi_1^*)$. Using the Elliptic Orbit Lemma, we compute that:

$$\mathcal{A} = 3(-1)^{\frac{n-1}{2}}\gamma_{n-3}^* + 2(n-3)(-1)^{\frac{n-1}{2}}\gamma_{n-2}^* + (-1)^{\frac{n-1}{2}}\gamma_{n-1}^* + \ldots.$$

The coefficients of the rest of the expression are irrelevant. Observe that if $n=3$, the coefficient of γ_{n-2}^* of $\mathcal{A}$ is zero. This proves this statement in this case. Otherwise, we need to apply $(\tau_e^*)^{\frac{n-3}{2}}$ to this expression. We find:

$$(\tau_e^*)^{\frac{n-3}{2}}(\mathcal{A}) = (-1)^{\frac{n-1}{2}}\Big(3\big(\tfrac{3-n}{2}\gamma_{n-4}^* + \gamma_{n-3}^* + \tfrac{3-n}{2}\gamma_{n-2}^*\big) + 2(n-3)\gamma_{n-2}^* + \big(\tfrac{3-n}{2}\gamma_{n-2}^* + \gamma_{n-1}^*\big)\Big) + \ldots.$$

These are the only terms which contribute to the coefficient of γ_{n-2}^*, so we see this coefficient is zero. ♠

Proof of Theorem 9.11 (The even case): We will again use the Stability Lemma. We will show that the coefficient of $\gamma_{n-2^{a+1}}^*$ is zero in $(\tau_o^*)^{\frac{1-b}{2}} \circ \big(\tau_o^* \circ (\tau_e^*)^{-1}\big)^{\frac{n}{2}}(\phi_1^*)$. Let $\mathcal{A} = \big(\tau_o^* \circ (\tau_e^*)^{-1}\big)^{\frac{n}{2}}(\phi_1^*)$. Using the Elliptic Orbit Lemma, we compute that:

$$\mathcal{A} = (-1)^{\frac{n}{2}}\Big((-2^{a+1}-1)\gamma_{n-2^{a+1}-1}^* + 2(n-2^a)\gamma_{n-2^{a+1}}^* + (-2^{a+1}+1)\gamma_{n-2^{a+1}+1}^*\Big) + \ldots.$$

The coefficients of the rest of the expression are irrelevant. Then,

$$\begin{aligned}(\tau_o^*)^{\frac{1-b}{2}}(\mathcal{A}) \;=\; & (-1)^{\frac{n}{2}}\Big((-2^{a+1}-1)(\tfrac{b-1}{2}\gamma_{n-2^{a+1}-2}^* + \gamma_{n-2^{a+1}-1}^* + \tfrac{b-1}{2}\gamma_{n-2^{a+1}}^*) + \\ & 2(n-2^a)\gamma_{n-2^{a+1}}^* + \\ & (-2^{a+1}+1)(\tfrac{b-1}{2}\gamma_{n-2^{a+1}}^* + \gamma_{n-2^{a+1}+1}^* + \tfrac{b-1}{2}\gamma_{n-2^{a+1}+2}^*)\Big) + \ldots.\end{aligned}$$

Only these terms contribute to the coefficient of $\gamma_{n-2^{a+1}}^*$. We compute this coefficient:

$$(-1)^{\frac{n}{2}}\big((-n+2^a+\frac{1-b}{2}) + (2n-2^{a+1}) + (-n+2^a+\frac{b-1}{2})\big) = 0.$$

♠

References

[BGKT98] M. Boshernitzan, G. Galperin, T. Krüger, and S. Troubetzkoy, *Periodic billiard orbits are dense in rational polygons*, Trans. Amer. Math. Soc. **350** (1998), no. 9, 3523–3535. MR 1458298 (98k:58179)

[CHK95] Barry Cipra, Robert M. Hanson, and Amy Kolan, *Periodic trajectories in right-triangle billiards*, Phys. Rev. E (3) **52** (1995), no. 2, 2066–2071. MR 1388476 (97e:58190)

[GZ03] G. Galperin and D. Zvonkine, *Periodic billiard trajectories in right triangles and right-angled tetrahedra*, Regul. Chaotic Dyn. **8** (2003), no. 1, 29–44. MR 1963966 (2004b:37081)

[HH00] Lorenz Halbeisen and Norbert Hungerbühler, *On periodic billiard trajectories in obtuse triangles*, SIAM Rev. **42** (2000), no. 4, 657–670 (electronic). MR 1814050 (2001k:37054)

[Hoo06] W. Patrick Hooper, *On the stability of periodic billiard paths in triangles*, Ph.D. thesis, SUNY Stony Brook, Stony Brook, New York, 2006.

[Hoo07] ———, *Periodic billiard paths in right triangles are unstable*, Geom. Dedicata **125** (2007), 39–46. MR 2322537

[HS09] W. Patrick Hooper and Richard Evan Schwartz, *Billiards in nearly isosceles triangles*, J. Mod. Dyn. **3** (2009), no. 2, 159–231.

[Mas86] Howard Masur, *Closed trajectories for quadratic differentials with an application to billiards*, Duke Math. J. **53** (1986), no. 2, 307–314. MR MR850537 (87j:30107)

[MT02] Howard Masur and Serge Tabachnikov, *Rational billiards and flat structures*, Handbook of dynamical systems, Vol. 1A, North-Holland, Amsterdam, 2002, pp. 1015–1089. MR 1928530 (2003j:37002)

[Sch06a] Richard Evan Schwartz, *Obtuse triangular billiards. I. Near the* $(2, 3, 6)$ *triangle*, Experiment. Math. **15** (2006), no. 2, 161–182. MR 2253003 (2007c:37034)

[Sch06b] ———, *Obtuse triangular billiards II: 100 degrees worth of periodic trajectories*, preprint, 2006.

[Tab95] Serge Tabachnikov, *Billiards*, Panor. Synth. (1995), no. 1, vi+142. MR 1328336 (96c:58134)

[Tro05] Serge Troubetzkoy, *Periodic billiard orbits in right triangles*, Ann. Inst. Fourier (Grenoble) **55** (2005), no. 1, 29–46. MR MR2141287 (2006b:37064)

[Vee89] W. A. Veech, *Teichmüller curves in moduli space, Eisenstein series and an application to triangular billiards*, Invent. Math. **97** (1989), no. 3, 553–583. MR 1005006 (91h:58083a)

[VGS92] Ya. B. Vorobets, G. A. Gal′perin, and A. M. Stëpin, *Periodic billiard trajectories in polygons: generating mechanisms*, Uspekhi Mat. Nauk **47** (1992), no. 3(285), 9–74, 207. MR 1185299 (93h:58088)

[Vor05] Yaroslav Vorobets, *Periodic geodesics on generic translation surfaces*, Algebraic and topological dynamics, Contemp. Math., vol. 385, Amer. Math. Soc., Providence, RI, 2005, pp. 205–258. MR 2180238 (2007d:37048)